Brain Research Bulletin 181 (2022) 144–156

Contents lists available at ScienceDirect

Brain Research Bulletin

journal homepage: www.elsevier.com/locate/brainresbull

Oral treatment of 4-methylumbelliferone reduced perineuronal nets and improved recognition memory in mice

Jana Dubisova [a,b], Jana Svobodova Burianova [a], Lucie Svobodova [a,c], Pavol Makovicky [d], Noelia Martinez-Varea [a,b], Anda Cimpean [a,b], James W. Fawcett [a,e], Jessica C.F. Kwok [a,f,*], Sarka Kubinova [a,g,**]

[a] Institute of Experimental Medicine of the Czech Academy of Sciences, Videnska 1083, 142 20 Prague, Czech Republic
[b] 2nd Medical Faculty, Charles University, V Úvalu 84, 150 06 Prague, Czech Republic
[c] Institute of Physiology of the Czech Academy of Sciences, Videnska 1083, 142 20 Prague, Czech Republic
[d] Department of Biology, Faculty of Education, J. Selye University, Slovakia
[e] John Van Geest Centre for Brain Repair, University of Cambridge, Cambridge, United Kingdom
[f] School of Biomedical Sciences, Faculty of Biological Sciences, University of Leeds, United Kingdom
[g] Institute of Physics of the Czech Academy of Sciences, Prague, Czech Republic

ARTICLE INFO

Keywords:
Perineuronal net
Hyaluronan
Memory
Neuroplasticity
Extracellular matrix

ABSTRACT

Hyaluronan (HA) is a core constituent of perineuronal nets (PNNs) that surround subpopulations of neurones. The PNNs control synaptic stabilization in both the developing and adult central nervous system, and disruption of PNNs has shown to reactivate neuroplasticity. We investigated the possibility of memory prolongation by attenuating PNN formation using 4-methylumbelliferone (4-MU), an inhibitor of HA synthesis. Adult C57BL/6 mice were fed with chow containing 5% (w/w) 4-MU for 6 months, at a dose ~6.7 mg/g/day. The oral administration of 4-MU reduced the glycosaminoglycan level in the brain to 72% and the spinal cord to 50% when compared to the controls. Spontaneous object recognition test (SOR) performed at 2, 3, 6 and 7 months showed a significant increase in SOR score in the 6-months treatment group 24 h after object presentation. The effect however did not persist in the washout group (1-month post treatment). Immunohistochemistry confirmed a reduction of PNNs, with shorter and less arborization of aggrecan staining around dendrites in hippocampus after 6 months of 4-MU treatment. Histopathological examination revealed mild atrophy in articular cartilage but it did not affect the motor performance as demonstrated in rotarod test. In conclusion, systemic oral administration of 4-MU for 6 months reduced PNN formation around neurons and enhanced memory retention in mice. However, the memory enhancement was not sustained despite the reduction of PNNs, possibly due to the lack of memory enhancement training during the washout period. Our results suggest that 4-MU treatment might offer a strategy for PNN modulation in memory enhancement.

Abbreviations

4-MU	4-methylumbelliferone
CNS	central nervous system
CSPGs	chondroitin sulfate proteoglycans
CTCF	Corrected Total Cell Fluorescence
ECM	extracellular matrix
GAGs	glycosaminoglycans
HAS	hyaluronan synthase
Hapln	hyaluronan and proteoglycan link protein
HA	hyaluronan
PNNs	perineuronal nets
SA	Spontaneous alternation test
SOR	spontaneous object recognition test
WFA	*Wisteria floribunda* agglutinin

* Corresponding author at: School of Biomedical Sciences, Faculty of Biological Sciences, University of Leeds, United Kingdom.
** Corresponding author at: Institute of Experimental Medicine of the Czech Academy of Sciences, Videnska 1083, 142 20 Prague, Czech Republic.
E-mail addresses: j.kwok@leeds.ac.uk (J.C.F. Kwok), kubinova@fzu.cz (S. Kubinova).

https://doi.org/10.1016/j.brainresbull.2022.01.011
Received 28 September 2021; Received in revised form 15 January 2022; Accepted 19 January 2022
Available online 21 January 2022

1. Introduction

The extracellular matrix (ECM) is a three-dimensional network that provides structural and biochemical support to surrounding cells. In the brain, ECM molecules exist both as a diffuse and a condensed forms, and play important roles in neuronal development, plasticity, and pathophysiology (Miyata and Kitagawa, 2017).

The most prominent form of condensed ECM in the central nervous system (CNS) is perineuronal nets (PNNs), which surround the soma and proximal dendrites of various neuronal subpopulations and have been shown to be responsible for the synaptic stabilization and receptor clustering, ultimately limits plasticity (Frischknecht et al., 2009; Pyka et al., 2011; Fawcett et al., 2019). PNNs have been shown to contribute to the multiple physiological brain functions, including learning and memory, and are involved in many disorders or pathologies, such as recovery from the spinal cord injury, schizophrenia, neurodegenerative diseases, epilepsy, autism and drug addiction (Sorg et al., 2016; Pantazopoulos and Berretta, 2016; Bozzelli et al., 2018).

Manipulation or disruption of PNNs have been shown to reactivate neuroplasticity, and improve learning and memory associated with the aging or neurological diseases, such as Alzheimer disease (Duncan et al., 2019). Several proof-of-concept approaches have been developed to manipulate or remove PNNs to increase the neuroplasticity, memory and CNS repair. These include enzymatic degradation of ECM molecules (Romberg et al., 2013; Kwok et al., 2008; Howell and Gottschall, 2012), antibodies blocking PNN inhibitory action (Yang et al., 2017), or genetic modifications such as knockout models with gene deletion of various PNN components (Romberg et al., 2013; Carulli et al., 2010). Genetic attenuation of PNNs through specific knock down of link protein *hapln1* in the CNS prolongs memory for familiar objects. Similarly, a localized digestion of PNNs with chondroitinase ABC, an enzyme that degrades the chondroitin sulfate proteoglycan components of ECM also enhances object recognition memory (Romberg et al., 2013).

In order to enhance PNN plasticity as a treatment, it is advantageous to develop a specific drug for this purpose. A promising strategy could be using small molecule compounds to prevent the biosynthesis of PNN components, such as hyaluronan (HA). In the CNS, HA is a major component of the loose ECM and PNNs, and has been shown to regulate the differentiation of neural stem cells (Su et al., 2017). It forms a backbone of mesh-like structure which holds the PNNs on neuronal surface and allows for the binding of other important components such as link proteins (*haplns*), chondroitin sulfate proteoglycans (CSPGs) and tenascin (Fawcett et al., 2019; Carulli et al., 2010; Kwok et al., 2010). Prevention of HA biosynthesis might be the effective target for PNN manipulation.

A well-established small molecule inhibitor of HA synthesis is 4-methylumbelliferone (4-MU), a coumarin derivative (7–hydroxy-4–methylcoumarin). 4-MU acts as a competitive substrate for uridine diphosphate (UDP)-glucuronyltransferase, an enzyme involved in HA synthesis, and causes depletion of cellular UDP-glucuronic acid, which is a building component of HA (Kakizaki et al., 2004). It was also shown that 4-MU downregulates the mRNA levels of HA synthase 2 and 3 (Kultti et al., 2009) or mRNA for UDP-glucose pyrophosphorylase and dehydrogenase (Vigetti et al., 2009). In addition, other mechanisms of 4-MU actions independent of inhibition of HA synthesis has also been suggested (Ishizuka et al., 2016).

4-MU, also called hymecromone, is already approved in multiple countries in Europe as choleretic and antispasmodic drug. Moreover, 4-MU prevents the up-regulation of HA and its beneficial effect have been reported in the treatment of cancers, and various animal models of inflammatory and autoimmune diseases, with the pathology associated with HA over-production (Nagy et al., 2015). Feeding of 4-MU was protective in experimental autoimmune encephalomyelitis model of multiple sclerosis in mice, where it modulates T-cell responses toward a FoxP3 + regulatory T-cell phenotype, related with disease prevention, and prevented suppression of the protective chemokine CXCL12 in CNS tissue (Kuipers et al., 2016; Mueller et al., 2014). In the model of lung staphylococcal enterotoxin B or LPS-induced lung inflammation in mice, 4-MU treatment led to a reduction in HA levels, and decreased lung permeability and pro-inflammatory cytokine production (McKallip et al., 2015, 2013). 4-MU treatment also inhibited development of rheumatoid arthritis (Yoshioka et al., 2013) and prevented liver fibrosis (Andreichenko et al., 2019).

In this study, we investigated the effect of 4-MU on the PNNs, the structures where HA plays an indispensable role. We observed a reduction of HA after a 6-month oral treatment of 4-MU. In addition, there is a reduction of PNNs with a concomitant enhancement in plasticity and an improvement in recognition memory with the use of spontaneous object recognition test in adult C57BL/6 mice. An assessment of the PNN structures around hippocampal neurons showed a reduction in PNN length on neurites and on the number of arborization. Histopathological studies showed a mild atrophy in articular cartilage but it did not affect the motor function of the mice as demonstrated in rotarod test.

2. Methods

2.1. Animals

Three months old mice C57BL/6JOlaHsd strain (males n = 12; females n = 28) (Jackson Laboratory, Bar Harbor, Maine) were used in this study. All experiments were performed in accordance with the European Communities Council Directive of 2020 September 2010 (2010/63/EU), regarding the use of animals in research and were approved by the Ethics committee of the Institute of experimental medicine CAS, Prague, Czech Republic. Animals had unrestricted access to food and water and were maintained on a 12 h light/dark cycle (lights off at 7:30 p.m.). All behavioural testing was conducted during the light phase of the cycle.

In the first group of mice (n = 16, female), we tested the different flavors of chow with 5% (w/w) 4-MU at a dose ~6.5 mg/g/day. The animals were randomly divided into 4 groups (n = 4 per group). 4 mice with the same treatment will be group-housed in one cage to avoid social isolation. Mice was fed *ad libitum* with 5% (w/w) 4-MU in Western diet (1.25% Cholesterol, Sniff GmbH, Germany) with chocolate, orange and banana flavor (4-methylubilliferone, DbPharma France). The mice and the consumed chow were weighed every 3 days for 28 days and compared with a control non-flavored chow (Western diet, Sniff GmbH, TD.88137, Germany) without 4-MU. While each mice was weighed individually (i.e. four data per time point from 4 mice), chow was being weighed from the food hopper and averaged for the calculation of chow consumption (i.e. one data per time point).

Second group of animals (n = 24) was fed *ad libitum* with 5% (w/w) 4-MU (8 male and 8 female) or control chocolate flavored Western diet (4 male and 4 female) for 6 months. Part of the animals were sacrificed directly after 6 months of the 4-MU treatment (4-MU n = 8, control n = 4) and organs (brain, spinal cord, spleen, liver, kidney and cartilage tissue) were dissected and used for biochemical, histological or qPCR analyses.

The rest of the animals were fed with 4-MU (n = 8) or a control chow (n = 4) for the 6 months and then with the control chow for the next 4-weeks to evaluate the wash-out effect. The animals were tested behaviorally for the memory and motor functions and sacrificed after 7 months when organs (brain, spinal cord, spleen, liver and cartilage tissue) were dissected and used for histological, immunohistochemical and qPCR analyses.

2.2. Behavioral tests

To observe the effect of 4-MU, series of memory and locomotor functional tests were performed. Spontaneous recognition tasks were used for the evaluation of changes in memory and plasticity of the brain. Rotarod and grip test were used for verifying the impact of the drug on

the motor functions, mobility of joints and muscular degeneration.

2.2.1. Spontaneous alternation test (SA)

SA tests hippocampus-dependent behavior as an attention toward novelty and spatial memory. Test was performed in a Y-maze with arms of identical dimensions and spaced at 120° angle from each other as described previously for rats (Ennaceur and Delacour, 1988; Winters et al., 2004) and mice (Bartko et al., 2011). The apparatus had high homogenous white non-transparent walls constructed from extruded polystyrene. All walls were 30 cm high, and each arm was 15.5 cm in length and 8 cm wide. A lamp illuminated the apparatus, and a video camera were mounted 40 cm above the apparatus to record trials. Each mouse was placed at the center of the Y-maze and allowed to move freely to explore the empty apparatus for 5 min. Over the course of multiple arm entries, the animals typically show a tendency to enter a less recently visited arm. The numbers of arm entries (activity) and alternation were recorded. Alternation was defined as an entry which was different from the two previously entered arms; no alternation was defined if the mouse went back to either of the two arms just previously visited. Percentage of alternation was calculated using this formula:

$$\% \text{ Alternation} = (\text{Number of alternation}/\text{Total number of entries}) \times 100\%$$

2.2.2. Spontaneous object recognition task (SOR)

In the SOR test, two familiar and one novel objects in the Y maze were used to determine the recognition memory of the mice. One arm of the Y maze was used as a start arm and the other two arms were used to display the objects (randomly shaped junk objects, dimensions ~10 cm × 5 cm × 5 cm). All mice were habituated to the Y maze in two-day sessions. To explore the Y-maze with the dimensions used for SOR test where 2 arms were 10 cm in length, 8 cm wide and the start arm was 4.5 cm in length and 8 cm wide. The following test sessions were separated by a minimum of 48 h. Each test session consisted of a sample phase and a choice phase. In the sample phase, two identical objects (Fig. 1A) were placed at the end of each arm. The animal was left to explore the objects for 5 min. The choice phase followed after a delay of 3 or 24 h which the animal spent in the home cage. The choice phase was procedurally identical to the sample phase, except that the object in one of the arms was replaced by a novel object whereas the other arm contained the familiar object (Fig. 1B). A different object pair was used for each session for a given animal. Time spent with object pairs were counter-balanced 1 h after exposition and objects with no preferences were selected for the experiment. The performance was recorded, and the time spent in exploring objects from each animal was assessed from the video recordings of the sample and choice phases. Occasions where an animal climbed or sat on an object were discarded. For the choice phase, a discrimination score was calculated by dividing the difference in exploration of the novel and familiar objects by the total object exploration time. Therefore, a score of 1 corresponded to exploration of the novel object only, whereas a score of 0 corresponded to the mouse equally exploring the novel and the familiar object (Bralett's test, one-way ANOVA).

2.2.3. Rotarod and grip test

Rotarod and grip test were performed after 6 months of 4-MU treatment. A rotarod machine with automatic timers and falling sensors with a 7 cm diameter drum (ROTA-ROD 47700, UGO BASILE S.R.L., Italy) was used for this test. Before the training sessions, mice (control n = 4; 4-MU n = 8) were habituated to stay on the stationary drum for 60 s and pre-trained for 5 rotations per minute (RPM) for 120 s. In the test phase, animals were tested for 300 s with 10 RPM in 3 different days follow the training.

For the grip test, grip strength test (BIO-GS3, Bioseb, Vitrolles, France) was used. Mice (control n = 4; treated n = 8) were test for the grip of hind limbs in 3 sessions in the 3 subsequent days.

2.3. Tissue processing and histology

The animals used for immunohistochemical and histological analysis (n = 4 for control, n = 7 for treated group) were deeply anesthetized with an intraperitoneal injection of overdose chloral hydrate (Sigma-Aldrich, St. Louis, Missouri, USA) and intracardially perfused with phosphate buffered saline (PBS), followed by 4% paraformaldehyde in 0.1 M phosphate buffer. Head was post-fixed in paraformaldehyde for 1 week. After the brain was dissected from the skull, it was transferred to solutions with increasing concentration of sucrose from 10% to 30% (w/v). Brain was then embedded with O.C.T compound (00411243; VWR), frozen and a series of 20 μm thick coronal sections were cut on cryostat (CryoStar NX70 ThermoScientific, Massachusetts, USA), placed on the glass tissue slides and stored at − 20 °C.

Before staining, brain coronal sections were permeabilized with 0.5% (v/v) Triton X-100 in PBS for 20 min at room temperature. Lipofuscin autofluorescence was quenched by ammonium acetate buffer 50 mM with $CuSO_4$. To block of endogenous biotin signal we used endogenous biotin blocking kit (#Ab64212, Abcam, Cambridge, GB).

PNNs were visualized by the *Wisteria floribunda* agglutinin (WFA), which specifically labels *N*-acetylgalactosamine beta 1 residues of glycoproteins within the ECM of the neurons (1:150; biotinylated WFA, L1516, Lectin from Wisteria floribunda, Sigma Aldrich), and aggrecan (1:150; Anti-aggrecan, rabbit polyclonal, #AB1031, Merck), one of the CSPGs bound to the HA chains in PNNs. Blocking of non-specific binding of aggrecan antibody and WFA was performed using 10% chemiblocker (#2170, Merck, Darmstadt, Germany) in 1X PBS with Triton 0.2% (v/v) at room temperature for 2 h.

Primary and secondary antibodies were diluted in the solution of the same composition as an immuno-blocking solution. Primary antibodies against aggrecan and biotinylated WFA were incubated overnight at 4 °C. WFA was visualized using streptavidin conjugated with Alexa Fluor 488 (1:200; S32354, Life Technologies, USA). Aggrecan was stained by goat-anti-rabbit secondary antibody conjugated with Alexa Fluor 594 (1:300; A11012, Life Technologies, USA). Nuclei were stained using DAPI (1:1000; D1306, Invitrogen). Slices were coverslipped

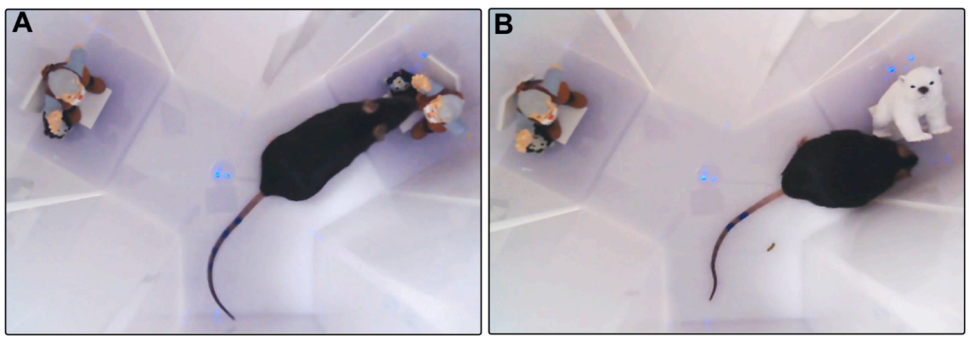

Fig. 1. The sample (a) and choice (b) phases of the SOR test used for the memory retention analysis.

mounted with the anti-fading medium Vectashield (#H-1000; Vector Laboratories, Burlingame, USA).

2.4. PNN analysis by immunohistochemistry

Images of fluorescent WFA staining was taken by Leica microscope (Leica DMI 6000B, ↱Wetzlar, Germany) using a 20× objective and analysed by ImageJ™ software (NIH). The number of WFA positive (WFA+) neurons was determined in the hippocampal area from four brain sections from each animal (n = 4 per group). The intensity of WFA staining was measured from WFA+ neurons in the CA1–3 area of the hippocampus. The value of the intensity was calculated as: Corrected Total Cell Fluorescence (CTCF) = Integrated density of selected cell – integrated density of background readings. In addition, the total number of cells surrounded by PNNs was counted from the number of WFA+ neurons in the CA1-CA3 area. For statistical analysis Bartlett's test, one-way ANOVA were used.

Fluorescent images of neurons (40 neurons per animal, n = 4 per group) stained for aggrecan were taken from CA2/CA3 area using Confocal Microscope Zeiss LSM 880 Airyscan (Zeiss, Oberkochen, Germany) with the 20x objective. Tracing of aggrecan stained PNNs was performed using fluorescent microscope (Leica DMRXA microscope) with Neurolucida2019 software (MBF Bioscience, Williston, Vermont, United States). The 3D tracing was performed manually, starting with neuronal soma. PNNs on dendritic branches were traced with a simultaneous slow movement along the z-axis to keep the traced segment at maximum focus. The final PNN tracings of particular neurons were saved and Neurolucida Explorer 2019 (MBF Bioscience) was used to conduct a detailed morphological structure analysis. The obtained data were further exported and statistically processed with GraphPad Prism Software (8.0). Differences between groups were analysed using Kruskal Wallis test, followed by Dunn's multiple comparisons test.

2.5. Glycosaminoglycan (GAG) extraction and quantification

GAG analyses were performed on 3 animals per group. GAGs purification was performed according to the protocol from (Lin et al., 2011). Briefly, brains and spinal cords were dissected, frozen on dry ice and stored at − 80 °C until purification. Acetone powder of the sample was prepared by homogenising the samples with chilled acetone and drying by desiccation at 4 °C. The dried powder was re-suspended in pronase solution (in buffer containing 0.1 M Tris-acetate, 10 mM calcium acetate, pH 7.8) at 37 °C overnight. Samples were then centrifuged, digested protein in the supernatant was precipitated with trichloroacetic acid (5% v/v final concentration). The supernatant was collected after centrifugation and was washed with diethyl ether. The GAGs present in the aqueous phase were precipitated with sodium acetate (5% w/v final concentration) and ice-cold ethanol (75% v/v final concentration) at 4 °C overnight. Precipitated GAG was recovered by centrifugation and dried at 4 °C. This whole GAG preparation was redissolved in water and stored at − 20 °C. The total GAG content in each sample were quantified using cetylpyridinium chloride (CPC) turbidimetry assay (Manley and Hawksworth, 1966). Chondroitin sulfate-A (Sigma Aldrich) was used to set up the standard curves.

2.6. Gene expression analysis

Changes in the mRNA expression of genes related to the HA synthesis (*has1, has2, has3*), hyaluronidases (*hyal1, hyal2, hyal3, tmem2, spam1*), chondroitin sulfate proteoglycans (*acan, bcan, ncan, vcan*), tenascine-C (*tnc*), synaptic growth (*ngf, gria2, syp*) and receptors for HA (*CD44, lyve1*) were determined after 6 months of the treatment for 4-MU and 4 weeks after the treatment by quantitative real-time PCR (qPCR), and plotted against the control untreated group of animals. RNA was isolated from paraformaldehyde-fixed frozen tissue sections using the High Pure RNA Paraffin Kit (Roche, Germany). RNA amounts were quantified using NanoPhotometer P 330 (Implen, Germany). Isolated RNA was reverse transcribed into complementary cDNA using the Transcriptor Universal cDNA Master (Roche) and T100 Thermal Cycler (Bio-Rad, USA). The qPCR reactions were performed using cDNA solution, FastStart Universal Probe Master (Roche) and TagMan Gene Expression Assays (Life Technologies, Carlsbad, CA, USA) (Supplementary Table 1).

The qPCR was carried out in a final volume of 10 µL containing 45 ng of extracted RNA. Amplification was performed on the real-time PCR cycler (QuantStudio 6, ThermoFisher, Massachusetts, USA). All amplifications were run under the same cycling conditions: 2 min at 50 °C, 10 min at 95 °C, followed by 40 cycles of 15 s at 95 °C and 1 min at 60 °C. All amplifications were run in duplicates and a negative control (water) was included in each array; with Gapdh as a reference gene. A log2 scale was used to display the symmetric magnitude for up and down regulated genes. The values of non-treated animals were set as zero line. Differences between the treated and non-treated groups were analysed for statistical significance with ΔCt values level, using a one-way ANOVA test with Kolmogorov-Smirnof.

2.7. Histopathological evaluation

For histopathological evaluation, spleen, liver, and kidney were sampled and fixed for a minimum of 24 h in 4% paraformaldehyde in 0.1 M PBS. Samples were processed according to standardized protocol using autotechnicon Leica ASP 6P25 (Leica Biosystems Nussloch GmbH, Germany) and paraffin blocks using embedding station Leica EG 1150 H (Leica Biosystems Nussloch GmbH, Germany). Approximately 10 µm slices were cut on a rotary microtome Leica RM2255 (Leica Biosystems Nussloch GmbH, Germany), placed onto standard slides (Bammed s.r.o., Czech Republic) and stained with haematoxylin-eosin (DiaPath, Italy).

Articular cartilage samples were fixed for a minimum of 24 h in 4% paraformaldehyde in 0.1 M PBS. Samples were afterward washed 4 times with distilled water during 24 h. Cartilages were treated with water solution of 15% EDTA (w/v), pH 8.0, which was changed every 3 days for 2 weeks. The samples were rinsed with distilled water and treated with increasing concentration of sucrose (10–20–30% w/v) in PBS and sections were cut on cryostat (CryoStar NX70 ThermoScientific), placed on the glass tissue slides and stored at − 20 °C. The H&E stained tissue slices were observed and imaged using Zeiss microscope (Zeiss Axioskop 2 Plus, Zeiss, Germany).

2.8. Statistical analysis

Data are presented as mean ± standard error of mean (SEM), statistical significance was analysed using SigmaPlot V13 (Systat Software Inc., USA) and GraphPad Prism Software (8.0) with the $^{*}p \leq 0.05$, $^{**}p \leq 0.01$, $^{***}p \leq 0.001$.

3. Results and discussion

3.1. Formulation for non-invasive oral administration of the 4-MU

PNNs present a promising treatment target for numerous brain diseases or CNS injuries. In this regard, 4-MU, a drug that inhibits HA synthesis, might have a wide potential in functional modulation of structures rich on HA. 4-MU is an approved drug for human consumption. Daily oral doses of 1200 mg/day for 3 months is well tolerated in humans without serious adverse effects and it serves as a dose for exploring new indications (Nagy et al., 2015; Trabucchi et al., 1986). However, to achieve and maintain an effective drug concentration in the organs such as the brain, a higher dose of 4-MU is required due to its rapid clearance and therefore low systemic bioavailability (< 3%) (Nagy et al., 2015). In this study, we used oral administration in a dose ~ 6.7 mg/g/day (5% w/w 4-MU in chow), which has been shown previously as therapeutically effective with a well-demonstrated tolerance (Nagy et al., 2015; Kuipers et al., 2016; Kuipers et al., 2016).

To avoid force feeding and facilitate spontaneous feeding behaviour, 4-MU (5% w/w) was mixed with different flavors (chocolate, orange and banana) in the chow and consumption was allowed *ad libitum*. To prevent the effect of weight loss in the animals after 4-MU consumption described before (Kuipers et al., 2016), we combined 4-MU treatment with the high fat diet recommended for rodents.

We first compared the amount of consumed chow with different flavors and the weight of the animals for 28 days (Fig. 2). When we used the chocolate and orange flavored 4-MU chow, the weight of the consumed chow as well as the weight of the animals did not differ from the control non-flavored chow. Surprisingly, a remarkable increase in 4-MU chow consumption was observed for banana flavor compared to all other groups ($p = 0.0001$). On the other hand, the enhanced feeding preference of banana-flavored chow had no effect on the weight of the animals (Fig. 2C).

We showed that incorporating 4-MU in a chocolate or orange favored chow is an easy and non-invasive method to administer the drug to the animals. To make our study comparable to the previous work (Kuipers et al., 2016; Tsuchiya et al., 2020), we chose chocolate flavor chow for the following 6-months 4-MU treatment.

3.2. 4-MU down-regulated GAGs in the CNS

To determine the effect of systemic 4-MU treatment on the HA synthesis, we first investigated the amount of GAG reduction in the CNS. HA belongs to the family of GAGs, which also include heparin/heparan sulfate, chondroitin sulfate, dermatan sulfate, and keratan sulfate. GAGs were isolated and analysed following our previously published protocol (Lin et al., 2011). In comparison to control fed mice, 4-MU treatment has led to a significant reduction of total GAGs by 50% in the spinal cord and 28% in the brain (Fig. 3). The stronger reduction of GAGs in the spinal cord could be due to differences in HA metabolism between the brain and spinal cord. The results, however, confirm that oral treatment of 4MU could effectively down-regulate HA in the CNS.

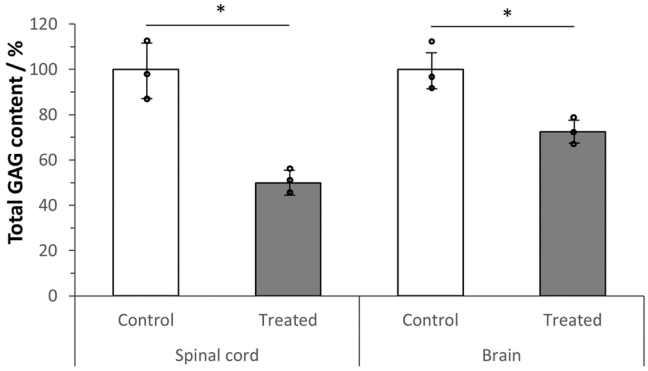

Fig. 3. 4-MU treatment has led to a reduction of GAGs in the CNS. Total GAG content (ug/mg of wet weight) was normalized to the quantity in the control treated mice. 4-MU treatment has led to a significant reduction of total GAG both in the spinal cords (from 100% to 49.93% ± 3.99%, $p = 0.0127$) and the brains (from 100% to 72.46% ± 4.51%, $p = 0.0300$). There is a stronger reduction in the spinal cord than in the brain (50.07% Vs 27.54%). $n = 3$, Student t-test, two tailed paired.

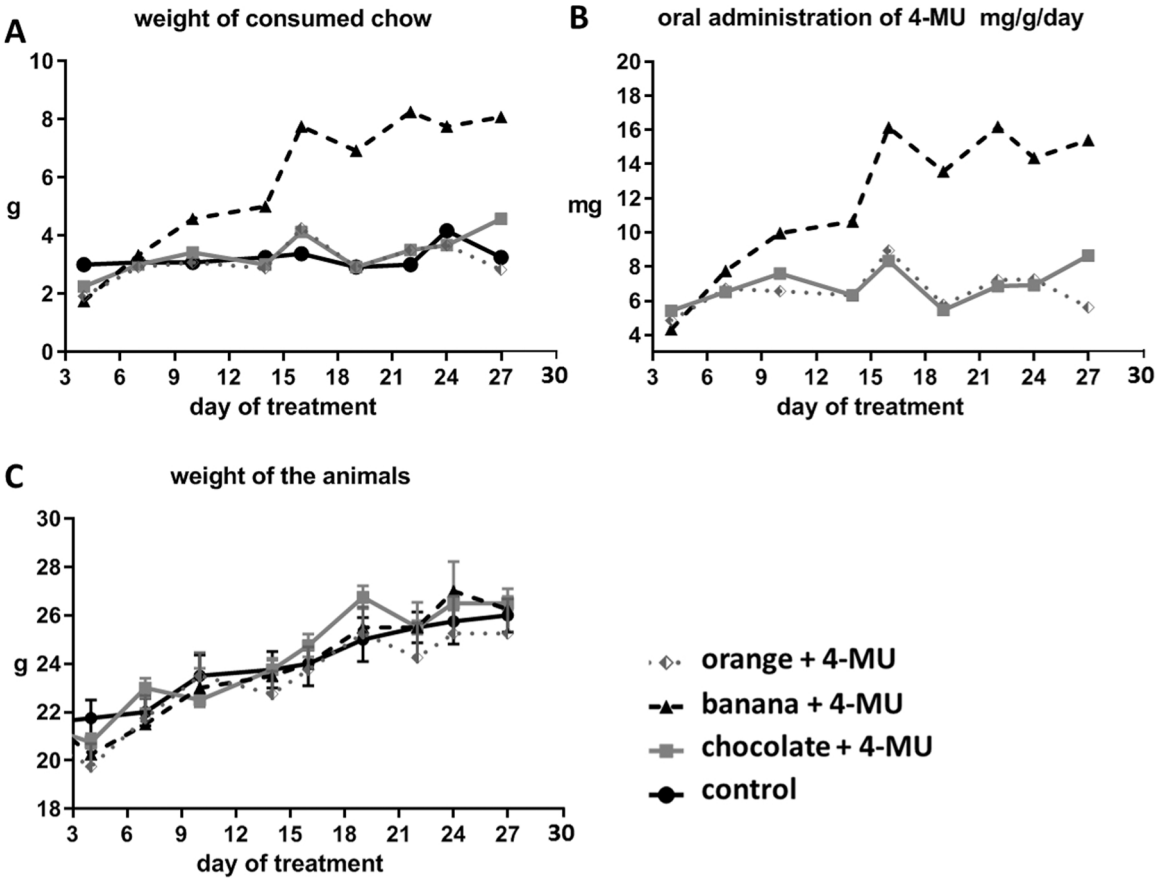

Fig. 2. The effect of flavor on the amount of consumed chow and weight of animals. Mice were fed with the control or 5% (w/w) 4-MU chow with a chocolate, orange or banana flavor ad libitum for the 28 days. (A) Remarkable enhancement of consumed chow was observed for banana flavor compared with all other groups. (One Way ANOVA; Dunn's Method; $p^{***} = 0.0001$). (B) The corresponding amount of consumed 4-MU. (C) The weight of the animals did not differ in all groups. $n = 4$ per group. (One Way ANOVA; Dunn's Method; $p^{***} = 0.0003$).

3.3. 4-MU improved memory retention

To investigate the effect of 4-MU in neuroplasticity, we used a set of behavioral tests focused on the short-term memory. Behavioural tests were started at 2 months after 4-MU treatment. This is mainly due to our previous observation in spinal cord injury that behavioural benefits from 4-MU treatment only appear at 6–7 weeks after treatment (Kwok et al., 2021). We thus decided to start our behavioural testing at 2 months after 4-MU treatment.

First, we examined the spontaneous alternation (SA) after 2 and 6 months of 4-MU treatment (Fig. 4A). This test is based on counting the alternation in three consecutive entrances to the arms which were not visit before, and it quantifies the willingness of the rodents to explore new environment as well as short term spatial memory. There is no difference in the total number of entries or alternations between the groups. This suggests that 4-MU did not affect the exploratory behaviour of the mice.

We then tested recognition memory after 2, 3 and 6 months of 4-MU treatment and after 1 month of 4-MU wash-out in the SOR test. This test is based on the tendency of rodents to interact more with a novel object than with a familiar object and animals are tested at various times after exposure to the objects to measure memory persistence. While 4-MU treatment showed a trend of memory enhancement in all time points of the treatment, significantly enhancement in 3-hour memory retention was found after 2 months of treatment compared to the washout group, and in 24-hour memory retention after 6 months of the treatment as compared to the control and washout group (Fig. 4B). Similar observation of memory enhancement in 24-hour object recognition tests have been previously observed with knock-out mice lacking the *Hapln1* gene, which encodes a link protein essential for PNN formation in the CNS, as well as after enzymatic degradation of PNN structures with chondroitinase ABC in the perirhinal cortex (Romberg et al., 2013). Our results suggest that oral treatment of 4-MU could improve memory retention via PNN down-regulation.

To investigate whether the effect of 4-MU is permanent, we performed SOR test one month after the termination of the 6-month 4-MU treatment (washout effect). We found that the memory-enhancing effect of 4-MU did not persist 1 month after the end of the 4-MU treatment, and the SOR score returned to the values as before the treatment. While the high level of neuroplasticity induced by the reduction of PNNs after 4-MU treatment facilitates memory retention, the lack of persistent memory benefits in the wash-out group suggests that a constant low PNN level is required. Alternatively, the observation in the wash-out group could be due to the lack of memory training during the wash-out period (Fig. 4). In addition, the results also suggest the involvement of other PNN-independent mechanism in the control of object recognition memory. Indeed, HA has been shown to differentially regulate the renewal, proliferation and differentiation of neural stem cells in the hippocampus (Su et al., 2017). It could be that the persistence low level of HA induced by the prolonged 4-MU administration hampers hippocampal neurogenesis which is instrumental in memory acquisition and formation.

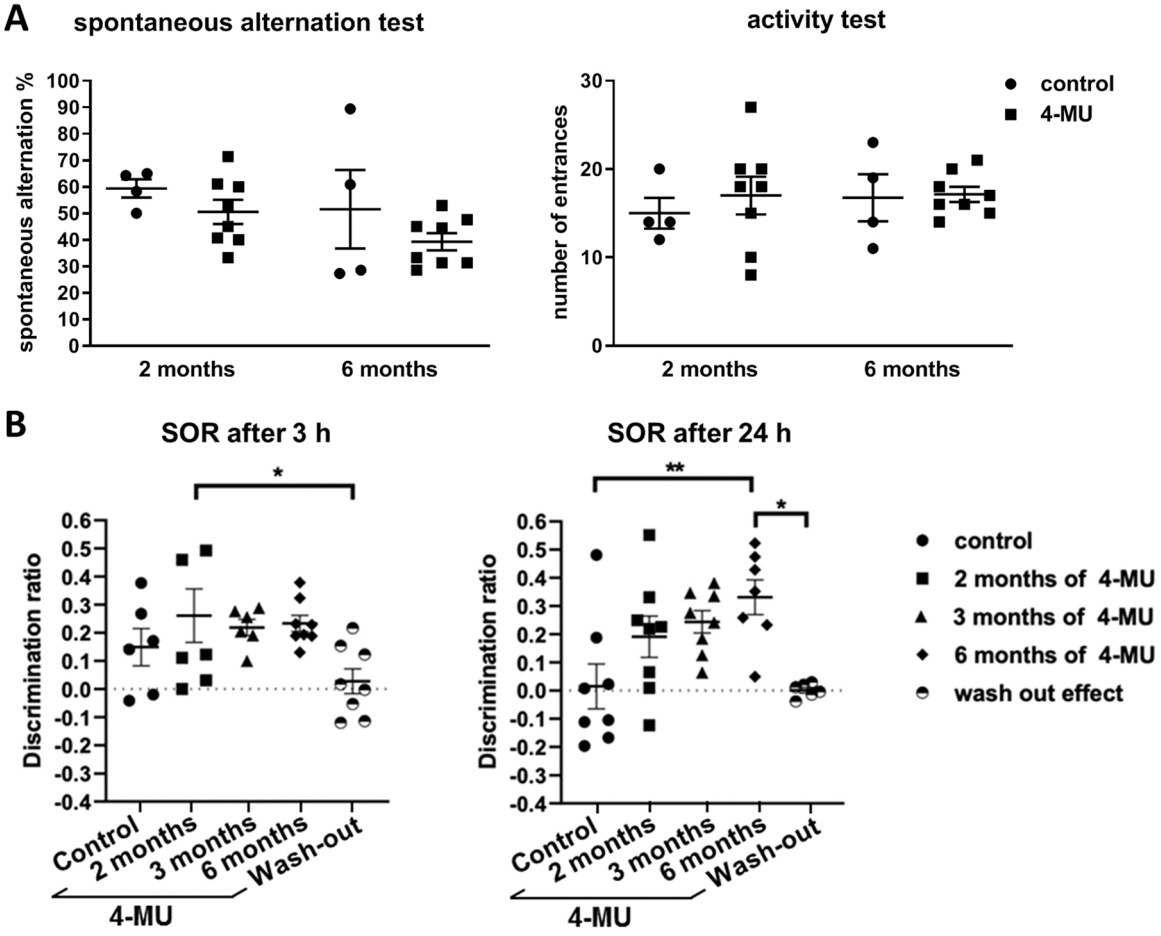

Fig. 4. The spontaneous alternation (SA) and activity test after 2 and 6 months of the 4-MU treatment. (A) SA as well as an activity test did not show any significantly changes after the administration of the 4-MU treatment compared to the control animals. (B) SOR test was done after 2/3/6 month of the 4-MU treatment and then after 1 month (washout). A significant enhancement of SOR score was found in the 3 h delay in animals treated with 4-MU after 2 months compared to the wash-out group and in 24 h delay after 6 months of treatment compared to control and wash out group of animals. SOR score decreased to the control level after 1 month wash-out, which suggests that the effect of 4-MU is temporal. *$p < 0.05$; **$p < 0.01$, One Way ANOVA; Tukey's multiple comparison test.

3.4. 4-MU reduced PNNs in the hippocampal area

It has been shown previously that recognition memory is related to the hippocampus and adjacent cortical areas including entorhinal, perirhinal, and parahippocampal cortex that are involved in normal memory function (Baxter, 2010). In the previous reports, reduction of PNNs by chondroitinase ABC in the perirhinal cortex altered SOR task (Romberg et al., 2013; Yang et al., 2015). These structures are highly integrated; the perirhinal cortex is involved in object recognition after short retention intervals, while the hippocampus is mainly associated with spatial navigation and in the encoding, consolidation and retrieval of non-spatial memory including object recognition memory. We thus investigated the effect of 4-MU in PNN expression in the hippocampus.

Here, we confirmed a reduction of PNNs after 4-MU treatment in the hippocampus. We used WFA staining that selectively labels the N-acetylgalactosamine-beta-1 residues of glycosaminoglycans of PNNs in the ECM to first evaluate the effect of 4-MU in the intensity of PNN and the total number of the neurons surrounded by PNNs (Fig. 5). While the total number of WFA positive neurons remains similar, there is a significant decrease in the WFA intensity around neuronal bodies in both the 4-MU treated and the wash-out groups (Fig. 5B).

Aggrecan is a CSPG which is present in almost all PNN-positive neurons in the brain and it forms an integral structure of the PNNs by binding to HA chains through the Haplns (Kwok et al., 2011; Galtrey et al., 2008). Previous study has shown changes in dendritic length and arborization during plasticity. To investigate the effect of 4-MU in dendritic plasticity, we performed immunohistochemical staining for aggrecan and quantified the dendritic arborization of PNNs around individual neurons in the hippocampus (Figs. 6 and 7). The single cell analysis using the aggrecan staining of hippocampal neurons after 6 months of 4-MU treatment revealed a reduction in the area and volume of PNNs per neuron, and the length of PNN on dendrite (Fig. 7, A–C). Analysis of the arborization also found a reduction in dendritic complexity covered by the PNNs, this is reflected in the number of arborization, nodes and ends of the dendrites (Fig. 7, D–F). Similar to WFA staining, the aggrecan staining around neurons did not recover after 1 month of 4-MU washout (Fig. 7).

These results confirmed that HA is an essential component for PNN formation and that an inhibition of HA synthesis leads to a significant reduction in PNN morphology in hippocampal neurons. However, this study focused on the hippocampal region of CA2/CA3 with the most pronounced aggrecan staining, and therefore the ubiquitous effect of 4-MU on total PNN in other areas have to be confirmed in a future study.

The results suggest a correlation of recognition memory enhancement and PNNs reduction after 6 months of 4-MU treatment. This finding also agrees with previous report which demonstrated that

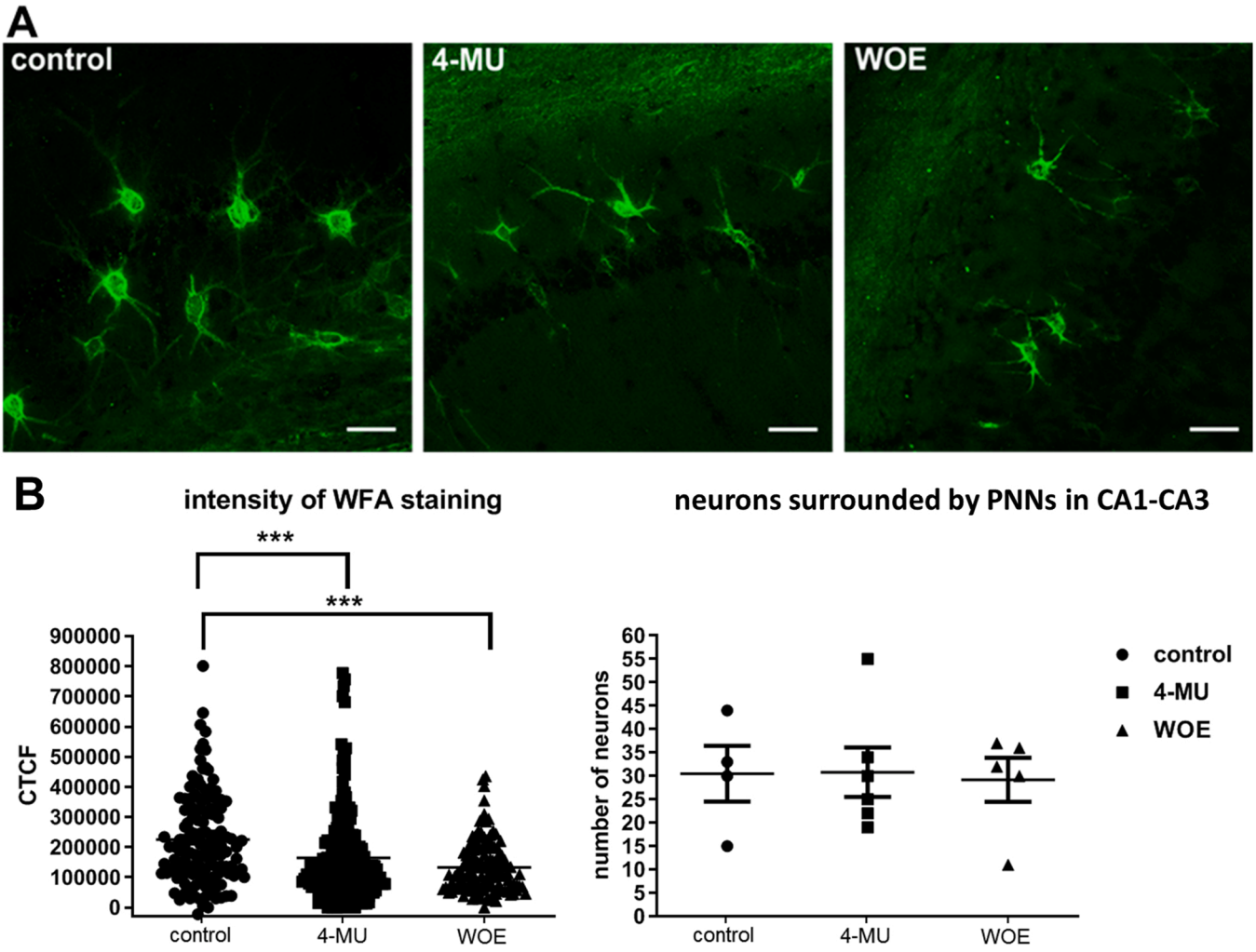

Fig. 5. (A) Representative images of immunofluorescence staining of WFA in CA1-CA3 of the hippocampal area in the control, 4-MU treated for 6 months and 4-MU treated animals after 1 month of the wash-out. (B) Intensity of WFA staining and total number of WFA positive cells determined in the hippocampal area (CA1–CA3). A significant decline of the WFA intensity staining was found after 6 months of 4-MU treatment and it persisted after 1 month of the wash-out when compared with the control. n = 4 per group, ***$p < 0.001$; one-way ANOVA test. WOE – wash-out effect. Scale: 50 μm.

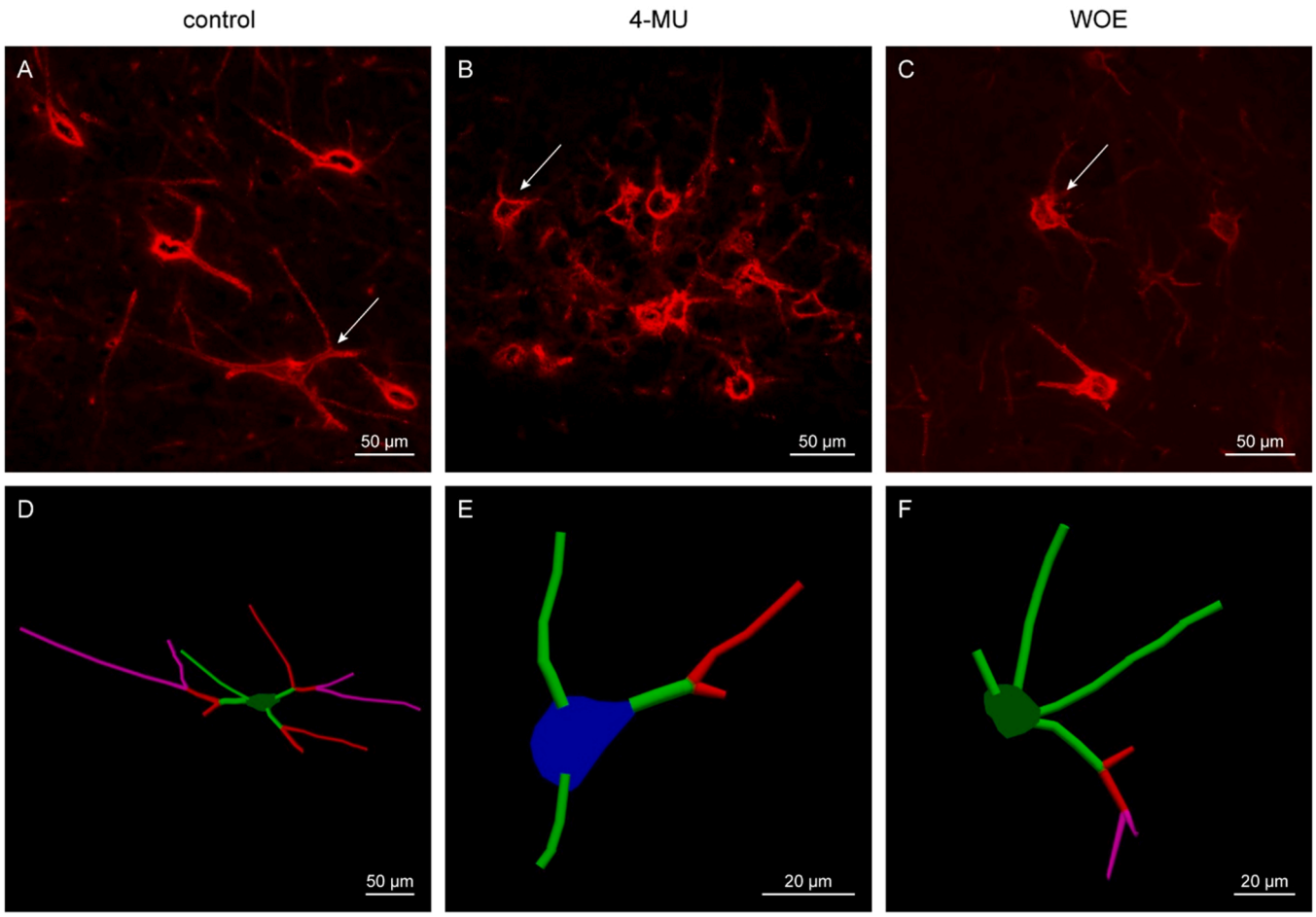

Fig. 6. (A–C) Illustrations of aggrecan stained PNNs in neurons in the hippocampal CA2/CA3 area in the (A) control, (B) 4-MU after 6 months of treatment and (C) WOE group. (D–F) Examples of PNN tracing in the (D) control, (E) 4-MU and (F) WOE. Arrows in A, B, C depict PNNs of neurons traced in D, E, F. WOE-washout effect. Scale: (A–D) 50 µm, (E, F): 20 µm.

improvement of recognition memory is related to attenuated PNNs in the hippocampus and its associated area such as perirhinal cortex (Romberg et al., 2013). Removal of hippocampal PNNs has been previously shown to disrupt contextual and trace fear memory, and a disruption of PNNs in the medial prefrontal cortex impaired long-term trace and conditioned stimulus-elicited fear memory in the trace fear conditioning task (Hylin et al., 2013). Notably, loss of PNNs in several brain regions has been suggested to contribute to cognitive impairment in disorders such as schizophrenia (Pantazopoulos and Berretta, 2016; Howell and Gottschall, 2012; Lewis et al., 2012) and PNN abnormalities are also associated with other neurological diseases (Wen et al., 2018). The opposing data demonstrate the complexity of PNNs in memory regulation.

It should be noted that much of the brain ECM exists as the diffuse compartment, and condensed ECM including PNNs represents a small proportion of the total ECM. Therefore, systemic inhibition of HA by 4-MU, which lacks specificity, can also cause the alteration of diffuse ECM. In this study, systemic HA inhibition caused a reduction of PNNs, which correlated with enhanced memory retention. On the other hand, one month after the end of 4MU treatment, the attenuation of PNNs still persisted, while the memory enhancing effect disappeared. This suggests that other PNN-independent, but ECM-related, mechanism is involved in the control of object recognition memory. HA and its receptor CD44 have been previously shown to regulate the hippocampal neurogenesis and hippocampal-dependent spatial memory (Su et al., 2017; Raber et al., 2014). It could be that the persistence low level of HA induced by the prolonged 4-MU administration hampers hippocampal neurogenesis which is instrumental in memory acquisition and formation.

Nonetheless, these data suggest that other factors in addition to PNNs might be involved in plasticity recovery after the treatment with 4-MU.

3.5. Changes in gene expressions using RT-qPCR

To examine the effect of 4-MU treatment on the expression of genes related to HA metabolism (*has1–3*, hyal1–3, *tmmem2*) and signalling (*CD44*) in the brain and neuroplasticity (*ngf, gria2, syp*), we used RT-qPCR analysis (Fig. 8). HA is synthesized by transmembrane enzymes HAS1–3 and extruded from the cell surface where it forms a PNN when interact with other soluble PNN molecules (Kwok et al., 2010). Each HAS isoform shows different enzyme activities and variable requirements for the cellular supply of UDP-sugars in vivo. HAS1 seems to produce low level of hyaluronan in cells with a low content of the nucleotide sugars, HAS3 produces HA at a high speed even with minimum substrate content (Rilla et al., 2013). In the cerebellum, HAS2 and HAS3 are produced by cerebellar PNN-bearing neurons (Carulli et al., 2006). On the other hand, it has been demonstrated that the genetic ablation of HA synthesis in the brain of *Has3*$^{-/-}$ mice revealed no detectable changes in the structure or composition of PNNs (Arranz et al., 2014), this could be due to compensatory regulation of other HASs. *In vitro*, 4-MU treatment downregulated HA biosynthesis and expression of HAS2 and/or 3 in various cancer cell lines (Kultti et al., 2009; Saito et al., 2013), bone marrow (Goncharova et al., 2012), or human articular chondrocytes (Ishizuka et al., 2016). We observed a reduced trend of *has3* expression in the 6 months treated group and a

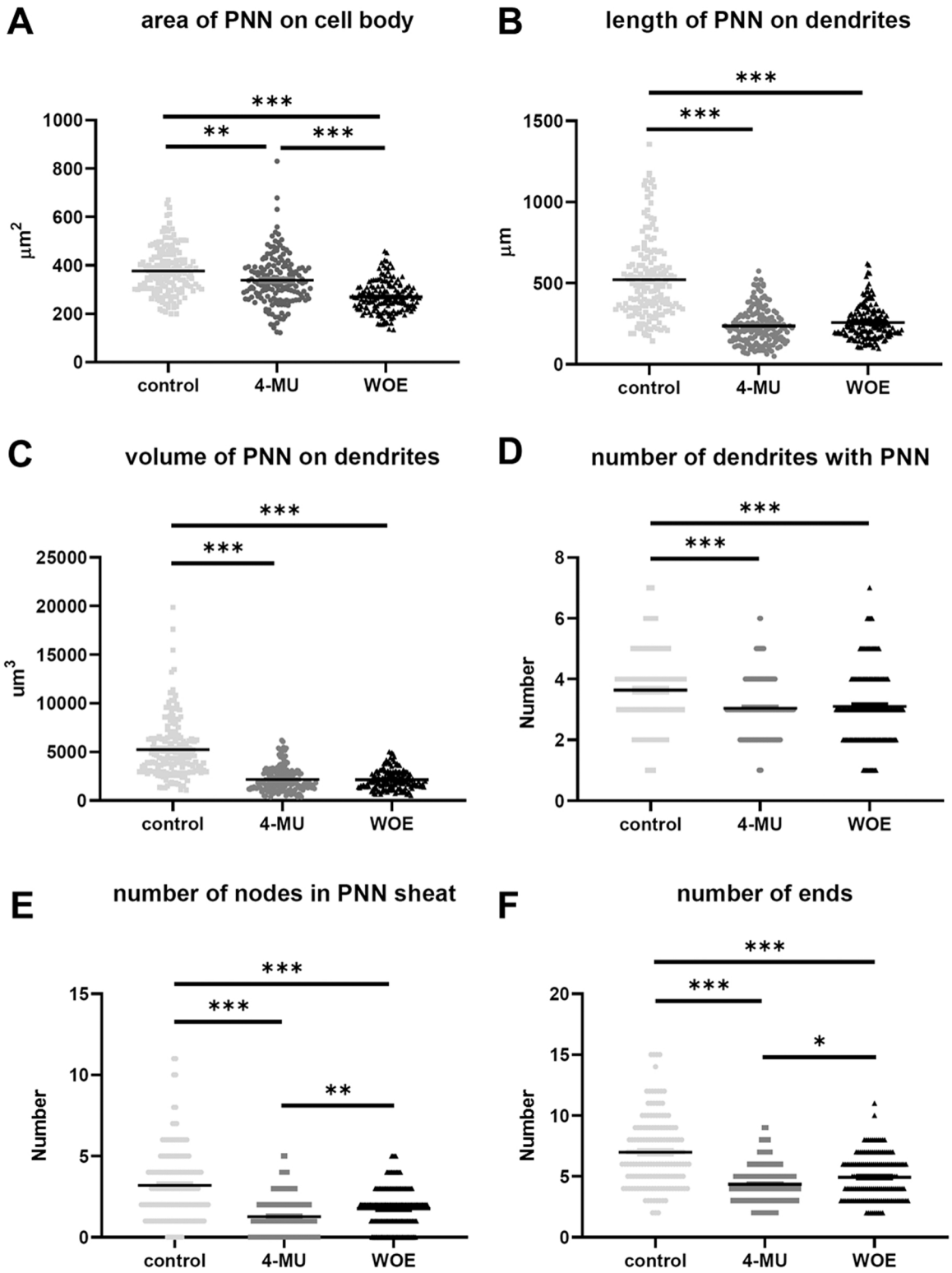

Fig. 7. Morphological parameters of PNNs in the hippocampal CA2/CA3 area in the control, 4-MU after 6 months of treatment, and WOE group. n = 4 per group, 40 neurons per animal, ***p < 0.001, ** p < 0.01, *p < 0.05, Kruskal Wallis test, followed by Dunn's multiple comparisons test.

significant reduction in the WOE group. The expression of the other isoforms *has1* and *has2,* and the HA degrading enzyme *hyal3* was not detected (Fig. 8). Moreover, we also observed a significant reduction in the expression of *CD44*, the receptor of HA. These data agrees with previous report that 4-MU regulates *has* expression (Kultti et al., 2009) and HA metabolism leading to the reduced formation of PNNs.

In terms of other key PNN components (*acan, bcan, ncan, vcan, tnc*), there is a significant reduction in the mRNA expression of neurocan (*ncan*) after 6 months of 4-MU application as well as 1 month after washout. Neurocan is one of the key HA binding CSPGs in the PNNs, and is a potent inhibitor of neuronal and glial adhesion, and neurite outgrowth. A reduction in ncan could potential lead to a more permissive environment favouring neuroplasticity.

In order to determine the effect of 4-MU and its associated down-

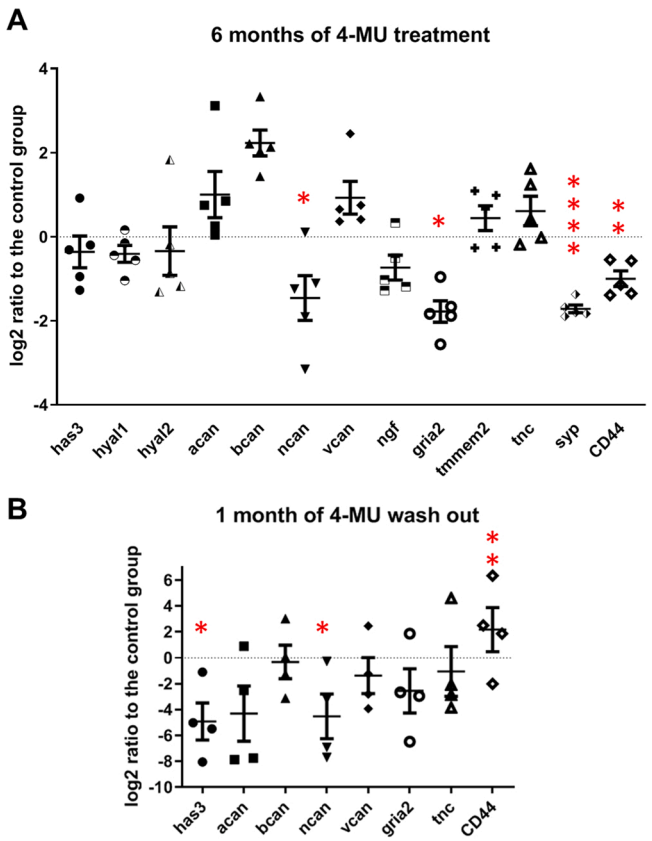

Fig. 8. mRNA expression of selected genes after(A) 6 months of 4-MU treatment and (B) 1 month of 4-MU wash-out. Significant changes of expression were observed in neurocan (ncan), glutamate ionotropic receptor AMPA type subunit 2 (gria2), synaptophysin (syp), (CD44) with 6 months of treatment, and in hyaluornan synthase 3 (has3), ncan and CD44 in the WOE group when compared with the control group. n(control) = 4, n(4-MU) = 5, n(WOE) = 4. * $p \leq 0.05$; ** $p \leq 0.01$; *** $p \leq 0.001$; ****$p \leq 0.0001$ vs. control, one-way ANOVA; Student-Newman-Keuls Method.

regulation of PNNs and ECMs in synaptic plasticity, we have also determine the expression for nerve growth factor (*ngf*), AMPA-selective glutamate receptor 2 (*gria2*) and synaptophysin (*syp*). We observed a significant down-regulation of *syp* after 6 months of 4-MU treatment. For *gria2*, the down-regulation was observed in both the 4-MU treated group and the wash-out group. This suggests that the effect of 4-MU on brain ECM was long-lasting and there is no recovery of PNN structures, neither on gene expression level or at the protein level even after 1 month after the end of treatment.

3.6. Histopathological examination after long-term 4-MU treatment

Apart from its weight bearing and lubricating function in cartilage, HA serves multiple physiological functions in the body. Systemic inhibition of hyaluronan synthesis by 4-MU (10 mg/g body wt) interfered with the protective function of the endothelial glycocalyx, facilitates leukocyte adhesion, subsequent inflammation, and progression of atherosclerosis in apolipoprotein E–deficient mice (Nagy et al., 2010). Disruption of HA production by intravenous injection of 4-MU (100 μL of 3 mM) decreased hematopoietic activity in vitro and lowers the migration of transplanted hematopoietic stem/progenitor cells into the marrow of irradiated mice (Goncharova et al., 2012). On the other hand, 4-MU diminished pro-inflammatory activation of articular chondrocytes and cartilage explants in vitro through a mechanism independent of HA (Ishizuka et al., 2016) or alleviates inflammatory responses in a model of murine arthritis (3 mg/g/day) and in human rheumatoid synovial fibroblasts (Yoshioka et al., 2013). Despite of the several studies of 4-MU administration on a variety of experimental disease models, a systematic histopathological study addressing the potential side effects of high doses of 4-MU is still lacking.

In the current study, we induced long-term non-specific inhibition of HA synthesis by the systemic 4-MU treatment in a dose ~ 6.7 mg/g. The dose is based on a previous publication (Nagy et al., 2015) but is much higher than the approved dose of hymecromone to treat biliary spasm. Notably, the LD_{50} of 4-MU for oral administration has been reported 2850 mg/kg in mice and 6200 mg/kg in rats (Bethesda (MD), 2021).

Despite exceeding the reported oral $LD_{50\ (mice)}$ by more than twice, no animal died during the 6 months of feeding in our study and there were no obvious behavioural sequelae. This suggests a much higher tolerability of oral administration of 4-MU than previously reported in the Pubchem database. The current LD_{50} for mice is reported from 1968 (Lontane et al., 1968), and drug preparation and impurity could have led to the observed difference. In our study, we used pharmaceutical grade 4-MU (5% w/w) that was showed tolerable in several previous studies, e.g., in a model of multiple sclerosis (Mueller et al., 2014), osteoarthritis (Tsuchiya et al., 2020) and diabetes (Sunkari et al., 2015). Undoubtedly, based on our data and recent reports, the LD50 for oral dose of 4-MU in mice needs revisiting.

To determine the potential adverse effect of systemic 4-MU administration on various tissues and their functions, we have performed histopathological observation of the cartilage, spleen, liver and kidney (Table S2), and investigated whether 4-MU treatment could impair the cartilage dependent motor capabilities, using rotarod and grip test after 6 months of the treatment.

In articular cartilage (Fig. 9), we observed an atrophy of the hyaline cartilage with changes in the structure of the cartilage in the 4-MU treated mice, where we observed bone trabeculae with residual, intermittent regenerating hyaline cartilage. However, motor deficit was not observed in rotarod and grip tests (Fig. 10), indicating that the animals were not suffering from joint pain. In both tests, we did not find any differences in balance, coordination, motor-planning and control of the forelimbs between the treated and non-treated group.

In the spleen (Fig. S1A, B), we observed extramedullary haematopoiesis and signs of anaemia in both the control and 4-MU treated groups, which might indicate a compensation for the disrupted haematopoiesis in the bone marrow after 4-MU treatment, described in (Goncharova et al., 2012). We did not observe clear pathological effect of 4-MU in the liver (Fig. S1 C, D). Steatosis as well as extramedullary haematopoiesis was detected in the liver of both control as well as 4-MU treated animals, which was probably due to the high fat in the Western diet (1.25% Cholesterol), which we used to reduce the weight loss of the animals after the 4-MU treatment (Kuipers et al., 2016). No noticeable change of glomeruli and tubules were detected in the kidney from both the control and treated groups (Fig. S2).

Taken together, the histopathological observation from such a high dose of 4-MU is rather mild and suggests a good tolerance. A prolonged systemic 4-MU treatment for 6 months has led to cartilage atrophy which did not affect motor functions. A further study should be performed to systemically interrogate all potential adverse effects of 4-MU in other organs.

4. Conclusions

Our study demonstrates that 6-month oral administration of 5% (w/w) 4-MU reduced GAG content in brain, improved memory retention and reduced PNNs in hippocampus in mice after 6 month of treatment. On the other hand, 1 month after the end of the 4-MU treatment, the memory-enhancing effect disappeared while the attenuation of PNNs in the hippocampus continued. Moreover, histopathology revealed mild atrophy of the articular cartilage. Overall, our results provide new knowledge about the effects of systemic inhibition of HA synthesis on the PNNs and suggest that inhibition of HA synthesis might offer a novel

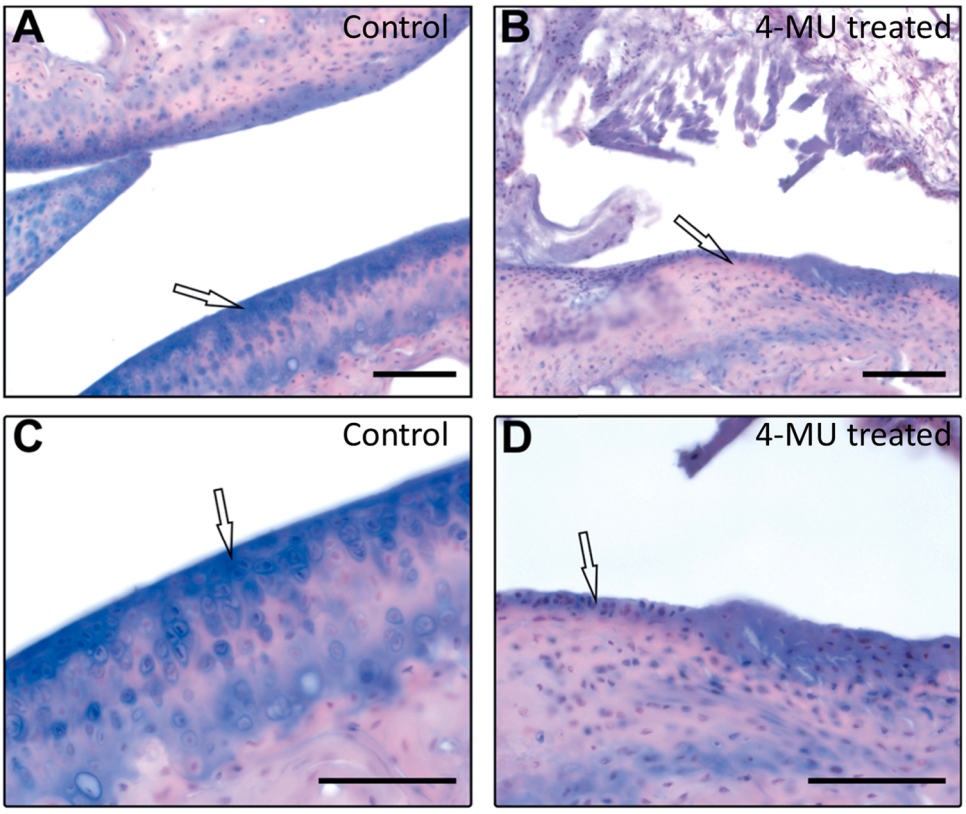

Fig. 9. Alcian blue staining of the articular cartilage. (A, C) Articulation in normal bones is covered by standard thick hyaline cartilages. (B, D) Atrophy of the hyaline cartilage with thin bones, and trabecula with residual, intermittent regenerating hyaline cartilages are observed after 4-MU treatment. Scale bar: A,B: 100 μm, C, D: 10 μm.

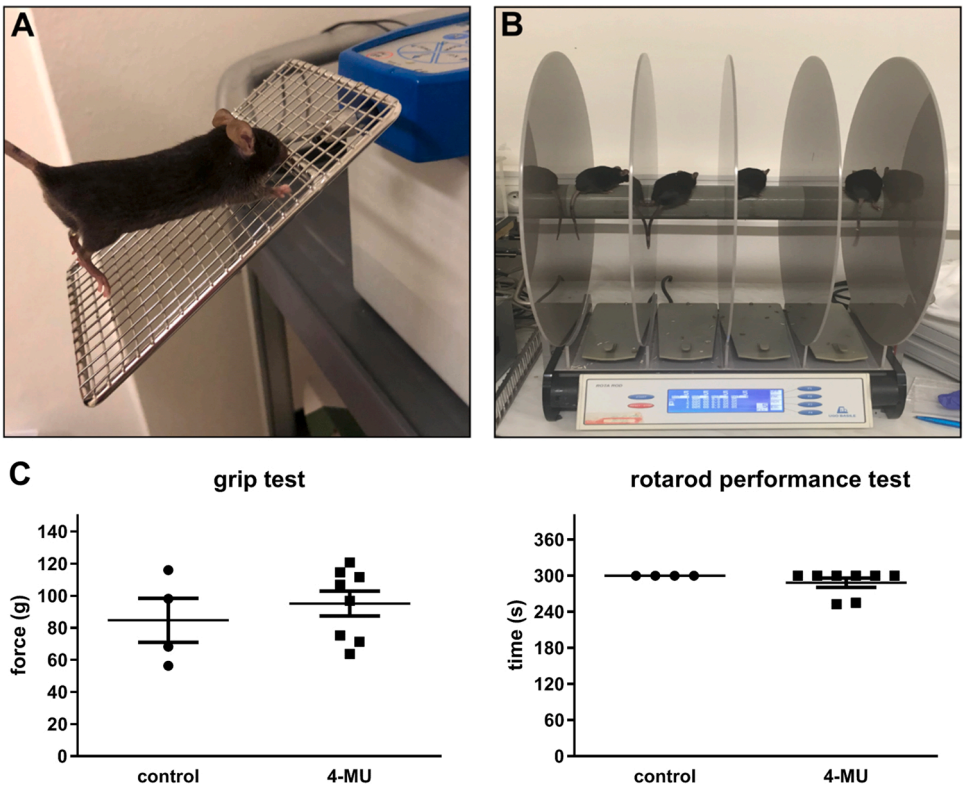

Fig. 10. (A) Grip test and (B) rotarod test. (C) The results between control and treated group didn't show any changes in the strength of the forelimbs period neither motor functions after 6 months of treatment. n = 4 in control and n = 8 in 4-MU group.

therapeutic intervention for PNNs modulation and thus enhancing synaptic plasticity in conditions such as Alzheimer's disease, aging and other disorders of cognition. On the other hand, the detail study of the effects of the systemic inhibition of HA synthesis on synaptic plasticity as well as pharmacological determination of the minimal effective dosage and safety analysis are needed for the future clinically relevant development of 4-MU in modulation of PNNs and their functions. Alternatively, finding non-invasive way to precisely target specific brain area without systemic effects remains a challenge for the future research.

Declaration of interest

Kwok has a patent 'Treatment of Conditions of the Nervous System' (PCT/EP2020/079979) issued.

Acknowledgements

Supported by: Center of Reconstruction Neuroscience – NEURORECON CZ.02.1.01/0.0/0.0/15_003/0000419 and Czech Science Agency 19-10365S. Wings for Life (WFL-UK-008-15) and Medical Research Council UK (Confidence in concept and Project grant MR/S011110/1) to JCFK, GAUK 870218.

CRediT authorship contribution statement

Jana Dubisova: Methodology, Data analysis, Investigation, Writing – original draft. **Jana Svobodova Burianova:** Data analysis, Investigation. **Lucie Svobodova:** Methodology. **Pavol Makovicky:** Investigation. **Noelia Martinez:** Data analysis. **Anda Cimpean:** Data analysis. **James W. Fawcett:** Conceptualization, Methodology, Writing – review & editing, Supervision. **Jessica C.F. Kwok:** Conceptualization, Methodology, Data analysis, Investigation, Writing – review & editing, Supervision. **Sarka Kubinova:** Conceptualization, Methodology, Writing – original draft, Writing – review & editing, Supervision.

Appendix A. Supporting information

Supplementary data associated with this article can be found in the online version at doi:10.1016/j.brainresbull.2022.01.011.

References

Miyata, S., Kitagawa, H., 2017. Formation and remodeling of the brain extracellular matrix in neural plasticity: roles of chondroitin sulfate and hyaluronan. Biochim. Biophys. Acta Gen. Subj. 1861 (10), 2420–2434.
Frischknecht, R., Heine, M., Perrais, D., Seidenbecher, C.I., Choquet, D., Gundelfinger, E. D., 2009. Brain extracellular matrix affects AMPA receptor lateral mobility and short-term synaptic plasticity. Nat. Neurosci. 12 (7), 897–904.
Pyka, M., Wetzel, C., Aguado, A., Geissler, M., Hatt, H., Faissner, A., 2011. Chondroitin sulfate proteoglycans regulate astrocyte-dependent synaptogenesis and modulate synaptic activity in primary embryonic hippocampal neurons. Eur. J. Neurosci. 33 (12), 2187–2202.
Fawcett, J.W., Oohashi, T., Pizzorusso, T., 2019. The roles of perineuronal nets and the perinodal extracellular matrix in neuronal function. Nat. Rev. Neurosci. 20 (8), 451–465.
Sorg, B.A., Berretta, S., Blacktop, J.M., Fawcett, J.W., Kitagawa, H., Kwok, J.C., Miquel, M., 2016. Casting a wide net: role of perineuronal nets in neural plasticity. J. Neurosci. 36 (45), 11459–11468.
Pantazopoulos, H., Berretta, S., 2016. In sickness and in health: perineuronal nets and synaptic plasticity in psychiatric disorders. Neural Plast. 2016, 9847696, 9847696: p.
Bozzelli, P.L., Alaiyed, S., Kim, E., Villapol, S., Conant, K., 2018. Proteolytic remodeling of perineuronal nets: effects on synaptic plasticity and neuronal population dynamics. Neural Plast. 2018, 5735789, 5735789: p.
Duncan, J.A., Foster, R., Kwok, J.C.F., 2019. The potential of memory enhancement through modulation of perineuronal nets. Br. J. Pharmacol. 176 (18), 3611–3621.
Romberg, C., Yang, S., Melani, R., Andrews, M.R., Horner, A.E., Spillantini, M.G., Bussey, T.J., Fawcett, J.W., Pizzorusso, T., Saksida, L.M., 2013. Depletion of perineuronal nets enhances recognition memory and long-term depression in the perirhinal cortex. J. Neurosci. 33 (16), 7057–7065.
Kwok, J.C., Afshari, F., García-Alías, G., Fawcett, J.W., 2008. Proteoglycans in the central nervous system: plasticity, regeneration and their stimulation with chondroitinase ABC. Restor. Neurol. Neurosci. 26 (2–3), 131–145.
Howell, M.D., Gottschall, P.E., 2012. Lectican proteoglycans, their cleaving metalloproteinases, and plasticity in the central nervous system extracellular microenvironment. Neuroscience 217, 6–18.
Yang, S., Hilton, S., Alves, J.N., Saksida, L.M., Bussey, T., Matthews, R.T., Kitagawa, H., Spillantini, M.G., Kwok, J., Fawcett, J.W., 2017. Antibody recognizing 4-sulfated chondroitin sulfate proteoglycans restores memory in tauopathy-induced neurodegeneration. Neurobiol. Aging 59, 197–209.
Carulli, D., Pizzorusso, T., Kwok, J.C., Putignano, E., Poli, A., Forostyak, S., Andrews, M. R., Deepa, S.S., Glant, T.T., Fawcett, J.W., 2010. Animals lacking link protein have attenuated perineuronal nets and persistent plasticity. Brain 133 (Pt 8), 2331–2347.
Su, W., Foster, S.C., Xing, R., Feistel, K., Olsen, R.H., Acevedo, S.F., Raber, J., Sherman, L. S., 2017. CD44 transmembrane receptor and hyaluronan regulate adult hippocampal neural stem cell quiescence and differentiation. J. Biol. Chem. 292 (11), 4434–4445.
Kwok, J.C.F., Carulli, D., Fawcett, J.W., 2010. In vitro modeling of perineuronal nets: hyaluronan synthase and link protein are necessary for their formation and integrity. J. Neurochem 114 (5), 1447–1459.
Kakizaki, I., Kojima, K., Takagaki, K., Endo, M., Kannagi, R., Ito, M., Maruo, Y., Sato, H., Yasuda, T., Mita, S., Kimata, K., Itano, N., 2004. A novel mechanism for the inhibition of hyaluronan biosynthesis by 4-methylumbelliferone. J. Biol. Chem. 279 (32), 33281–33289.
Kultti, A., Pasonen-Seppänen, S., Jauhiainen, M., Rilla, K.J., Kärnä, R., Pyöriä, E., Tammi, R.H., Tammi, M.I., 2009. 4-Methylumbelliferone inhibits hyaluronan synthesis by depletion of cellular UDP-glucuronic acid and downregulation of hyaluronan synthase 2 and 3. Exp. Cell Res. 315 (11), 1914–1923.
Vigetti, D., Rizzi, M., Viola, M., Karousou, E., Genasetti, A., Clerici, M., Bartolini, B., Hascall, V.C., De Luca, G., Passi, A., 2009. The effects of 4-methylumbelliferone on hyaluronan synthesis, MMP2 activity, proliferation, and motility of human aortic smooth muscle cells. Glycobiology 19 (5), 537–546.
Ishizuka, S., Askew, E.B., Ishizuka, N., Knudson, C.B., Knudson, W., 2016. 4-methylumbelliferone diminishes catabolically activated articular chondrocytes and cartilage explants via a mechanism independent of hyaluronan inhibition. J. Biol. Chem. 291 (23), 12087–12104.
Nagy, N., Kuipers, H.F., Frymoyer, A.R., Ishak, H.D., Bollyky, J.B., Wight, T.N., Bollyky, P.L., 2015. 4-methylumbelliferone treatment and hyaluronan inhibition as a therapeutic strategy in inflammation, autoimmunity, and cancer. Front. Immunol. 6, 123.
Kuipers, H.F., Rieck, M., Gurevich, I., Nagy, N., Butte, M.J., Negrin, R.S., Wight, T.N., Steinman, L., Bollyky, P.L., 2016. Hyaluronan synthesis is necessary for autoreactive T-cell trafficking, activation, and Th1 polarization. Proc. Natl. Acad. Sci. USA 113 (5), 1339–1344.
Mueller, A.M., Yoon, B.H., Sadiq, S.A., 2014. Inhibition of hyaluronan synthesis protects against central nervous system (CNS) autoimmunity and increases CXCL12 expression in the inflamed CNS. J. Biol. Chem. 289 (33), 22888–22899.
McKallip, R.J., Ban, H., Uchakina, O.N., 2015. Treatment with the hyaluronic Acid synthesis inhibitor 4-methylumbelliferone suppresses LPS-induced lung inflammation. Inflammation 38 (3), 1250–1259.
McKallip, R.J., Hagele, H.F., Uchakina, O.N., 2013. Treatment with the hyaluronic acid synthesis inhibitor 4-methylumbelliferone suppresses SEB-induced lung inflammation. Toxins 5 (10), 1814–1826.
Yoshioka, Y., Kozawa, E., Urakawa, H., Arai, E., Futamura, N., Zhuo, L., Kimata, K., Ishiguro, N., Nishida, Y., 2013. Suppression of hyaluronan synthesis alleviates inflammatory responses in murine arthritis and in human rheumatoid synovial fibroblasts. Arthritis Rheum. 65 (5), 1160–1170.
Andreichenko, I.N., Tsitrina, A.A., Fokin, A.V., Gabdulkhakova, A.I., Maltsev, D.I., Perelman, G.S., Bulgakova, E.V., Kulikov, A.M., Mikaelyan, A.S., Kotelevtsev, Y.V., 2019. 4-methylumbelliferone prevents liver fibrosis by affecting hyaluronan deposition, FSTL1 expression and cell localization. Int. J. Mol. Sci. 20 (24).
Ennaceur, A., Delacour, J., 1988. A new one-trial test for neurobiological studies of memory in rats. 1: Behavioral data. Behav. Brain Res. 31 (1), 47–59.
Winters, J.M., Feng, X., Wang, Y., Johnson, L.M., Foil, J., 2004. Progress toward universal interface technologies for telerehabilitation. Conf. Proc. IEEE Eng. Med. Biol. Soc. 2004, 4777–4780.
Bartko, S.J., Vendrell, I., Saksida, L.M., Bussey, T.J., 2011. A computer-automated touchscreen paired-associates learning (PAL) task for mice: impairments following administration of scopolamine or dicyclomine and improvements following donepezil. Psychopharmacology 214 (2), 537–548.
Lin, R., Rosahl, T.W., Whiting, P.J., Fawcett, J.W., Kwok, J.C., 2011. 6-Sulphated Chondroitins Have a Positive Influence on Axonal Regeneration. PLoS One 6, 7.
Manley, G., Hawksworth, J., 1966. Diagnosis of Hurler's syndrome in the hospital laboratory and the determination of its genetic type. Arch. Dis. Child 41 (215), 91–96.
Trabucchi, E., Baratti, C., Centemero, A., Zuin, M., Rizzitelli, E., Colombo, R., 1986. Controlled-study of the effects of tiropramide on biliary dyskinesia. Pharmatherapeutica 4 (9), 541–550.
Kuipers, H.F., Nagy, N., Ruppert, S.M., Sunkari, V.G., Marshall, P.L., Gebe, J.A., Ishak, H. D., Keswani, S.G., Bollyky, J., Frymoyer, A.R., Wight, T.N., Steinman, L., Bollyky, P. L., 2016. The pharmacokinetics and dosing of oral 4-methylumbelliferone for inhibition of hyaluronan synthesis in mice. Clin. Exp. Immunol. 185 (3), 372–381.
Tsuchiya, S., Ohashi, Y., Ishizuka, S., Ishiguro, N., O'Rourke, D.P., Knudson, C.B., Knudson, W., 2020. Suppression of murine osteoarthritis by 4-methylumbelliferone. J. Orthop. Res. 38 (5), 1122–1131.
Kwok, J.C.F., R. Foster, J.A. Duncan, Treatment of conditions of the nervous system. PCT/EP2020/079979, 2021. 2021-4-29.
Baxter, M.G., 2010. "I've seen it all before": explaining age-related impairments in object recognition. theoretical comment on Burke et al. (2010). Behav. Neurosci. 124 (5), 706–709.

Yang, S., Cacquevel, M., Saksida, L.M., Bussey, T.J., Schneider, B.L., Aebischer, P., Melani, R., Pizzorusso, T., Fawcett, J.W., Spillantini, M.G., 2015. Perineuronal net digestion with chondroitinase restores memory in mice with tau pathology. Exp. Neurol. 265, 48–58.
Kwok, J.C., Dick, G., Wang, D., Fawcett, J.W., 2011. Extracellular matrix and perineuronal nets in cns repair. Dev. Neurobiol. 71 (11), 1073–1089.
Galtrey, C.M., Kwok, J.C., Carulli, D., Rhodes, K.E., Fawcett, J.W., 2008. Distribution and synthesis of extracellular matrix proteoglycans, hyaluronan, link proteins and tenascin-R in the rat spinal cord. Eur. J. Neurosci. 27 (6), 1373–1390.
Hylin, M.J., Orsi, S.A., Moore, A.N., Dash, P.K., 2013. Disruption of the perineuronal net in the hippocampus or medial prefrontal cortex impairs fear conditioning. Learn Mem. 20 (5), 267–273.
Lewis, D.A., Curley, A.A., Glausier, J.R., Volk, D.W., 2012. Cortical parvalbumin interneurons and cognitive dysfunction in schizophrenia. Trends Neurosci. 35 (1), 57–67.
Wen, T.H., Binder, D.K., Ethell, I.M., Razak, K.A., 2018. The perineuronal 'safety' net? perineuronal net abnormalities in neurological disorders. Front. Mol. Neurosci. 11, 270.
Raber, J., Olsen, R.H., Su, W., Foster, S., Xing, R., Acevedo, S.F., Sherman, L.S., 2014. CD44 is required for spatial memory retention and sensorimotor functions. Behav. Brain Res. 275, 146–149.
Kwok, J.C.F., Carulli, D., Fawcett, J.W., 2010. In vitro modeling of perineuronal nets: hyaluronan synthase and link protein are necessary for their formation and integrity. J. Neurochem. 114 (5), 1447–1459.
Rilla, K., Oikari, S., Jokela, T.A., Hyttinen, J.M., Kärnä, R., Tammi, R.H., Tammi, M.I., 2013. Hyaluronan synthase 1 (HAS1) requires higher cellular UDP-GlcNAc concentration than HAS2 and HAS3. J. Biol. Chem. 288 (8), 5973–5983.
Carulli, D., Rhodes, K.E., Brown, D.J., Bonnert, T.P., Pollack, S.J., Oliver, K., Strata, P., Fawcett, J.W., 2006. Composition of perineuronal nets in the adult rat cerebellum and the cellular origin of their components. J. Comp. Neurol. 494 (4), 559–577.
Arranz, A.M., Perkins, K.L., Irie, F., Lewis, D.P., Hrabe, J., Xiao, F., Itano, N., Kimata, K., Hrabetova, S., Yamaguchi, Y., 2014. Hyaluronan deficiency due to Has3 knock-out causes altered neuronal activity and seizures via reduction in brain extracellular space. J. Neurosci. 34 (18), 6164–6176.
Saito, T., Dai, T., Asano, R., 2013. The hyaluronan synthesis inhibitor 4-methylumbelliferone exhibits antitumor effects against mesenchymal-like canine mammary tumor cells. Oncol. Lett. 5 (3), 1068–1074.
Goncharova, V., Serobyan, N., Iizuka, S., Schraufstatter, I., de Ridder, A., Povaliy, T., Wacker, V., Itano, N., Kimata, K., Orlovskaja, I.A., Yamaguchi, Y., Khaldoyanidi, S., 2012. Hyaluronan expressed by the hematopoietic microenvironment is required for bone marrow hematopoiesis. J. Biol. Chem. 287 (30), 25419–25433.
Nagy, N., Freudenberger, T., Melchior-Becker, A., Röck, K., Ter Braak, M., Jastrow, H., Kinzig, M., Lucke, S., Suvorava, T., Kojda, G., Weber, A.A., Sörgel, F., Levkau, B., Ergün, S., Fischer, J.W., 2010. Inhibition of hyaluronan synthesis accelerates murine atherosclerosis: novel insights into the role of hyaluronan synthesis. Circulation 122 (22), 2313–2322.
Bethesda (MD): National Library of Medicine (US), National Center for Biotechnology Information; 2004–. PubChem Compound Summary for CID 5280567, Hymecromone. PubChem [Internet], 2021.
Lontane, L., et al., 1968. Toxicological and teratological study of 4-methylumbelliferone. Therapie XXIII, 359–371.
Mueller, A.M., Yoon, B.H., Sadiq, S.A., 2014. Inhibition of hyaluronan synthesis protects against central nervous system (CNS) autoimmunity and increases CXCL12 expression in the inflamed CNS. J. Biol. Chem. 289 (33), 22888–22899.
Sunkari, V., et al., 2015. Inhibition of hyaluronan synthesis restores normoglycemia and promotes a regenerative wound phenotype in obese and diabetic mice. Wound Repair Regen. 23 (2) p. A41-A41.

TISSUE ENGINEERING: Part C
Volume 23, Number 6, 2017

DOI: 10.1089/ten.tec.2017.0089

termis
Tissue Engineering
& Regenerative Medicine
International Society

METHODS ARTICLE

Extracellular Matrix Hydrogel Derived from Human Umbilical Cord as a Scaffold for Neural Tissue Repair and Its Comparison with Extracellular Matrix from Porcine Tissues

Zuzana Kočí,[1,2] Karel Výborný,[1,2] Jana Dubišová,[1,2] Irena Vacková, PhD,[1] Aleš Jäger, PhD,[3] Oleg Lunov, PhD,[3] Klára Jiráková, PhD,[1] and Šárka Kubinová, PhD[1]

Extracellular matrix (ECM) hydrogels prepared by tissue decellularization have been reported as natural injectable materials suitable for neural tissue repair. In this study, we prepared ECM hydrogel derived from human umbilical cord (UC) and evaluated its composition and mechanical and biological properties in comparison with the previously described ECM hydrogels derived from porcine urinary bladder (UB), brain, and spinal cord. The ECM hydrogels did not differ from each other in the concentration of collagen, while the highest content of glycosaminoglycans as well as the shortest gelation time was found for UC-ECM. The elastic modulus was then found to be the highest for UB-ECM. In spite of a different origin, topography, and composition, all ECM hydrogels similarly promoted the migration of human mesenchymal stem cells (MSCs) and differentiation of neural stem cells, as well as axonal outgrowth *in vitro*. However, only UC-ECM significantly improved proliferation of tissue-specific UC-derived MSCs when compared with the other ECMs. Injection of UC-ECM hydrogels into a photothrombotic cortical ischemic lesion in rats proved its *in vivo* gelation and infiltration with host macrophages. In summary, this study proposes UC-ECM hydrogel as an easily accessible biomaterial of human origin, which has the potential for neural as well as other soft tissue reconstruction.

Keywords: extracellular matrix, hydrogel, umbilical cord, mesenchymal stromal cells, neural tissue, regeneration

Introduction

The limited repair capacity of the central nervous system (CNS) is a considerable medical challenge as there is currently no available treatment that would enable the recovery of damaged connections. Promising alternatives for the reconstruction of neural tissue structures are offered by various biomaterials developed to activate endogenous restorative mechanisms and/or to provide structural and biochemical support for engraftment of transplanted cells.[1–3]

In contrast to artificially designed tissue-engineered materials that fail to mimic the complex structure and chemistry of the cell microenvironment seen *in vivo*, biologic scaffolds comprising native extracellular matrix (ECM) represent structures very similar to those of the uninjured host tissue with many advantages, such as complex natural composition, three-dimensional structure, retention of growth factors, and bioactive properties, including stimulation of angiogenesis and migration of endogenous progenitor cells or modulation of immune reaction.[4] These unique features of ECM scaffolds ensure functional remodeling of the lesioned area, which is in contrast to scar tissue formation that usually takes place during standard healing.[5]

Biological ECM scaffolds have been used for the reconstruction of numerous tissues, including myocardium,[6] skeletal muscles,[7] musculotendinous tissues,[8,9] lung,[10] urinary tract,[11,12] esophagus,[13] peripheral nerve,[14] or dura mater,[15] and have already been utilized for the treatment of many patients with tolerable tissue responses and positive clinical outcomes.[16]

Both allogeneic and xenogeneic biological ECM materials are currently being transplanted for tissue and organ

[1]Institute of Experimental Medicine, Academy of Sciences of the Czech Republic, Prague, Czech Republic.
[2]Second Medical Faculty, Charles University, Prague, Czech Republic.
[3]Institute of Physics, Academy of Sciences of the Czech Republic, Prague, Czech Republic.

replacement. As xenografts, ECMs from nonprimate mammals (typically pigs) are commonly used, which might be associated with adverse host tissue inflammatory reactions due to the human immune response against mammalian ECM by anti-Gal and anti-nonGal antibodies.[17] Despite the fact that the role of α gal-specific antibodies in xenogeneic ECM implantation appears to be minimal,[18,19] human-derived biomaterials could be more desirable as they avoid concerns related to potential immune responses as well as xenogeneic disease transfer.

Besides xenogeneic ECM, acellular allografts of human origin are being commonly prepared from cadavers and used, for example, as bone, valves, cornea, or skin grafts.[20] Remarkably, the age of the donor tissue is an important parameter that causes significant differences between ECM properties harvested from the same source. It has been shown that with age, there is an increasing ECM cross-linking due to nonenzymatic protein glycation,[21] adipose tissue deposition, and fibrosis, while biologic materials derived from younger animals are associated with a more constructive, site-appropriate tissue remodeling response than scaffolds derived from older animals.[22,23] On the other hand, cadaveric tissues might differ in age of the human donors and are supposed to be considerably older than the porcine sources. For instance, comparison of human versus porcine tissue sources for an injectable myocardial matrix hydrogel revealed that despite the similarity of these matrices, there is an increased difficulty in the processing of human tissue and significant patient-to patient variability.[24]

In contrast to adult tissue, the ECM from fetal or neonatal tissue comprises more immature collagen with few crosslinks, which promotes more effective tissue remodeling.[25–27] It is therefore conceivable that ECM derived from fetal or neonatal tissue would induce more efficient and constructive tissue remodeling than ECM derived from adult or old tissues.

In this context, umbilical cord (UC) represents the suitable neonatal tissue source, which is easily accessible in sufficient amounts without any ethical constraints. Of note, UC is commonly used in regenerative medicine for isolation of mesenchymal stem cells (MSCs) and endothelial cells and it can also serve as a source for hyaluronic acid isolation. Being an extraembryonic tissue, it eliminates age-related impediments such as ECM remodeling, fibrosis, oxidative stress, and other negative changes.[26]

As a scaffold for neural tissue repair, injectable *in situ* gelling hydrogels have been considered more appropriate than fibrous ECM as these materials can easily conform to lesion irregularity with minimal tissue damage during delivery. To form injectable hydrogels, ECM from various decellularized tissues can be enzymatically solubilized to a liquid form, which self-assembles into a hydrogel under physiological pH and temperature.[27–29] Previously described injectable ECM hydrogels prepared by decellularization of porcine brain (B-ECM), spinal cord (SC-ECM), and porcine urinary bladder (UB-ECM) revealed *in vitro* neurotrophic properties.[30,31] Moreover, ECM hydrogels from UB-ECM and SC-ECM proved to be beneficial for providing a supportive environment *in vivo* after injection into an experimentally induced cavity in stroke[32] or spinal cord injury.[33]

In this study, we propose human UC as a suitable source of ECM and introduce an optimized decellularization protocol to prepare UC-derived ECM hydrogel (UC-ECM). UC-ECM hydrogel is characterized in terms of its structure, composition, mechanical properties, and neurotrophic potential *in vitro* and compared with previously described UB-ECM, SC-ECM, and B-ECM. In addition, UC-ECM hydrogel was injected into cortical photothrombotic lesions in rats to prove its *in situ* gelation and *in vivo* biocompatibility.

Materials and Methods

Tissue decellularization and preparation of ECM hydrogels

Porcine UBs, spinal cords, and brains were obtained from an abattoir (Český Brod, Czech Republic); the age of the animals was 6 months. ECM hydrogels were prepared according to previously described protocols.[30,34] Human UCs were obtained from healthy full-term neonates after spontaneous delivery with the informed consent of donors, using the guidelines approved by the Institutional Committee at University Hospital (Pilsen, Czech Republic). About 10–15 cm of umbilical tissues were frozen (>16 h at −20°C), aseptically transported into the laboratory, and subsequently thawed and transversely cut into pieces (<0.5 cm length). Tissue pieces were agitated in 0.1 M phosphate-buffered saline (PBS; IKEM, Czech Republic) bath (48 h at 120 rpm, 4°C). The PBS bath was exchanged three to five times before the tissue pieces were soaked in 0.02% trypsin/0.05% EDTA (120 min at 120 rpm, 37°C) and afterward in 0.1% peracetic acid in 4.0% ethanol bath (120 min at 300 rpm; Penta, Czech Republic), and in a series of PBS and deionized water (dH_2O) soaks. Finally, tissue pieces were lyophilized for 24 h (FreeZone® 2.5; Labconco Corporation) and powdered (Mini-Mill Cutting Mills; Thomas Scientific). For the *in vivo* application, the powdered ECM was sterilized in ethylene oxide at 37°C overnight.

To prepare the hydrogel, powdered ECM samples were solubilized with 1.0 mg/mL pepsin in 0.01 N HCl (Sigma) at a concentration of 10 mg ECM/mL and stirred at room temperature for 48 h to form a pregel solution (pH ~2). The pepsin-HCl ECM solution was neutralized to pH 7.4 with 0.1 N NaOH, isotonically balanced with 10×PBS, and diluted with 1×PBS to the final concentration of 8 mg/mL, which allows *in vivo* gelation.[32,33] To form the hydrogel, the neutralized pregel was placed at 37°C for ~45 min.

ECM hydrogel characterization

Nanoscale topography. The surface topography of UC-ECM, UB-ECM, SC-ECM, and B-ECM hydrogels was analyzed by scanning electron microscopy (SEM) mode, applying previously published methodology.[35] Briefly, a gel was placed on the glass slide, fixed in cold 2.5% glutaraldehyde (Electron Microscopy Sciences) for 24 h, and washed in PBS. Hydrogels were then dehydrated in a graded series of alcohol, followed by subsequent chemical drying with hexamethyldisilazane (Sigma). The dried samples were cut to expose their inner structure and used for SEM studies. Micrographs were taken using an FEI Quanta 3D FEG scanning electron microscope at an acceleration voltage of 2 kV to prevent charging of unconductive samples. ImageJ (Rasband, W.S.; U.S. National Institutes of Health, Bethesda, MD) software was used for image processing and micrograph quantification. Using special plug-in for ImageJ

(FibrilTool),[36] image analysis was performed in terms of anisotropy score calculation.

Efficiency of tissue decellularization. The absence of cell nuclei in decellularized tissues was proved by hematoxylin and eosin (H&E) staining. The nuclei were stained using 4′,6-diamidino-2-phenylindole fluorescent dye (DAPI, 1:1000; Invitrogen). Double-strain DNA (dsDNA) was isolated from native and decellularized tissue according to the manufacturer's instructions (DNeasy® Blood & Tissue Kit; Qiagen) and quantified using a spectrophotometer (NanoPhotometer™ P-Class). DNA content was normalized to the initial dry weight of the samples. For each native and decellularized tissue, the assay was repeated three times. Base pair length of residual DNA was determined on 2% agarose gel (Sigma) containing 0.5% SYBR Safe DNA Gel Stain (Thermo Fisher Scientific) and visualized with ultraviolet transillumination using a reference 50-base pair (bp) ladder (Cleaver Scientific).

Immunohistochemical analysis. To visualize the content of acid mucopolysaccharides, collagen, laminin, and fibronectin, the decellularized ECM was fixed in 4% paraformaldehyde in PBS and embedded in paraffin blocks. Sections of 5 μm thickness were mounted onto slides, deparaffinized, and stained with Alcian blue (pH 2.5; all acid mucosubstances, blue or greenish blue) together with Weigert's iron hematoxylin (nuclei, black) and Van Gieson's staining (acid fuchsin in saturated aqueous picric acid; collagen—red). In addition, immunohistochemistry using primary antibodies against collagen I (COL-I) (mouse monoclonal IgG1, clone COL-I, 1:1000), laminin (rabbit polyclonal IgG, 1:200), and fibronectin (rabbit polyclonal IgG, 1:200, all from Abcam) was performed. Goat anti-mouse IgG conjugated with Alexa Fluor 488 (1:400) for collagen, goat anti-rabbit IgG conjugated with Alexa Fluor 488 (1:400) for fibronectin, and goat anti-rabbit IgG conjugated with Alexa Fluor 594 (1:400) for laminin (all from Life Technologies) served as secondary antibodies. Images were taken using the LEICA CTR 6500 microscope (Leica Microsystems).

Collagen and glycosaminoglycan quantification. The collagen content in ECM hydrogels was assessed using colorimetric assay Sircol™ Insoluble Collagen Assay Kit (Biocolor Ltd.). Sulfated glycosaminoglycan (sGAG) concentrations in ECM hydrogels were determined using the Blyscan Sulfated Glycosaminoglycan Assay Kit (Biocolor). Absorbance of the samples was recorded at 555 nm for collagen and at 656 nm for sGAG content using a Tecan Spectra plate reader (Tecan). All assays were performed according to the manufacturer's recommended protocol from three independent samples measured in triplicates. The collagen and sGAG content was normalized to the initial dry weight of the samples.

Rheometry. Dynamic oscillatory shear tests were used to investigate the viscoelastic properties of ECM hydrogels. ECM hydrogels were subjected to a sinusoidal deformation in a 40-mm parallel plate rheometer (AR-G2; TA Instruments) at 1 Pa stress and 10°C to determine their mechanical response (displacement or strain) as a function of time. A dynamic time sweep was run with the parameters of 5% strain, 1 rad/s (0.159 Hz), and increasing the temperature from 10°C to 37°C to induce gelation as indicated by a sharp increase and plateau phase of the storage modulus (G'). The assay was repeated three times with three independent samples in triplicates.

Turbidity gelation measurement. The turbidimetric gelation kinetics were determined on a spectrophotometer (Infinite® 200 Pro; Tecan), which was preheated to 37°C. ECM hydrogel samples (8 mg/mL) were kept on ice at 4°C until 100 μL was pipetted into each well of a 96-well plate and inserted into a spectrophotometer. Absorbance was measured at 405 nm every 10 min for 100 min. Normalized absorbance time to reach 50% and 95% maximal absorbance were determined as $t_{1/2}$ and t_{95}.[37] The lag time (t_{lag}) was defined as the point where a line representing the slope at log $t_{1/2}$ intersects the turbidimetry baseline with 0% absorbance. The gelation rate (S) was defined as the slope of the linear region of the gelation curve. The measurements were repeated three times with three independent samples in triplicates.

In vitro *characterization on cell culture*

Mesenchymal stem cells. Human bone marrow (hBM) MSCs were obtained from Bioinova, Ltd. (Czech Republic), and cultured as described previously[38] in complete medium comprising MEM Alpha (Lonza) media, 5% platelet lysate (Bioinova, Ltd.), and gentamicin (10 μg/mL; gentamicin Lek®; Lek Pharmaceuticals).

Human adipose tissue-derived MSCs (hASCs) were obtained from healthy volunteers who underwent liposuction procedures for esthetic reasons and signed an informed consent. The lipoaspirate was repeatedly washed in PBS and enzymatically digested by collagenase (0.3 PzU/mL, Collagenase NB 6 GMP; Serva Electrophoresis GmbH) at 37°C, centrifuged at 1000 rpm/min for 5 min, and the cells were cultured under standard conditions.

Human Wharton's jelly (hWJ) MSCs were collected from fresh human UCs as described in the Tissue Decellularization and Preparation of ECM Hydrogels section. About 10–15 cm of UC was aseptically transported into sterile PBS with antibiotic–antimycotic solution (Sigma) at 4°C. After removal of blood vessels, the remaining tissue was chopped into small pieces (1–2 mm^3) and transferred to 10-cm Nunc culture dishes (Schoeller, Czech Republic) containing the complete medium. On day 10, the explants were removed from the culture dishes and remaining adherent cells were cultured for 3 weeks or until 90% confluence.

All hMSCs were cultivated at 37°C and 5% CO_2 in a humidified atmosphere; the medium was changed twice a week. Cells in the third passage were analyzed for surface markers and used for the ECM hydrogel evaluation.

Using a flow cytometer (FACSAria™; Becton Dickinson), all three types of MSCs were proved, for characteristic surface markers, positive for CD90, CD73, CD29, CD10, CD44 (Exbio, Czech Republic), CD105 (BioLegend), and HLA ABC (BD Pharmingen) and negative for CD14, CD34, CD45 (Exbio), CD133 (Miltenyi Biotec), VEGFR2 (BioLegend), CD31, and HLA-DR (Pharmingen). Data analysis was performed using BD FASCDiva software.

Human neural stem cells. A conditionally immortalized human fetal neural stem cell (NSC) line SPC-01 was generated from 8-week-old human fetal spinal cord as described previously.[35] Cells were cultured in tissue culture flasks, freshly coated with laminin (10 μg/mL) in DMEM/F12 (Gibco, Life Technologies), and supplemented with human serum albumin (0.03%; Baxter Healthcare Ltd.), human apotransferrin (100 μg/mL), putrescine DiHCl (16.2 μg/mL), human recombinant insulin (5 μg/mL), progesterone (60 ng/mL), L-glutamine (2 mM), sodium selenite (40 ng/mL), 4-OHT (100 nM) (all from Sigma), human EGF (20 ng/mL), human bFGF (10 ng/mL) (PeproTech), and primocin 100 μg/mL (InvivoGen) at 37°C and 5% CO_2 in a humidified atmosphere.

Cell growth and proliferation. To determine *in vitro* MSC proliferation, ECM hydrogels were placed into a 96-well plate (90 μL/well) and seeded with cells (5000 cells/cm^2 in 100 μL media). Cells seeded on wells without hydrogel (tissue culture plastic) served as a control. Cell proliferation was measured using WST-1 assay (Roche) after 1, 3, 7, and 14 days of the culture. Ten microliters of WST-1 reagent was added to each well containing 100 μL culture media, and the plates were incubated for 2 h at 37°C. The absorbance was measured using a Tecan Spectra plate reader at 450 nm. Each type of hydrogel was seeded in triplicate. Six independent experiments of three hydrogel batches were performed for each hydrogel type.

The morphology of MSCs grown on hydrogels was examined by immunofluorescence staining for actin filaments. After fixation in 4% paraformaldehyde in PBS for 15 min, the cells were washed with PBS and stained with Alexa Fluor 568 phalloidin (1:400; Molecular Probes); the nuclei were visualized using DAPI fluorescent dye (1:1000; Invitrogen).

NSC growth and differentiation were analyzed after their seeding (100,000/cm^2) on laminin-coated coverslips or ECM hydrogel disks formed inside a cylindrical mold with a diameter of 0.8 cm (Scaffdex). After 7 and 14 days of culture, the cells were fixed in 4% paraformaldehyde in PBS for 15 min, washed with PBS, and stained using Alexa Fluor 568 phalloidin. Next, immunohistochemical staining against light neurofilaments (70 kDa) using mouse monoclonal IgG1 (NF70, 1:400; clone DA2, Merck Millipore) and mouse monoclonal IgG against microtubule-associated protein 2 (MAP2, 1:1000; clone AP20; Millipore) was performed. The nuclei were visualized using DAPI fluorescent dye (1:1000, Invitrogen). Images were taken using the confocal microscope Zeiss LSM 5 DUO (Carl Zeiss, MicroImaging GmbH).

Cell migration. To assess the chemotactic capacity of ECM hydrogels for hMSCs, xCELLigence® RTCA DP Instrument was used to perform Cell Invasion and Migration Assay (Acea Biosciences, Inc.). ECM hydrogels (6% v/v solutions in media without supplements) were placed into a lower chamber of CIM-Plate 16, and hBM-MSCs, hASCs, and hWJ-MSCs (10^5 cells in 100 μL of media without supplements) were then pipetted into an upper chamber. The impedance signal was reduced when cells adhered to the microporous membrane to migrate toward ECM hydrogels. As a positive control, chemokine stromal cell-derived factor 1 (SDF-1, 20 ng/mL; Sigma) was used; culture medium without supplements served as a negative control. Recorded impedance signal was then used to assess the rate of cell migration. The assay was repeated five times.

Dorsal root ganglia explant culture. Dorsal root ganglia (DRGs) were extracted from four 3–5-day-old Wistar rats (Velaz, Czech Republic). Briefly, the spinal cords were dissected and DRGs from low thoracic and lumbar parts were isolated, placed in cold Hank's balanced salt solution without Ca^{2+}/Mg^{2+} solution (Invitrogen), and cleaned of peripheral nerve processes. DRG explants were then placed on ECM hydrogels or Matrigel (Matrigel® Growth Factor Reduced Basement Membrane Matrix, Phenol Red-Free; Corning) in 24-well plates, and cultured in neurobasal medium (Invitrogen) supplemented with 2% B27 (Life Technologies), 2 mM L-glutamine (Invitrogen), 0.5% NGF (50 ng/mL; PeproTech), uridine (17.5 μg/mL; Sigma), and primocin (2 μL/mL; PeproTech) in a humidified atmosphere at 37°C and 5% CO_2. The medium was changed every 3 days. After 7 days of culture, DRGs were fixed with 4% paraformaldehyde in PBS for 10 min and stained for anti-NF160 antibody (clone NN18, 1:200; Sigma), Alexa Fluor 488 secondary antibody (1:200; Invitrogen), and cell nuclei (DAPI, 1:1000; Invitrogen). Fluorescent images were taken using the Leica fluorescence microscope (Leica DMI 6000B) and TissueGnostic software (TissueGnostics GmbH). The neurite extension area and the longest neurite length were determined using a special plug-in for ImageJ (NeuriteJ).[39] The assay was repeated three times for each hydrogel.

Injection of UC-ECM hydrogels into a rat model of cortical photothrombotic lesion

To test biocompatibility of UC-ECM hydrogel *in vivo*, a focal brain photochemical lesion was created in the motor cortex in rats. Eight male Wistar rats (330 ± 30 g) were maintained at 22°C on a 12-h light/12-h dark schedule and given water and food *ad libitum*. To cause the lesion, the animal was placed into the stereotactic apparatus under isoflurane (3%) anesthesia, the scalp incision was created in the midline, and the pericranial tissue was dissected to expose the bregma. Focal cerebral ischemia was performed according to[40] as follows: Bengal Rose (Sigma) was injected through the right femoral vein (0.08 g/mL saline; 1 μL/g of the animal weight), and the skull was illuminated above the primary motor cortex (2 mm rostral and 2 mm dextrolateral to the bregma) with a fiber-optic bundle of a cold light source (KL 1500 LCD; Zeiss) for 10 min. The skin overlying the cranium was then sutured.

Seven days after the focal cerebral ischemia, a small opening in the lesion site was drilled into the scull of the animal and 10 μL of UC-ECM ($n = 4$) or saline ($n = 4$) was injected into the lesion (in a depth of 2 mm) using a Hamilton syringe (Hamilton Company, Bonaduz, Switzerland) and stereotactic apparatus.

Animals were sacrificed 24 h after the implantation with an overdose of anesthesia and perfused with 4% paraformaldehyde in 0.1 M PBS intracardially. The brains were removed, fixed in 4% paraformaldehyde for 10 days, and cut in frozen mode (local temperature −24°C). Coronal slides, 40 μm thick, were stained for cell nuclei with DAPI (1:1000; Life Technologies), mouse monoclonal IgG1 to CD68 (ED1, 1:150; Abcam), goat polyclonal IgG to CD206 (c-20; 1:250; Santa Cruz), or mouse monoclonal IgG1 to COL-I (1:1000, COL-I; Abcam) diluted in 0.1 M PBS containing goat (or donkey–depending on the host organism of secondary antibodies) serum (1:10 both; Sigma) and Triton X-100 (0.1%) overnight in 4°C. Staining solution lacking Triton X-100 was used only

in the case of extracellular anticollagen staining. As secondary antibodies, goat anti-mouse IgG conjugated with Alexa Fluor 594 (1:400) for COL-I, donkey anti-mouse IgG conjugated with Alexa Fluor 488 (1:400) for CD68, and donkey anti-goat IgG conjugated with Alexa Fluor 594 (1:400) for CD206 (all from Life Technologies) were used.

Fluorescent images were taken using confocal microscope Zeiss LSM 5 DUO. The relative number of macrophages in the hydrogel area was determined from three randomly selected sections using a 20× objective and ImageJ software.

All experiments on animals were performed in accordance with the European Communities Council Directive of 24th November 1986 (86/609/EEC) regarding the use of animals in research and were approved by the Ethics Committee of the Institute of Experimental Medicine Academy of Sciences, Czech Republic, Prague.

Statistical analysis

Data are presented as mean ± standard error of mean. The statistical significance was analyzed using one-way ANOVA with Tukey's multiple comparison *post hoc* analysis (GraphPad Prism) with a level of $p < 0.05$ considered statistically significant.

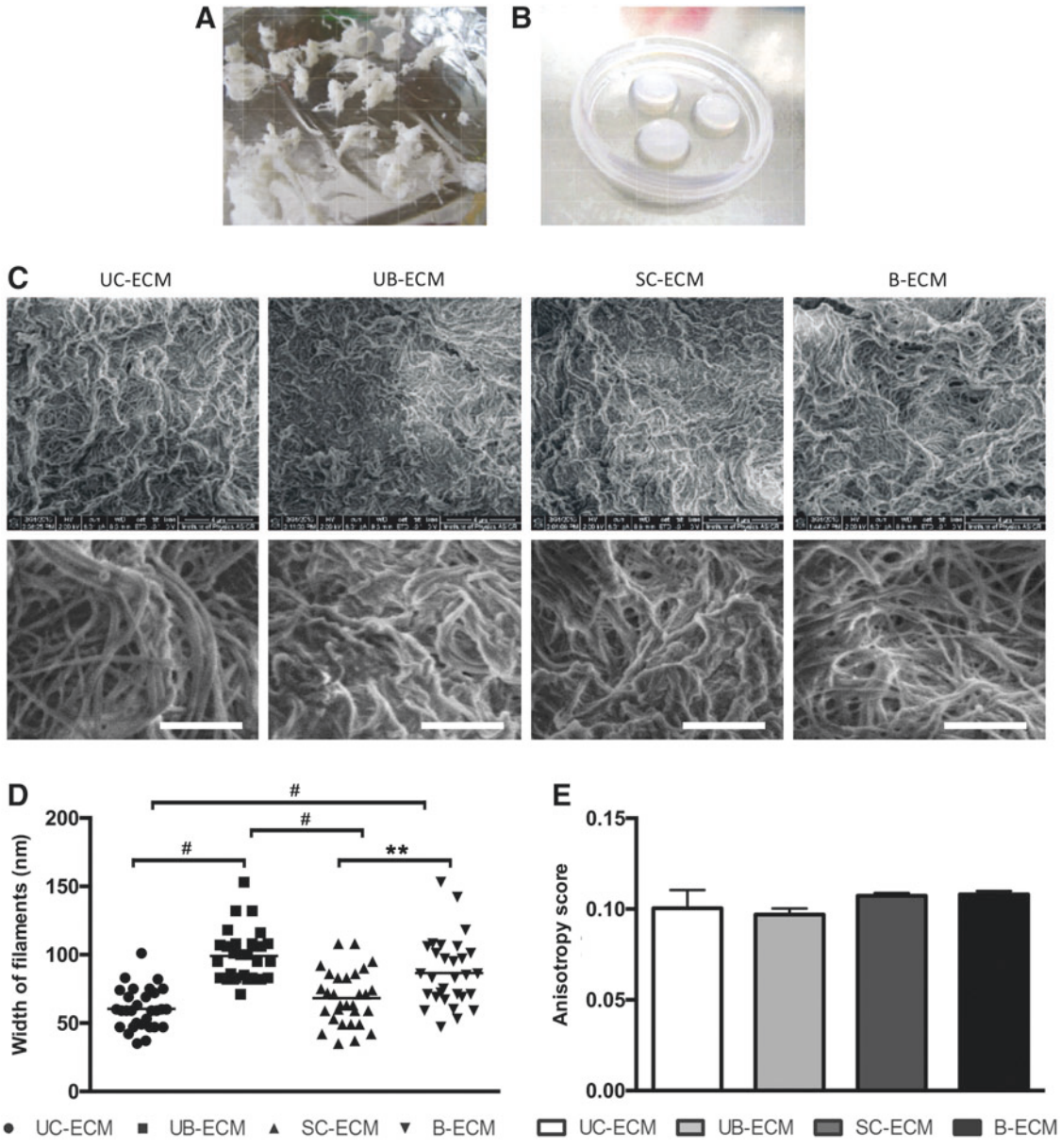

FIG. 1. **(A)** UC-ECM after the decellularization process. **(B)** UC-ECM in a form of hydrogel. **(C)** Representative scanning electron micrograph of UC-ECM, UB-ECM, SC-ECM, and B-ECM. Scale bars represent 1 μm. **(D)** Fiber diameter distribution and **(E)** anisotropy score in UC-ECM, UB-ECM, SC-ECM, and B-ECM. UC-ECM and SC-ECM have a smaller fiber width when compared with UB-ECM and B-ECM. No difference in anisotropy score was found between the ECM hydrogels. Data are shown as mean ± standard error of mean, $n = 30$. One-way ANOVA with Newman–Keuls multiple comparison test was used, $^{**}p < 0.01$, $^{\#}p < 0.001$. B-ECM, brain extracellular matrix; SC-ECM, spinal cord extracellular matrix; UB-ECM, urinary bladder extracellular matrix; UC-ECM, umbilical cord extracellular matrix.

Results

Structure of ECM hydrogels

B-ECM, SC-ECM, and UB-ECM hydrogels were prepared by decellularization protocols as described previously.[30,34] Due to a high amount of hyaluronic acid, which causes massive tissue swelling in water, the decellularization procedure of UC-ECM required more washing steps in dH_2O and PBS to thoroughly remove the cells from the ECM. Importantly, we found that agitation of the tissue in trypsin/EDTA was a necessary step to achieve gelation of the resultant ECM hydrogel (Fig. 1A, B).

The fiber network topology of different ECM hydrogels was examined on SEM images (Fig. 1C). Microscopic comparison of these gels shows that fiber width of UC-ECM (60.47 ± 2.73 nm) and SC-ECM (68.23 ± 43.61 nm) was significantly smaller in comparison with UB-ECM (99.00 ± 3.37 nm) and B-ECM (86.57 ± 4.53 nm, Fig. 1D). To extract quantitative data on fibril orientation, circular statistics were used, which are adapted to directional data, to analyze the properties of the tangent direction over the region of interest. The circular variance of the tangent direction defines the score, determining whether the fibrils are well ordered (fibril array anisotropy, Fig. 1E). With regard to the anisotropy score, the following conventions were used: 0 for no order (purely isotropic arrays) and 1 for perfectly ordered, that is, parallel fibrils (purely anisotropic arrays).[36] Indeed, there was no difference with regard to the anisotropy score between all types of ECMs (Fig. 1E).

Composition of ECM hydrogels

Similarly to porcine ECMs, UC-ECM was successfully decellularized with minimal cellular content within the scaffold (Fig. 2). H&E and DAPI staining confirmed the absence of residual cell nuclei (Fig. 2A). Quantification of dsDNA showed that in all ECM samples, the residual dsDNA was less than 50 ng per mg dry ECM (Fig. 2B, C). Previous studies[4,32,41] show that DNA contained in ECM should not exceed 50 ng/mg of the tissue in order not to elicit an immune reaction on the recipient's site. Our protocol of UC decellularization ensured efficient cell removal, and resulting UC-ECM contained <50 ng or no residual dsDNA, and therefore met the basic requirement for clinical application.

An important parameter, which shows efficacy of ECM harvesting, is the ECM yield, expressed as the percentage of dry weight of ECM to wet weight of the initial source tissue (Table 1). The highest ECM yield was found for UB-ECM $8.06\% \pm 4.66\%$ ($n = 6$), followed by UC-ECM $0.96\% \pm 0.51\%$ ($n = 6$). In contrast, the decellularization of CNS tissues, which requires more complex decellularization procedures due to the high amount of myelin, resulted in a very low ECM

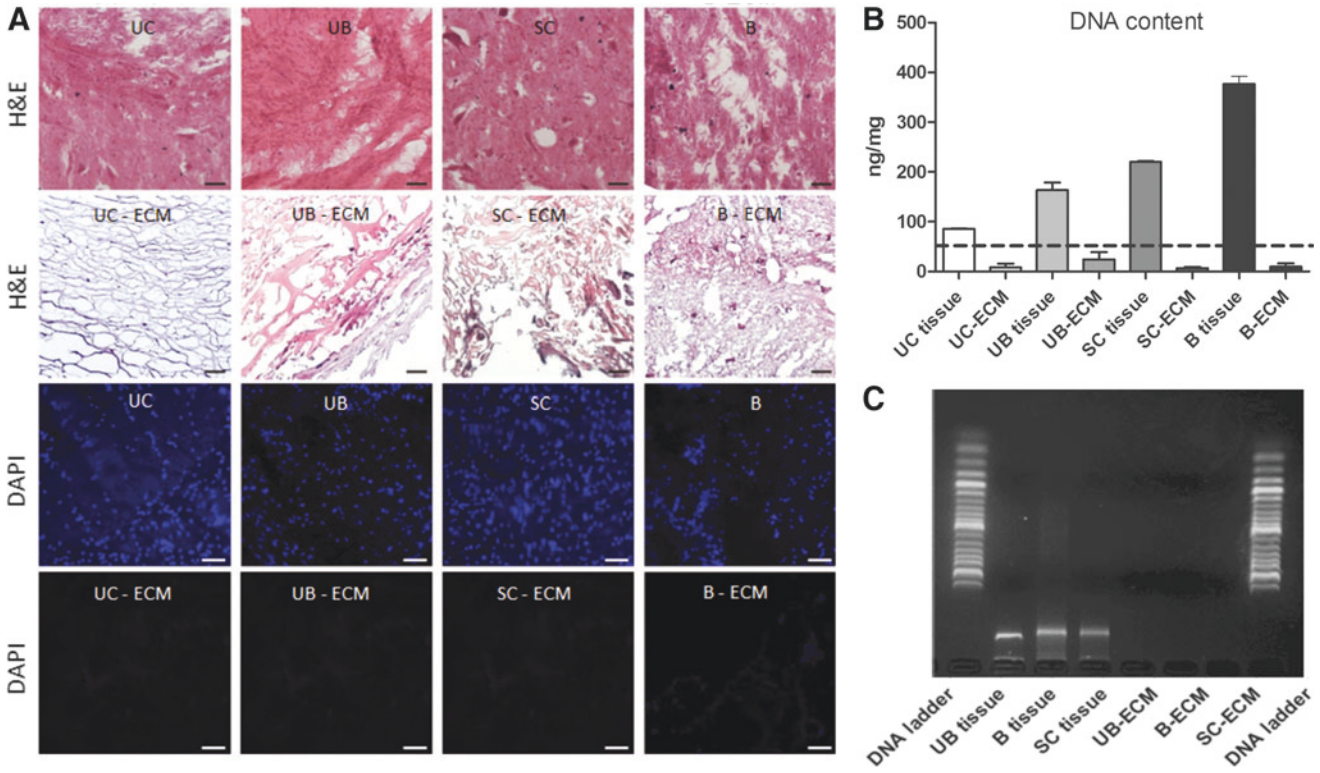

FIG. 2. **(A)** *First row*: H&E staining of (from *left* to *right*) UC, UB, spinal cord (SC), and brain (B) tissue sections before decellularization. *Second row*: H&E staining of UC-ECM, UB-ECM, SC-ECM, and B-ECM after decellularization. *Third row*: DAPI staining for DNA of (from *left* to *right*) UC, UB, SC, and B sections of tissue before decellularization. *Fourth row*: DAPI staining for residual DNA content in UC-ECM, UB-ECM, SC-ECM, and B-ECM. Scale bars represent 50 µm. **(B)** dsDNA quantification. The *dotted line* shows the maximum allowed amount of dsDNA (50 ng/mg) per mg of dry weight. Data are shown as mean ± standard error of mean, $n = 3$. **(C)** DNA base pair (bp) quantification using electrophoresis. On the *left* and the *right* side of the gel is a DNA ladder depicting 50–1500 bp. DAPI, 4′,6-diamidino-2-phenylindole; dsDNA, double-strain DNA; H&E, hematoxylin and eosin.

Table 1. Extracellular Matrix Yield and the Time Required to Reach Lag Phase (T_{LAG}), Half of the Final Turbidity ($T_{1/2}$), 95% of the Final Turbidity (T_{95}), and Gelation Rate (S) of Extracellular Matrix Hydrogels Derived from Human Umbilical Cord, Porcine Urinary Bladder, Porcine Spinal Cord, and Porcine Brain

	Physical properties of ECM			
	UC-ECM	*UB-ECM*	*SC-ECM*	*B-ECM*
Number of batches	6	6	6	6
ECM yield (%)	0.96 ± 0.51	8.06 ± 4.66	0.25 ± 0.14	0.12 ± 0.07
t_{lag} (min)	0.20 ± 0.57	30.78 ± 0.98	19.77 ± 0.98	22.88 ± 1.98
$t_{1/2}$ (min)	12.00 ± 0.75	43.70 ± 0.48	28.19 ± 1.92	32.31 ± 1.26
t_{95} (min)	40.06 ± 5.15	79.00 ± 5.92	55.30 ± 6.77	60.00 ± 3.64
S (min^{-1})	0.10 ± 0.01	0.09 ± 0.01	0.13 ± 0.02	0.10 ± 0.01

ECM yield is expressed as a percentage of the dry weight of ECM to the wet weight of the initial tissue.
ECM, extracellular matrix.

yield; 0.25% ± 0.14% for SC-ECM ($n = 6$) and 0.12% ± 0.07% for B-ECM ($n = 6$), respectively.

Alcian blue was used to stain acid polysaccharides such as GAGs (Fig. 3A). Immunohistochemical staining showed that ECM scaffolds comprise collagen (Fig. 3B), laminin (Fig. 3C), and fibronectin (Fig. 3D).

Collagen concentration did not significantly differ among all the ECM types. The highest amount of collagen was found for UC-ECM (542.6 ± 1.78 μg/mg of dry ECM weight), then for UB-ECM (476.1 ± 45.38 μg/mg), B-ECM (408.1 ± 141.0 μg/mg), and SC-ECM (384.7 ± 147.6 μg/mg) (Fig. 3E).

It has been shown that the concentration of hyaluronic acid within ECM is high in fetal and newborn tissues, including UCs.[42] Indeed, the significantly highest amount of sGAG was found in UC-ECM (6.59 ± 1.24 μg/mg) when compared with UB-ECM (3.46 ± 0.99 μg/mg), SC-ECM (1.84 ± 1.26 μg/mg), and B-ECM (1.47 ± 0.79 μg/mg of dry ECM weight) (Fig. 3F).

Rheological and turbidimetric measurements

In rheological experiments, we determined the flow and mechanical properties of ECM hydrogels. Increasing the strain, G' of ECM hydrogels, started a decline of 10% amplitude when they became more viscose, which was observed for all ECM hydrogels, irrespective of their origin (Fig. 4A). The storage modulus of the matrix was found to be the highest for UB-ECM, while the softest material was B-ECM.

Turbidimetric gelation kinetic curves showed a sigmoidal shape for UC-ECM, whereas other ECMs had an exponential

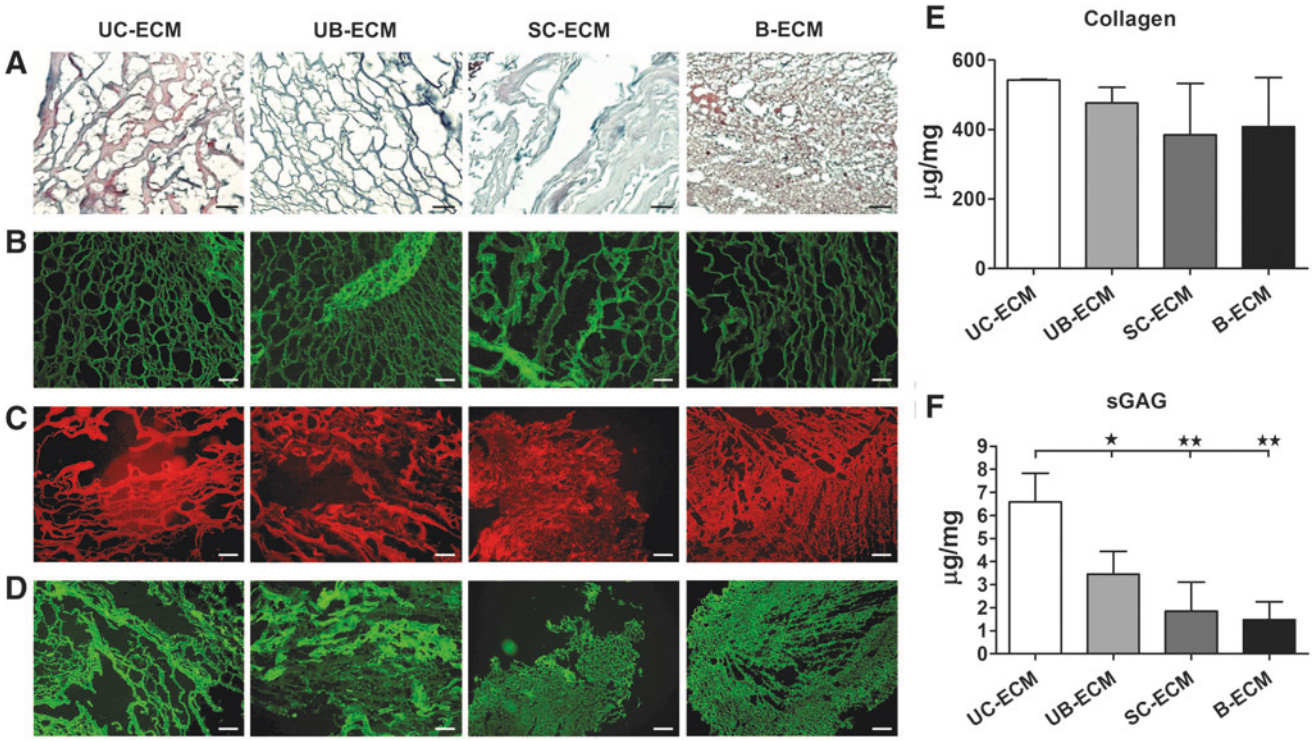

FIG. 3. **(A)** Alcian blue staining for acid mucopolysaccharides in human UC-ECM, porcine UB-ECM, SC-ECM, and B-ECM. **(B)** Immunohistochemical localization of collagen, **(C)** laminin, and **(D)** fibronectin. Scale bars represent 100 μm. **(E)** Collagen and **(F)** sGAG content per mg of dry weight of individual ECM using colorimetric assays. Data are shown as mean ± standard error of mean. $*p < 0.05$, $**p < 0.01$, $n = 3$. sGAG, sulfated glycosaminoglycan.

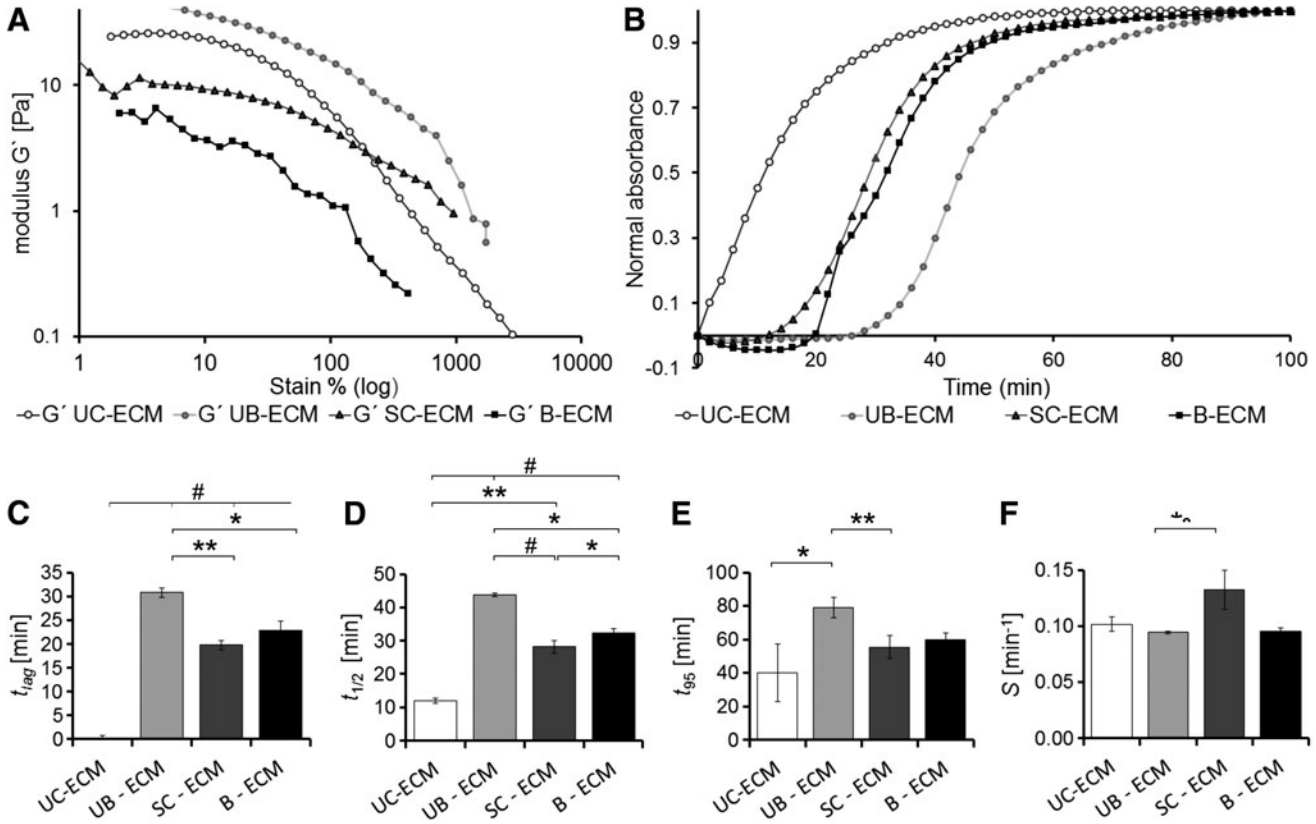

FIG. 4. **(A)** Dynamic oscillatory shear test for viscoelastic property analysis of human UC-ECM, porcine UB-ECM, SC-ECM, and B-ECM. Strain is depicted on the x axis and storage modulus (G') on the y axis. **(B)** Representative curve for turbidimetric gelation kinetics of UC-ECM, UB-ECM, SC-ECM, and B-ECM. **(C)** Lag time (t_{lag}) of ECM hydrogels determined as an intercept point of the slope at log $t_{1/2}$ and turbidimetry baseline with 0% absorbance. **(D)** Time to reach 50% ($t_{1/2}$) and **(E)** 95% (t_{95}) maximal absorbance. **(F)** The gelation rate S defined as the slope of the linear region of the gelation curve. Data are shown as mean ± standard error of mean. $^{*}p<0.05$, $^{**}p<0.01$, $^{\#}p<0.001$, $n=3$.

shape (Fig. 4B). A significantly longer lag phase as well as the longer time required to reach half of the final turbidity ($t_{1/2}$) and 95% of the final turbidity (t_{95}) was found for UB-ECM than for other ECM hydrogels, while the shortest gelation time was found for UC-ECM (Table 1 and Fig. 4B–E). However, the velocity to complete gelation or gelation rate (S) was significantly higher for SC-ECM when compared with UB-ECM (Fig. 4F). These results suggest that hydrogel assembly was fastest for UC-ECM, followed by SC-ECM and B-ECM, while the UB-ECM hydrogels had the longest gelation time.

Cell growth, proliferation, and migration on ECM hydrogels

Proliferation of hBM-MSCs, hASCs, and hWJ-MSCs on ECM hydrogels was determined using WST-1 assay after 1, 3, 7, and 14 days of the culture. While BM-MSCs on UC-ECM proliferated similarly as in the control tissue culture well, lower proliferation of BM-MSCs was found on all porcine-derived hydrogels, UB-ECM, SC-ECM, and B-ECM. On the other hand, proliferation of hASCs on all types of ECM hydrogels did not significantly differ from controls. Notably, proliferation of hWJ-MSCs at 14 days was significantly higher on tissue-specific UC-ECM than on other ECM hydrogels or even in controls (Fig. 5).

Using migration assay, all ECM hydrogels revealed chemotactic properties and stimulated the migration of all types of MSCs, which was significantly higher when compared with cell migration to the control culture medium alone (Fig. 6A–C).

The ability of ECM hydrogels to support neurite outgrowth was observed using DRG explant cultures. After 7 days of culture, neurites densely extended from DRG bodies with no significant differences in neurite length or neurite area between individual hydrogels and Matrigel, which served as a positive control (Fig. 6D–F).

It is well known that the unique compositions and microstructural features of ECM have been shown to be influential in directing cell fate or morphology.[43] To reveal the neurotrophic properties of ECM hydrogels, we determined neural differentiation of NSC culture. NSCs grew on all ECM hydrogels, and after 7 days, displayed an expression of the early neuronal marker NF70 (Fig. 7). Of note, in contrast to the dispersed NSCs cultured on laminin-coated glass coverslips, the NSCs grown on the ECM hydrogels tend to grow in distinct clusters with delimitated borders. After 14 days in culture, NSCs proliferated and differentiated into neuronal cells positive for neuronal marker MAP2, without any remarkable differences between particular ECM hydrogels (Fig. 7).

In vivo *evaluation of ECM hydrogels*

To prove the *in vivo* gelation and biocompatibility of UC-ECM, the hydrogel was injected into the focal

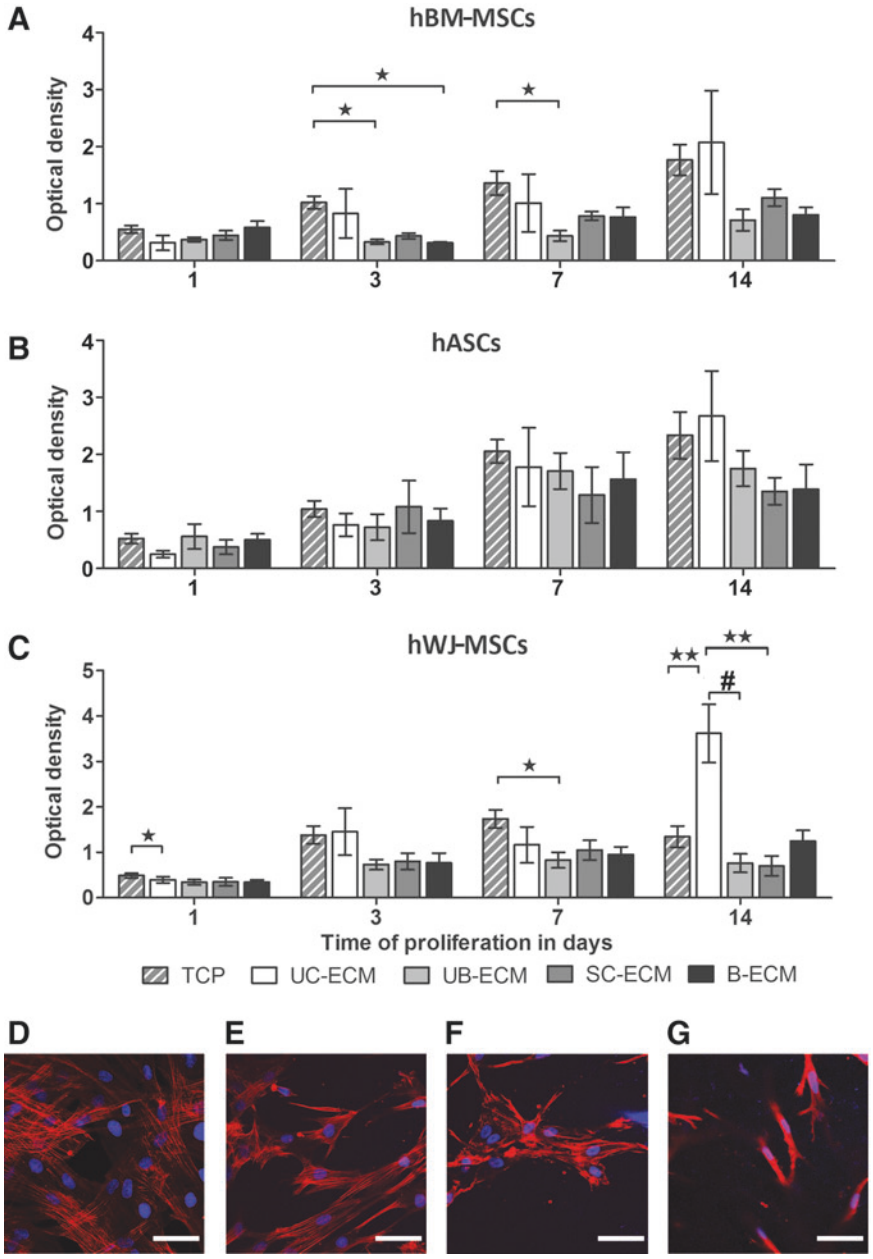

FIG. 5. **(A)** Comparison of proliferation of hBM-MSCs, **(B)** hASCs, **(C)** and hWJ-MSCs on human UC-ECM, porcine UB-ECM, SC-ECM, B-ECM, and control TCP on 1, 3, 7, and 14 days using WST-1 reagent. The proliferation rate was assessed on a spectrophotometer and illustrated as optical density. **(D)** The morphology of proliferating hWJ-MSCs on UC-ECM, **(E)** UB-ECM, **(F)** SC-ECM, and **(G)** B-ECM was depicted after 14 days. Data are shown as mean ± standard error of mean. Scale bars represent 50 μm. $*p < 0.05$, $**p < 0.01$, $^{\#}p < 0.001$, $n = 6$. hASCs, human adipose tissue-derived stromal cells; hBM-MSCs, human mesenchymal stem cells isolated from human bone marrow; hWJ, human Wharton's jelly; TCP, tissue culture plastic.

ischemic lesion created in the rat motor cortex. As is illustrated in Figure 8 on collagen and DAPI staining after 24 h, the UC-ECM formed a compact hydrogel within the lesion, which was highly populated by endogenous cells. The host macrophages were the prevalent cell type present within the lesion and also infiltrating the hydrogel (75.7% ± 5.0% of all infiltrating cells in the gel, $n = 3$). As is apparent from Figure 8C, the macrophages detected within the UC-ECM hydrogel revealed predominant positivity for marker of M2 macrophages ($CD206^+$ cells), which represented 77.1% ± 6.5% of all macrophages within the hydrogel.

Discussion

Acellular tissue-specific ECMs can be utilized as biological scaffolds for many applications in tissue engineering. For reconstruction of neural or other soft tissues, ECMs in the form of hydrogels are clinically more acceptable as these materials retain biologic activity, with the advantage of injectability and *in situ* polymerization, which offer minimally invasive delivery techniques. Indeed, injectable ECM hydrogels derived from different tissue sources have been previously demonstrated for the treatment of spinal cord injury,[33] stroke,[27] postmyocardial infarction,[44] critical limb ischemia,[45] and new adipose tissue development.[46]

In this study, we optimized the decellularization protocol as described by Medberry *et al.*[30] to prepare an injectable hydrogel from human UC tissue, which combines the advantages of neonatal tissue of human origin with the ease of availability, without any ethical or regulatory constraints. In contrast to other previously used ECMs extracted from the porcine UB, brain, or spinal cord, UC-ECM contained a significantly higher amount of sGAG, which is generally high in fetal and newborn tissues, including the UC.[42]

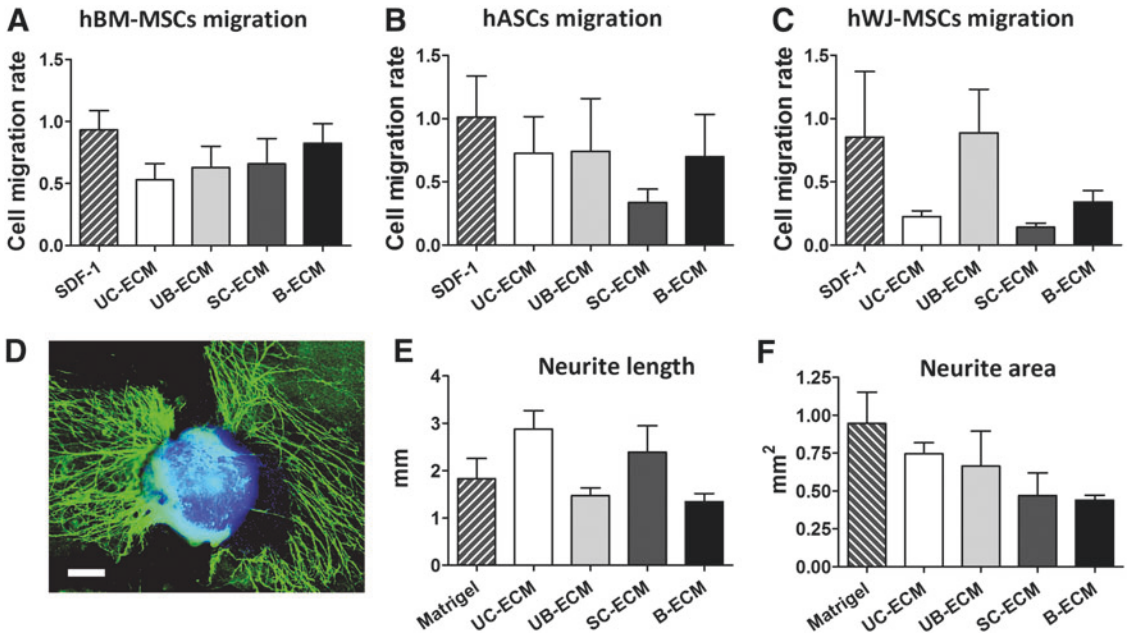

FIG. 6. Chemotactic properties of ECM hydrogels investigated using xCELLigence® RTCA DP Cell Invasion and Migration Assay showing migration of **(A)** hBM-MSCs, **(B)** hASCs, and **(C)** WJ-MSCs toward UC-ECM, UB-ECM, SC-ECM, and B-ECM at 6 h after seeding. Results are normalized to the control (culture medium without supplements) ($n = 5$). **(D)** DRG explant culture on UC-ECM hydrogel stained with DAPI and NF160. DRGs were cultivated for 7 days on the Matrigel or ECM hydrogels and the longest neurite length **(E)** and neurite area **(F)** were determined using NeuriteJ ImageJ plug-in. Data are shown as mean ± standard error of mean, ($n = 3$). Scale bars represent 200 μm. DRG, dorsal root ganglion.

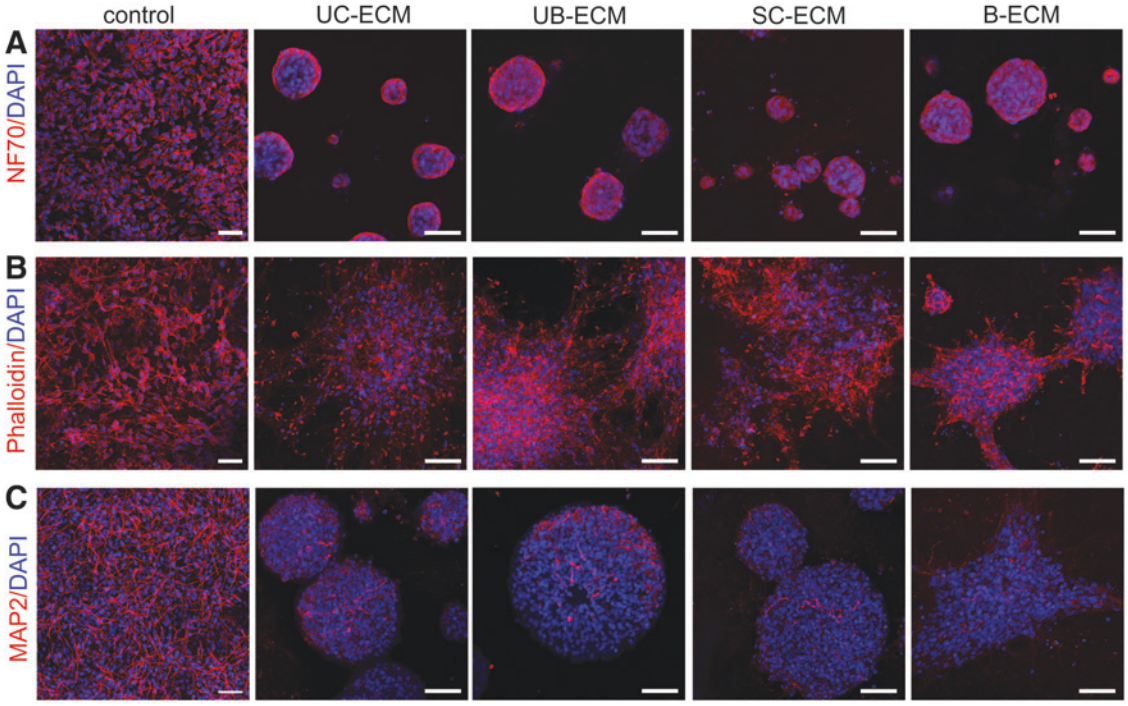

FIG. 7. **(A)** Growth and differentiation of NSC line SPC-01 on laminin-coated glass coverslips (control) and on UC-ECM, UB-ECM, SC-ECM, and B-ECM. Immunostaining for neurofilaments NF70 and DAPI after 1 week in culture, **(B)** phalloidin and DAPI after 2 weeks in culture, and **(C)** MAP2 and DAPI after 2 weeks in culture. Scale bars represent 50 μm. NSC, neural stem cell.

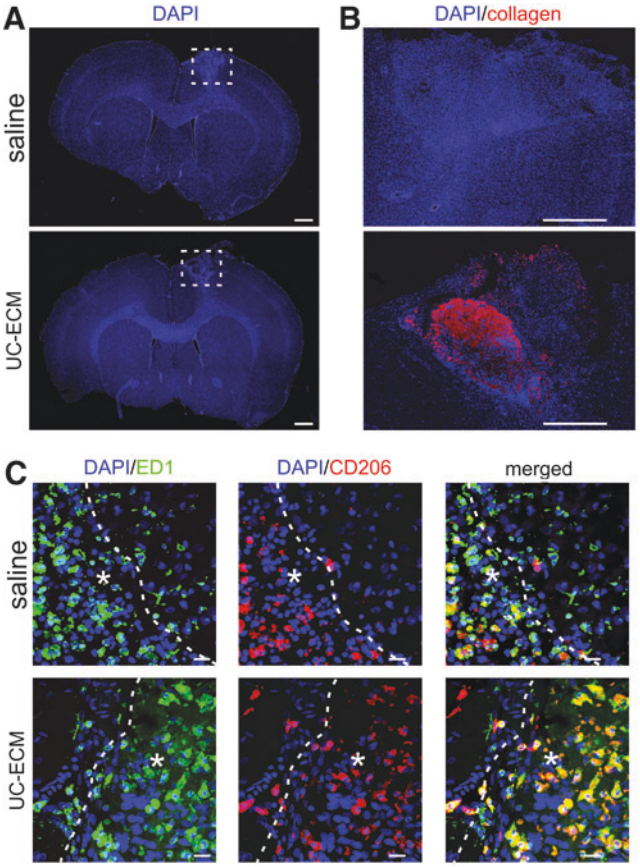

FIG. 8. Coronal brain sections illustrating *in vivo* gelation and cellular infiltration of UC-ECM hydrogel 24 h after implantation into the photothrombotic ischemic lesion in the rat motor cortex. **(A, B)** Saline (control lesion, *first row*) and UC-ECM hydrogel (*second row*) were injected into the lesion site 7 days after lesion induction. **(A)** Staining for cell nuclei (DAPI). Scale bars represent 1 mm. **(B)** Staining for DAPI (*blue*) and collagen I (*red*). Scale bars represent 500 μm. **(C)** Infiltration of macrophages into the control lesion and UC-ECM hydrogel is depicted by ED1 (*green*) and CD206 (*red*) staining. Cell nuclei were stained for DAPI (*blue*). The *dotted line* shows the border of the lesion and intact brain tissue, the *asterisk* represents the lesion site. Scale bars represent 20 μm.

Moreover, the sGAG present in ECM includes chondroitin sulfates, heparin, heparan sulfate, and hyaluronic acid, and these structures can bind cytokines and growth factors such as bFGF and contribute to neural tissue reconstruction.[34,47–50]

The concentration of sGAG has been shown to alter gelation kinetics and mechanical properties of ECM hydrogels.[30] Indeed, UC-ECM revealed the fastest gelation rate when compared with porcine ECMs with lower sGAG. Notably, even if the B-ECM, SC-ECM, and UB-ECM were prepared by the same decellularization protocols, they displayed slight differences in collagen and sGAG concentrations as well as in gelation time and rheologic properties when compared with those described by Medberry *et al.*[30] These differences might result from different origin as well as the age of porcine tissues used for decellularization.

It has been suggested that ECM scaffolds derived from the same tissue type as that of the injury site may have a unique composition of molecular constituents to induce constructive tissue-specific remodeling. For instance, cardiac ECM has demonstrated the capability to provide tissue-specific cues for cardiac cell growth and differentiation.[6] Tissue-specific skeletal muscle ECM revealed better outcomes for critical limb ischemia treatment compared with UC-ECM.[45] In addition, the B-ECM hydrogel, being the tissue-specific matrix, unlike the SC-ECM and UB-ECM, increased the length of neurite extensions of the neuroblastoma cell line.[30]

On the contrary, other studies have not shown an advantage of CNS-derived ECM versus non-CNS-derived ECM materials with respect to their effects on *in vitro* neurite outgrowth[34,41] or *in vivo* neurotrophic properties in spinal cord injury repair.[33]

Similarly, in this study, despite dissimilarities in nanoscale topography, sGAG content, mechanical properties, and the speed of gelation, we did not observe any significant differences in chemotactic or neurotrophic properties between the CNS- and non-CNS-derived ECM materials of human or porcine origin, which does not indicate an advantage of tissue specificity for ECM hydrogels in neural tissue repair. Of note, to achieve effective cell removal, CNS-derived tissues required the more complex decellularization procedures compared with, for example, UB-ECM or UC-ECM, which may result in the removal of neurosupportive proteins and growth factors and consequent loss of CNS tissue-specific bioactivity.

On the other hand, we found a tissue-specific effect of UC-ECM, which selectively promoted proliferation of hWJ-MSCs when compared with the other types of ECMs and MSCs.

A significant, but neglected, feature of ECM hydrogels is their contraction in 3D fibroblast-like culture. This well-known phenomenon is a characteristic of collagen gels seeded with fibroblasts, which generate tension on the matrix during both extension and retraction of pseudopodia.[51] A similar effect has also been described for ECM hydrogels derived from porcine dermis and UB seeded with fibroblasts.[52] We previously reported that porcine SC-ECM and UB-ECM significantly contracted when combined with hWJ-MSCs in a 3D culture[33]; in this study, we demonstrated contraction also for UC-ECM and B-ECM. The contraction rate, however, occurred slower for UC-ECM and B-ECM in comparison with SC-ECM and UB-ECM (Supplementary Data; Supplementary Data are available online at www.liebertpub.com/tec).

When used as an MSC vehicle *in vivo* to fill the lesion cavity, rapid gel contraction may then result in an inhomogeneous scaffold distribution within the lesion, which should be taken into consideration, when applying ECM hydrogels as cell carriers in *in vivo* settings. On the other hand, other cell types such as NSCs can be cultured in ECM hydrogel without causing contraction.

Finally, we proved *in vivo* UC-ECM gelation and biocompatibility using a rat model of photothrombotic lesion. The UC-ECM was densely infiltrated by resident macrophages with a predominating M2-like phenotype. An M2-like macrophage phenotype was also found using SC-ECM and UB-ECM hydrogel in rat spinal cord injury[33] and UB-ECM injected into rat middle cerebral ischemia lesion cavities.[32] An M2-positive macrophage infiltration in response to acellular ECM has been positively correlated with constructive host tissue remodeling, while M1 phenotype resulted in the deposition of dense connective tissue and

scarring.[25,53] Nevertheless, future work is needed to determine the *in vivo* UC-ECM degradation and its replacement by the host tissue in a longer time period.

In summary, our results expand the previously described ECM hydrogels and have proved UC-ECM to be an easily accessible material of human origin that provides appropriate mechanical and bioactive properties suitable for CNS repair.

Conclusion

In this study, we prepared injectable ECM hydrogel by decellularization of human UC tissue and compared its properties with CNS and non-CNS ECM hydrogels derived from porcine UB, brain, and spinal cord. Despite differences in nanoscale topography, sGAG content, and speed of gelation, all ECMs revealed similar *in vitro* neurotrophic properties, which do not indicate a benefit of tissue-specific ECM for neural tissue repair. After injection into the cortical photothrombotic lesion in rats, the UC-ECM formed a hydrogel *in situ* and was densely populated by host macrophages. Further *in vivo* studies are needed to consider the potential of ECM hydrogels for clinical translation.

Acknowledgments

This work was supported by GACR 15-01396S, GAUK 1846214, Ministry of Education, Youth and Sports of CR within the LO1309, BIOCEV (CZ.1.05/1.1.00/02.0109), CZ.02.1.01/0.0./0.0/15_003/0000419, and the J.E. Purkyně fellowship awarded by Academy of Sciences of the Czech Republic. The authors thank Stephen F. Badylak and Christopher J. Medberry for the initial training and providing the decellularization protocols.

Disclosure Statement

No competing financial interests exist.

References

1. Kubinova, S., and Sykova, E. Biomaterials combined with cell therapy for treatment of spinal cord injury. Regen Med **7,** 207, 2012.
2. Kubinova, S. New trends in spinal cord tissue engineering. Future Neurol **10,** 129, 2015.
3. Saldin, L.T., Cramer, M.C., Velankar, S.S., White, L.J., and Badylak, S.F. Extracellular matrix hydrogels from decellularized tissues: structure and function. Acta Biomater **49,** 1, 2017.
4. Crapo, P.M., Gilbert, T.W., and Badylak, S.F. An overview of tissue and whole organ decellularization processes. Biomaterials **32,** 3233, 2011.
5. Badylak, S.F. The extracellular matrix as a scaffold for tissue reconstruction. Semin Cell Dev Biol **13,** 377, 2002.
6. Wang, R.M., and Christman, K.L. Decellularized myocardial matrix hydrogels: in basic research and preclinical studies. Adv Drug Deliv Rev **96,** 77, 2016.
7. Agrawal, V., Brown, B.N., Beattie, A.J., Gilbert, T.W., and Badylak, S.F. Evidence of innervation following extracellular matrix scaffold-mediated remodelling of muscular tissues. J Tissue Eng Regen Med **3,** 590, 2009.
8. Badylak, S., Arnoczky, S., Plouhar, P., Haut, R., Mendenhall, V., Clarke, R., and Horvath, C. Naturally occurring extracellular matrix as a scaffold for musculoskeletal repair. Clin Orthop Relat Res **367 Suppl,** S333, 1999.
9. Zantop, T., Gilbert, T.W., Yoder, M.C., and Badylak, S.F. Extracellular matrix scaffolds are repopulated by bone marrow-derived cells in a mouse model of achilles tendon reconstruction. J Orthop Res **24,** 1299, 2006.
10. Petersen, I. [Morphological and molecular pathology of lung cancer]. Pathologe **31 Suppl 2,** 204, 2010.
11. Dedecker, F., Grynberg, M., and Staerman, F. [Small intestinal submucosa (SIS): prospects in urogenital surgery]. Prog Urol **15,** 405, 2005.
12. Wood, J.D., Simmons-Byrd, A., Spievack, A.R., and Badylak, S.F. Use of a particulate extracellular matrix bioscaffold for treatment of acquired urinary incontinence in dogs. J Am Vet Med A **226,** 1095, 2005.
13. Badylak, S.F., Vorp, D.A., Spievack, A.R., Simmons-Byrd, A., Hanke, J., Freytes, D.O., Thapa, A., Gilbert, T.W., and Nieponice, A. Esophageal reconstruction with ECM and muscle tissue in a dog model. J Surg Res **128,** 87, 2005.
14. Karabekmez, F.E., Duymaz, A., and Moran, S.L. Early clinical outcomes with the use of decellularized nerve allograft for repair of sensory defects within the hand. Hand (N Y) **4,** 245, 2009.
15. Bejjani, G.K., Zabramski, J., and Durasis Study, G. Safety and efficacy of the porcine small intestinal submucosa dural substitute: results of a prospective multicenter study and literature review. J Neurosurg **106,** 1028, 2007.
16. Parmaksiz, M., Dogan, A., Odabas, S., Elcin, A.E., and Elcin, Y.M. Clinical applications of decellularized extracellular matrices for tissue engineering and regenerative medicine. Biomed Mater **11,** 022003, 2016.
17. Galili, U. Avoiding detrimental human immune response against Mammalian extracellular matrix implants. Tissue Eng Part B Rev **21,** 231, 2015.
18. Raeder, R.H., Badylak, S.F., Sheehan, C., Kallakury, B., and Metzger, D.W. Natural anti-galactose alpha 1,3 galactose antibodies delay, but do not prevent the acceptance of extracellular matrix xenografts. Transpl Immunol **10,** 15, 2002.
19. Badylak, S.F., and Gilbert, T.W. Immune response to biologic scaffold materials. Semin Immunol **20,** 109, 2008.
20. Taylor, D.A. From stem cells and cadaveric matrix to engineered organs. Curr Opin Biotechnol **20,** 598, 2009.
21. Semba, R.D., Nicklett, E.J., and Ferrucci, L. Does accumulation of advanced glycation end products contribute to the aging phenotype? J Gerontol A Biol Sci Med Sci **65,** 963, 2010.
22. Sicari, B.M., Johnson, S.A., Siu, B.F., Crapo, P.M., Daly, K.A., Jiang, H.B., Medberry, C.J., Tottey, S., Turner, N.J., and Badylak, S.F. The effect of source animal age upon the in vivo remodeling characteristics of an extracellular matrix scaffold. Biomaterials **33,** 5524, 2012.
23. Tottey, S., Johnson, S.A., Crapo, P.M., Reing, J.E., Zhang, L., Jiang, H.B., Medberry, C.J., Reines, B., and Badylak, S.F. The effect of source animal age upon extracellular matrix scaffold properties. Biomaterials **32,** 128, 2011.
24. Johnson, T.D., Dequach, J.A., Gaetani, R., Ungerleider, J., Elhag, D., Nigam, V., Behfar, A., and Christman, K.L. Human versus porcine tissue sourcing for an injectable myocardial matrix hydrogel. Biomater Sci **2014,** 60283D, 2014.
25. Badylak, S.F. Decellularized allogeneic and xenogeneic tissue as a bioscaffold for regenerative medicine: factors that influence the host response. Ann Biomed Eng **42,** 1517, 2014.
26. Kurtz, A., and Oh, S.J. Age related changes of the extracellular matrix and stem cell maintenance. Prev Med **54 Suppl,** S50, 2012.

27. Freytes, D.O., Martin, J., Velankar, S.S., Lee, A.S., and Badylak, S.F. Preparation and rheological characterization of a gel form of the porcine urinary bladder matrix. Biomaterials **29,** 1630, 2008.
28. DeQuach, J.A., Mezzano, V., Miglani, A., Lange, S., Keller, G.M., Sheikh, F., and Christman, K.L. Simple and high yielding method for preparing tissue specific extracellular matrix coatings for cell culture. PLoS One **5,** e13039, 2010.
29. Okada, M., Payne, T.R., Oshima, H., Momoi, N., Tobita, K., and Huard, J. Differential efficacy of gels derived from small intestinal submucosa as an injectable biomaterial for myocardial infarct repair. Biomaterials **31,** 7678, 2010.
30. Medberry, C.J., Crapo, P.M., Siu, B.F., Carruthers, C.A., Wolf, M.T., Nagarkar, S.P., Agrawal, V., Jones, K.E., Kelly, J., Johnson, S.A., Velankar, S.S., Watkins, S.C., Modo, M., and Badylak, S.F. Hydrogels derived from central nervous system extracellular matrix. Biomaterials **34,** 1033, 2013.
31. DeQuach, J.A., Yuan, S.H., Goldstein, L.S., and Christman, K.L. Decellularized porcine brain matrix for cell culture and tissue engineering scaffolds. Tissue Eng **17,** 2583, 2011.
32. Ghuman, H., Massensini, A.R., Donnelly, J., Kim, S.M., Medberry, C.J., Badylak, S.F., and Modo, M. ECM hydrogel for the treatment of stroke: characterization of the host cell infiltrate. Biomaterials **91,** 166, 2016.
33. Tukmachev, D., Forostyak, S., Koci, Z., Zaviskova, K., Vackova, I., Vyborny, K., Sandvig, I., Sandvig, A., Medberry, C.J., Badylak, S.F., Sykova, E., and Kubinova, S. Injectable extracellular matrix hydrogels as scaffolds for spinal cord injury repair. Tissue Eng **22,** 306, 2016.
34. Crapo, P.M., Medberry, C.J., Reing, J.E., Tottey, S., van der Merwe, Y., Jones, K.E., and Badylak, S.F. Biologic scaffolds composed of central nervous system extracellular matrix. Biomaterials **33,** 3539, 2012.
35. Pollock, K., Stroemer, P., Patel, S., Stevanato, L., Hope, A., Miljan, E., Dong, Z., Hodges, H., Price, J., and Sinden, J.D. A conditionally immortal clonal stem cell line from human cortical neuroepithelium for the treatment of ischemic stroke. Exp Neurol **199,** 143, 2006.
36. Boudaoud, A., Burian, A., Borowska-Wykret, D., Uyttewaal, M., Wrzalik, R., Kwiatkowska, D., and Hamant, O. FibrilTool, an ImageJ plug-in to quantify fibrillar structures in raw microscopy images. Nat Protoc **9,** 457, 2014.
37. Gelman, R.A., Williams, B.R., and Piez, K.A. Collagen fibril formation. Evidence for a multistep process. J Biol Chem **254,** 180, 1979.
38. Sponer, P., Filip, S., Kucera, T., Brtkova, J., Urban, K., Palicka, V., Koci, Z., Syka, M., Bezrouk, A., and Sykova, E. Utilizing autologous multipotent mesenchymal stromal cells and beta-tricalcium phosphate scaffold in human bone defects: a prospective, controlled feasibility trial. BioMed Res Int **2016,** 2076061, 2016.
39. Torres-Espin, A., Santos, D., Gonzalez-Perez, F., del Valle, J., and Navarro, X. Neurite-J: an image-J plug-in for axonal growth analysis in organotypic cultures. J Neurosci Meth **236,** 26, 2014.
40. Anderova, M., Kubinova, S., Jelitai, M., Neprasova, H., Glogarova, K., Prajerova, I., Urdzikova, L., Chvatal, A., and Sykova, E. Transplantation of embryonic neuroectodermal progenitor cells into the site of a photochemical lesion: immunohistochemical and electrophysiological analysis. J Neurobiol **66,** 1084, 2006.
41. Crapo, P.M., Tottey, S., Slivka, P.F., and Badylak, S.F. Effects of biologic scaffolds on human stem cells and implications for CNS tissue engineering. Tissue Eng **20,** 313, 2014.
42. Leung, A., Crombleholme, T.M., and Keswani, S.G. Fetal wound healing: implications for minimal scar formation. Curr Opin Pediatr **24,** 371, 2012.
43. Bonnans, C., Chou, J., and Werb, Z. Remodelling the extracellular matrix in development and disease. Nat Rev Mol Cell Biol **15,** 786, 2014.
44. Singelyn, J.M., and Christman, K.L. Injectable materials for the treatment of myocardial infarction and heart failure: the promise of decellularized matrices. J Cardiovasc Transl Res **3,** 478, 2010.
45. Ungerleider, J.L., Johnson, T.D., Hernandez, M.J., Elhag, D.I., Braden, R.L., Dzieciatkowska, M., Osborn, K.G., Hansen, K.C., Mahmud, E., and Christman, K.L. Extracellular matrix hydrogel promotes tissue remodeling, arteriogenesis, and perfusion in a rat hindlimb ischemia model. JACC Basic Translat Sci **1,** 32, 2016.
46. Young, D.A., Ibrahim, D.O., Hu, D., and Christman, K.L. Injectable hydrogel scaffold from decellularized human lipoaspirate. Acta Biomater **7,** 1040, 2011.
47. Badylak, S.F. Xenogeneic extracellular matrix as a scaffold for tissue reconstruction. Transpl Immunol **12,** 367, 2004.
48. Seif-Naraghi, S.B., Horn, D., Schup-Magoffin, P.J., and Christman, K.L. Injectable extracellular matrix derived hydrogel provides a platform for enhanced retention and delivery of a heparin-binding growth factor. Acta Biomater **8,** 3695, 2012.
49. Wang, T.W., and Spector, M. Development of hyaluronic acid-based scaffolds for brain tissue engineering. Acta Biomater **5,** 2371, 2009.
50. Horn, E.M., Beaumont, M., Shu, X.Z., Harvey, A., Prestwich, G.D., Horn, K.M., Gibson, A.R., Preul, M.C., and Panitch, A. Influence of cross-linked hyaluronic acid hydrogels on neurite outgrowth and recovery from spinal cord injury. J Neurosurg Spine **6,** 133, 2007.
51. Brown, R.A. In the beginning there were soft collagen-cell gels: towards better 3D connective tissue models? Exp Cell Res **319,** 2460, 2013.
52. Wolf, M.T., Daly, K.A., Brennan-Pierce, E.P., Johnson, S.A., Carruthers, C.A., D'Amore, A., Nagarkar, S.P., Velankar, S.S., and Badylak, S.F. A hydrogel derived from decellularized dermal extracellular matrix. Biomaterials **33,** 7028, 2012.
53. Brown, B.N., Valentin, J.E., Stewart-Akers, A.M., McCabe, G.P., and Badylak, S.F. Macrophage phenotype and remodeling outcomes in response to biologic scaffolds with and without a cellular component. Biomaterials **30,** 1482, 2009.

Address correspondence to:
Šárka Kubinová, PhD
Institute of Experimental Medicine
Academy of Sciences of the Czech Republic
Videnska 1083
Prague 1420
Czech Republic

E-mail: sarka.k@biomed.cas.cz

Received: February 22, 2017
Accepted: May 1, 2017
Online Publication Date: May 25, 2017

SCIENTIFIC REPORTS

OPEN

Genipin and EDC crosslinking of extracellular matrix hydrogel derived from human umbilical cord for neural tissue repair

Received: 13 August 2018
Accepted: 3 July 2019
Published online: 23 July 2019

Karel Výborný[1,2], Jana Vallová[1,2], Zuzana Kočí[1], Kristýna Kekulová[1,2], Klára Jiráková[1], Pavla Jendelová[1], Jiří Hodan[3] & Šárka Kubinová[1]

Extracellular matrix (ECM) hydrogels, produced by tissue decellularization are natural injectable materials suitable for neural tissue repair. However, the rapid biodegradation of these materials may disrupt neural tissue reconstruction *in vivo*. The aim of this study was to improve the stability of the previously described ECM hydrogel derived from human umbilical cord using genipin and N-(3-Dimethylaminopropyl)-N′-ethylcarbodiimide hydrochloride (EDC), crosslinking at concentration of 0.5–10 mM. The hydrogels, crosslinked by genipin (ECM/G) or EDC (ECM/D), were evaluated *in vitro* in terms of their mechanical properties, degradation stability and biocompatibility. ECM/G, unlike ECM/D, crosslinked hydrogels revealed improved rheological properties when compared to uncrosslinked ECM. Both ECM/G and ECM/D slowed down the gelation time and increased the resistance against *in vitro* enzymatic degradation, while genipin crosslinking was more effective than EDC. Crosslinkers concentration of 1 mM enhanced the *in vitro* bio-stability of both ECM/G and ECM/D without affecting mesenchymal stem cell proliferation, axonal sprouting or neural stem cell growth and differentiation. Moreover, when injected into cortical photochemical lesion, genipin allowed *in situ* gelation and improved the retention of ECM for up to 2 weeks without any adverse tissue response or enhanced inflammatory reaction. In summary, we demonstrated that genipin, rather than EDC, improved the bio-stability of injectable ECM hydrogel in biocompatible concentration, and that ECM/G has potential as a scaffold for neural tissue application.

Restoration of the neural tissue architecture and functions plays a crucial role in the treatment of the injured central nervous system (CNS). Several strategies have been developed and implemented in animal models to reconstruct the damaged neural tissue. One of these strategies – the tissue engineering approach - is bridging the lesion with the use of a biomimetic scaffold which is able to fill the lesion cavity and provide the necessary microenvironment for the neural tissue remodelling. Various synthetic and natural hydrogels have been used as tissue-engineered scaffolds for neural tissue repair[1–4], but these materials usually fail to mimic the complex structure and composition of the native tissue. In contrast, biological scaffolds, composed of natural extracellular matrix (ECM), have many advantages including a three-dimensional (3D) structure, low immunogenicity and a complex biomolecular composition[5,6].

Such scaffolds are commonly produced by whole tissue decellularization and may be prepared in injectable form by solubilisation of the obtained ECM into the hydrogel, using pepsin digestion at pH ~ 2. These ECM hydrogels have physical properties (e.g. the ability to be physically crosslinked *in situ* at physiological pH and temperature) and adequate mechanical strength similar to the soft nervous tissue that allow them to be non-invasively injected into the defect caused by the injury with minimal surrounding tissue damage. ECM-based scaffolds, obtained from a variety of tissues, have been used for the reconstruction of e.g. myocardium, muscles, blood vessels, valves, bones, kidney, liver, as well as CNS tissues[7–9].

[1]Institute of Experimental Medicine of the Czech Academy of Sciences, Prague, Czech Republic. [2]2nd Medical Faculty, Charles University, Prague, Czech Republic. [3]Institute of Macromolecular Chemistry of the Czech Academy of Sciences, Prague, Czech Republic. Correspondence and requests for materials should be addressed to Š.K. (email: sarka.kubinova@iem.cas.cz)

In our recent study, we optimized the effective, reproducible decellularization techniques for the preparation of ECM-based hydrogel from human umbilical cord tissue and proved its neuro-promoting capacity, which was comparable to ECMs, derived from porcine tissues such as urinary bladder, spinal cord and brain[9,10]. In this context, due to neonatal and human origin, high accessibility and no ethical constraints, umbilical cord-derived ECM represents a promising tissue source for hydrogel preparation.

The control of ECM scaffold degradation is essential for the constructive tissue remodelling process, since the degrading biomaterial is gradually replaced by endogenous cells, which build a new functional ECM equivalent as opposed to scar tissue[5]. As shown in our previous studies and those of others, in inflammatory conditions the implanted ECM hydrogels are quickly populated with the resident cells, significantly accelerating the degradation rate of ECM-based scaffolds[10]. Therefore, the implementation of non-toxic, biocompatible and reproducible techniques to prolong and control the degradability of ECM-derived hydrogels, represents a challenging issue in applying such biomaterials for neural regeneration.

On the other hand, a long-term retention (12 weeks) but sparse endogenous cell invasion was found for ECM hydrogel derived from porcine urinary bladder injected into subacute stroke cavity in the brain, which indicates a marked difference of biodegradation of ECM hydrogel in the various types of CNS lesion[11].

A common method to reduce the degradation of various biomaterials is chemical crosslinking. Formaldehyde or glutaraldehyde are common agents to stabilize ECM scaffolds[12,13], however, the high cytotoxicity and potential induction of inflammatory response impedes these compounds the use as implants in neural tissue[14,15]. For that reason, non-cytotoxic crosslinkers, such as genipin or N-(3-Dimethylaminopropyl)-N′-ethylcarbodiimide hydrochloride (EDC) have been selected as candidates to improve the stability of ECM hydrogels[16,17].

Genipin is a natural crosslinking low-toxic agent, derived from the gardenia fruit which can bridge free amino groups of lysine or hydroxylysine residues of different polypeptide chains by monomeric or oligomeric crosslinks in collagen[16–19]. To stabilize ECM scaffolds, genipin crosslinking was used in myocardial matrix hydrogel[20], decellularized spinal cord[21] or whole-liver decellularized grafts[22], where it proved to have a lower cytotoxicity and *in vivo* immunogenicity than their glutaraldehyde-treated counterparts. In addition, genipin possesses a range of key pharmacological properties, such as anti-inflammatory, neuroprotective, neurogenic, and antidepressant effects which gives this compound therapeutic potential for diseases of the CNS[23].

In contrast to genipin, EDC activates carboxyl groups of glutamic or aspartic acid residues to conjugate to amino groups between proteins and/or peptide molecules and is used for the crosslinking of proteins and polysaccharides. Collagen scaffolds crosslinked with EDC have been shown to decrease degradation rates[24,25] while supporting the growth of human keratinocytes[26], smooth muscle cells[27], and fibroblasts[28].

Therefore, due to the different reactions, fixation in genipin and EDC may produce distinct crosslinking structures that may affect the crosslinking characteristics, mechanical properties, and resistance against enzymatic degradation of the fixed material[16,17].

In this study we used ECM derived from human umbilical cord, crosslinked by genipin and EDC to improve the structural stability, and evaluated feasibility of the obtained materials for neural tissue repair. Rheology, turbidimetry, and *in vitro* enzymatic degradation assays were used to characterize the kinetics of genipin and EDC cross-linking, and the effects of cross-linking on the gelation time, storage modulus and enzymatic degradation resistance. The *in vitro* biocompatibility of the crosslinked hydrogels was determined by the evaluation of human mesenchymal stem cell (MSCs) proliferation, axonal growth of dissociated adult rat dorsal root ganglion neurons and growth and differentiation of human fetal neural stem cells. In addition, *in situ* gelation and a prolonged retention of ECM/G hydrogels were confirmed after injection into a subacute photothrombotic cortical ischemic lesion in rats.

Results

Composition of ECM hydrogels. In our previous study we characterized the structure and composition of umbilical cord derived ECM hydrogel, while the amount of total collagen (543 μg/mg of dry ECM weight) and glycosaminoglycans (6.6 μg/mg of dry ECM weight) was determined[9]. In addition to this, the detailed proteomics of ECM matrix was performed in this study using high-resolution LC–tandem mass spectrometry and compared to the protein profile of the native umbilical cord tissue (Supplementary Table 1).

The composition of the ECM hydrogel confirms the previous conclusions on chemical compounds of ECM[9,29]. The most abundant proteins detected in the ECM are Collagen alpha-1(I) chain, Collagen alpha-2(I) chain, Collagen alpha-1(III) chain and Collagen alpha-1(II) chain, which were relatively enhanced in ECM in comparison with the native tissue. On the other hand, the decellularization process leads to a decrease of other types of collagen, such as Collagen alpha-1(IV, V, VI, XI, XII) chain, Collagen alpha-2(IV, V, VI, XI) chain or Collagen alpha-3(VI) chain, as well as to a substantial decrease of Fibronectin, Fibrillin-1, 2, Tenascin and Laminin subunit beta-1 and gamma-1. Some of the cytoskeletal or cytoplasmic proteins, such as Actin. aortic smooth muscle, Actin. cytoplasmic 2, Myosin-11, Filamin-A, Tropomyosin beta chain and alpha-1 chain, Caveolin-1, Myosin-10 and 9 were still preserved in ECM matrix, but to a very low extent (Supplementary Table 1).

Crosslinking degree evaluation. The 2,4,6-trinitrobenzene sulfonic acid (TNBSA) protocol was used to determine the relative amount of free amino group[30,31]. As is apparent in Fig. 1A, with the increasing concentration of genipin and EDC (0.5 mM; 1.0 mM and 10 mM), the crosslinking degree significantly increased from 31.3% to 52.5% in ECM/G but only from 28.6% to 35.1% in ECM/D. The uncrosslinked ECM keeps 0% baseline. The crosslinking degree of ECM/G increased with rising genipin concentration which shows that genipin reacts with the free amino groups in ECM and can form intra- and intermolecular crosslinking networks. On the other hand, EDC crosslinking efficiency is limited due to the need of both primary amine and carboxyl groups in the peptide or proteins. Moreover, EDC crosslinking is considered to be most efficient in acidic (pH 4.5) conditions while phosphate buffers and neutral pH (up to 7.2) conditions result in lower efficiency; nevertheless, an increasing amount of EDC in a reaction solution up to 10 mM was not able to compensate for the reduced crosslinking efficiency.

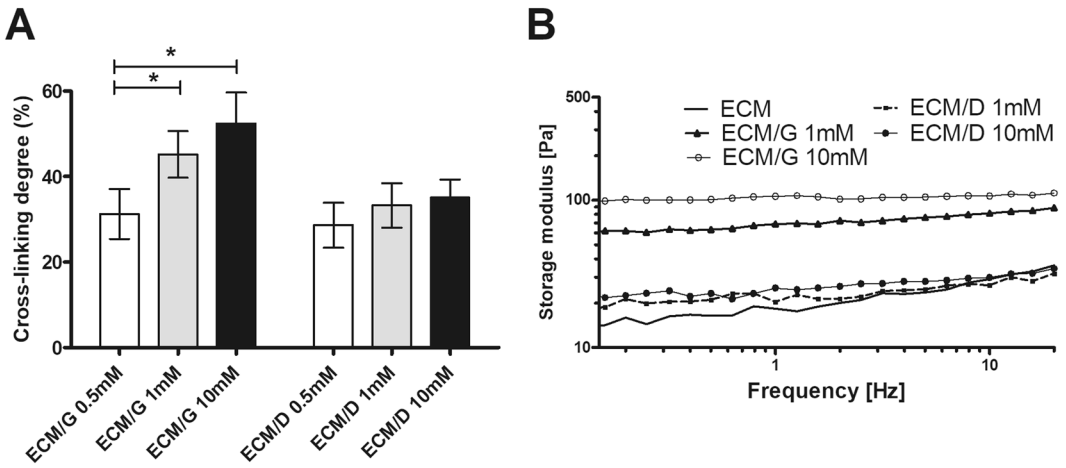

Figure 1. (**A**) The cross-linking degree and (**B**) strain sweep of ECM, ECM/G and ECM/D crosslinked by 0.5 – 10 mM genipin or EDC, (*$p < 0.05$, $n = 3$).

Rheological and turbidimetric measurements. In rheological experiments, we tested the storage modulus to determine the flow and deformation properties of the crosslinked ECM hydrogels with crosslinkers concentration 1 mM and 10 mM. Increasing the frequency, the storage modulus of ECM and ECM/D retains nearly the same value and has an increasing trend. On the other hand, the storage modulus of ECM/G remarkably increased (Fig. 1B). These data reflect the lower efficiency of the ECM/D crosslinking degree assessed by the TNBSA protocol (Fig. 1A).

Turbidimetric gelation kinetic curves revealed a sigmoidal shape for uncrosslinked ECM and near-linear shape for ECM/G and ECM/D at a concentration of 1 mM and 10 mM (Fig. 2A). Notably, the gelation of uncrosslinked gel starts more rapidly than that for both the crosslinked ECMs and reached the plateau after ~100 min, compared to ~120 min for the crosslinked ECMs.

The time required to reach half of the final turbidity ($t_{1/2}$) as well as the time required to reach 95% of the final turbidity (t_{95}) was significantly longer for both crosslinkers at both tested concentrations than for the uncrosslinked ECM (Fig. 2B,C, Supplementary Table 2). On the other hand, a significantly higher lag time and gelation velocity at $t_{1/2}$ (delta S) was found for ECM/D when compared with uncrosslinked ECM (Fig. 2D,E). These results suggest that hydrogel assembly was fastest for the uncrosslinked ECM while the crosslinking hydrogels required a longer gelation time.

***In vitro* enzymatic degradation.** 1-D degradation test was used to analyse the ECM hydrogel endurance to enzymatic degradation in relation to the hydrogel maturation (Fig. 3). The % of the remaining weight was determined after 3 hours of exposure to 0.1% collagenase, while ECM, ECM/G and ECM/D hydrogels were allowed to mature for 1–72 hours. The collagenase concentration (0.1 wt %, 163 U/mg) was chosen to provide a standardized, accelerated assay for gel degradation in order to compare the effect of crosslinkers concentration on *in vitro* gel stability. It should be noted that the concentration of collagenase is much higher than of that which could be found *in vivo*, while the number of other matrix degrading proteases are present in the inflamed body setting. Generally, all concentrations of genipin and EDC provided a substantial resistance to collagenase-associated degradation, which increased with crosslinker concentration and maturation time, but a higher resistance and shorter maturation time were found for genipin rather than for EDC. After 24 h maturation and crosslinker concentration 1 mM, the degradation resistance was 2-fold higher in ECM/D and almost 4-fold higher in ECM/G than in the uncrosslinked ECM. Degradation of the hydrogels did not further increase after 24 h of maturation for ECM/G or after 48 h for ECM/D, which reflects that crosslinked ECM/G mature earlier than ECM/D, even in higher concentrations of the EDC.

A 3-D degradation model was used to further investigate the hydrogel's stability (Fig. 4). ECM, ECM/G and ECM/D hydrogels were matured for 1 h (Fig. 4A,B) and 48 h (Fig. 4C,D) after the initial crosslinking and the degradation was determined as % of the initial weight after 30, 60, 90 and 120 min incubation in collagenase. ECM hydrogels which matured for 48 h showed a greater resistance to degradation than those which matured for 1 h, even in the case of uncrosslinked ECM. Similarly, as for the 1-D degradation, the resistance was higher for ECM/G than for ECM/D. Half-life calculations showed that ECM hydrogels matured for 1 h exhibited half-life times 96.37 min for 1.0 mM ECM/D and 170.38 min for 1.0 mM ECM/G hydrogels (Table 1).

Cell proliferation in the presence of genipin and EDC. Using MSC culture, various concentrations of free genipin and EDC added to the culture media were tested after 1, 4 and 7 days of the culture to evaluate the toxicity and effect of the crosslinkers on cell proliferation. As is apparent from Fig. 5A,B, proliferation of MSCs significantly decreased when the concentration of genipin as well as EDC in the culture media was 5 mM and higher.

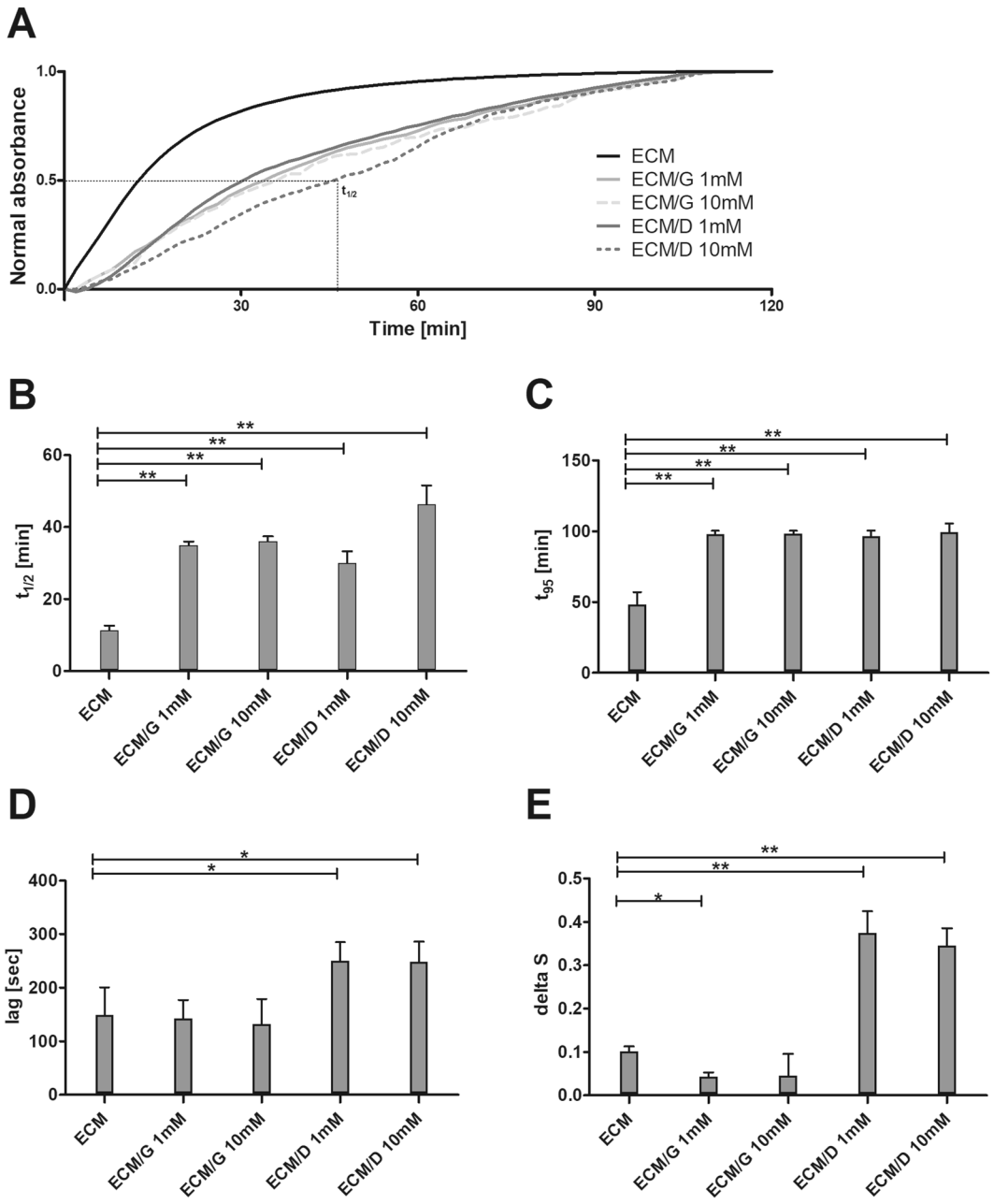

Figure 2. (**A**) The representative normalized turbidimetric gelation kinetics of ECM, ECM/G and ECM/D crosslinked by 1 mM and 10 mM genipin or EDC. (**B**) Time to reach 50% and (**C**) 95% maximal absorbance. (**D**) Lag time of ECM hydrogels determined as an intercept point of the slope at log $t_{1/2}$ and turbidimetry baseline with 0% absorbance. (**E**) The gelation rate delta S defined as the slope of the linear region of the gelation curve (*$p < 0.05$, **$p < 0.01$, $n = 3$).

Cell proliferation on the crosslinked ECM hydrogels. The proliferation of MSCs seeded on ECM/D and ECM/G hydrogels with an increasing concentration of crosslinkers, was determined after 3, 7 and 14 days of the culture (Fig. 5C,D, Supplementary Fig. 1). A significantly decreased cell proliferation was found on the ECM hydrogels crosslinked with a genipin or EDC concentration of 5 mM and higher in comparison with the uncrosslinked ECM, while a crosslinker concentration of 1 mM was found biocompatible without remarkable effects on MSC proliferation. It is apparent that the cytotoxic effect of the crosslinked hydrogels occurs at a higher crosslinker concentration than in the case of free crosslinkers added into the culture media. The cytotoxic effect in higher crosslinker concentrations is most likely caused by the residual or unbound crosslinkers within the matrix.

ECM hydrogel contraction. The mechanical stability of the crosslinked ECM hydrogels was evaluated in a 3-D cell culture, which result in the hydrogel contraction. Figure 6A depicts a contraction of ECM hydrogels seeded by MSCs (5×10^5 in 200 µl of the hydrogel disc) after 4 h, 24 h and 48 h. In uncrosslinked ECM hydrogels,

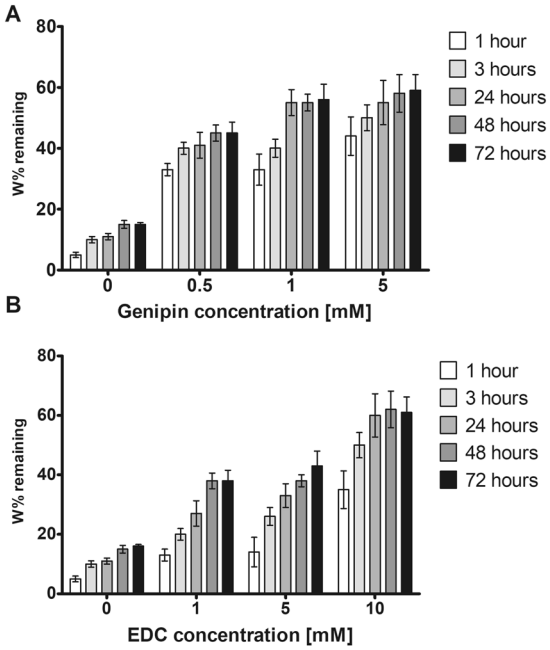

Figure 3. 1-D enzymatic degradation of (**A**) ECM/G and (**B**) ECM/D in different concentrations of crosslinkers after hydrogel maturation time 1–72 hours. Data are reported as % of remaining weight expressed as the dry weight of the ECM hydrogels exposed to the collagenase for 3 hours related to the dry weight of control ECM gel exposed to PBS for the same time (n = 3).

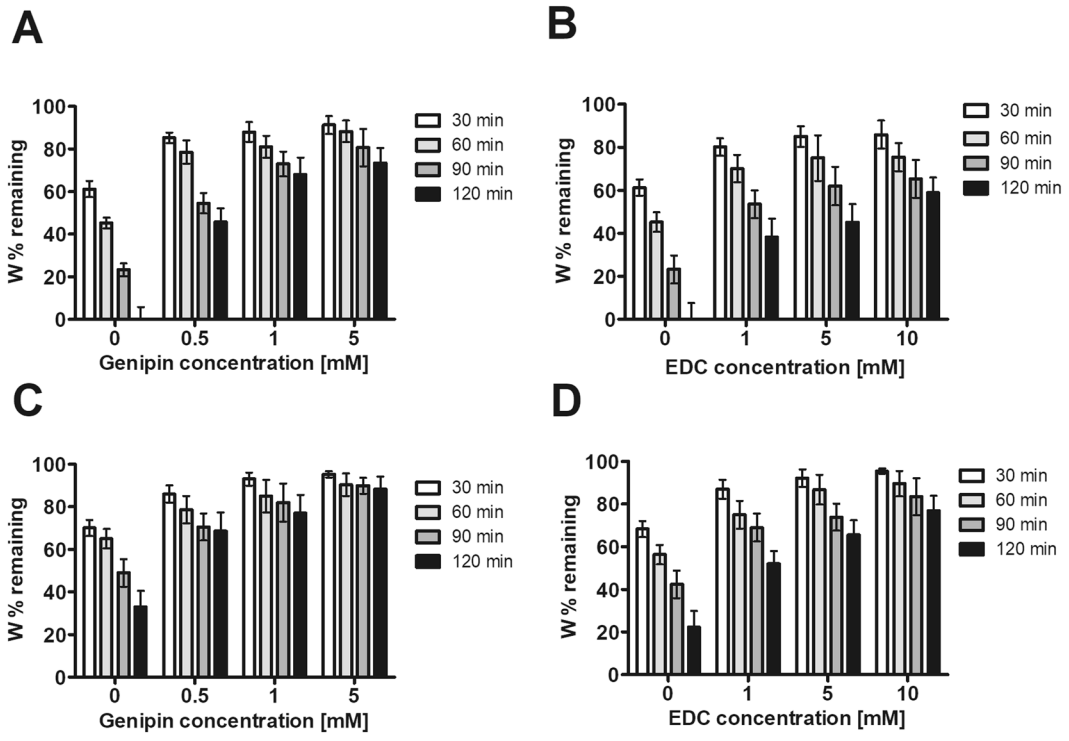

Figure 4. 3-D degradation assay of ECM/G and ECM/D hydrogels in different concentrations of (**A**,**C**) genipin and (**B**,**D**) EDC, with a maturation time of (**A**,**B**) 1 hour and (**C**,**D**) 48 hours. Data are reported as % of remaining weight expressed as the dry weight of the ECM hydrogels after 30, 60, 90, 120 min exposure in collagenase solution related to the dry weight of control ECM gel exposed to PBS for the same time (n = 3).

a significant contraction leads to the shrinkage of the hydrogel disc area to 24% within 24 hours. However, crosslinking of the ECM hydrogels by 1 mM genipin or EDC reduced the contraction to 49.9% (ECM/G) and 51.3% (ECM/D) (within 24 h) of the initial hydrogel disc area, while using this concentration, no decrease in

Crosslinker concentration [mM]	Hydrogel type	Half-life time [min]	
		1-hour treatment	48-hours treatment
0	ECM	75.21 ± 8.27	43.52 ± 5.11
0.5	ECM/G	104.25 ± 6.86	234.11 (est.)
1	ECM/G	170.38 (est.)	310.82 (est.)
1	ECM/D	96.37 ± 8.54	130.11 (est.)
5	ECM/G	225.42 (est.)	605.21 (est.)
5	ECM/D	112.63 ± 6.41	173.89 (est.)
10	ECM/D	150.12 (est.)	305.82 (est.)

Table 1. Half-life calculation of ECM, ECM/G and ECM/D hydrogels after 3-D degradation in 0.1% type I collagenase, (est.) estimated calculation using linear progression method, (n = 3).

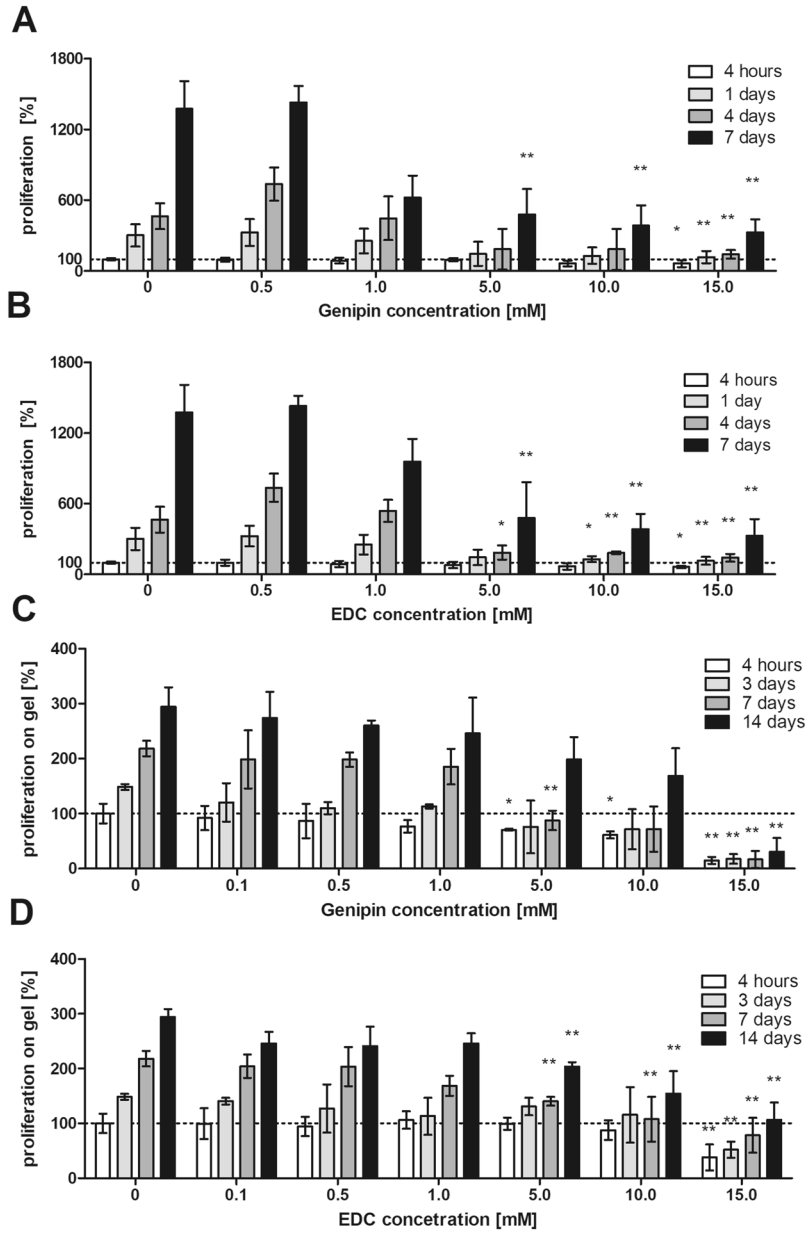

Figure 5. MSC proliferation in different concentrations of (**A**,**B**) free genipin and EDC, and (**C**,**D**) on ECM/G and ECM/D hydrogels crosslinked with different concentrations of genipin and EDC. Cell proliferation was assessed using Alamar Blue assay. The data are normalized to the initial values obtained at the beginning of the experiment on the uncrosslinked ECM which were set as 100% cell viability (dotted baseline), (*$p < 0.05$, **$p < 0.01$ vs. uncrosslinked ECM, n = 6).

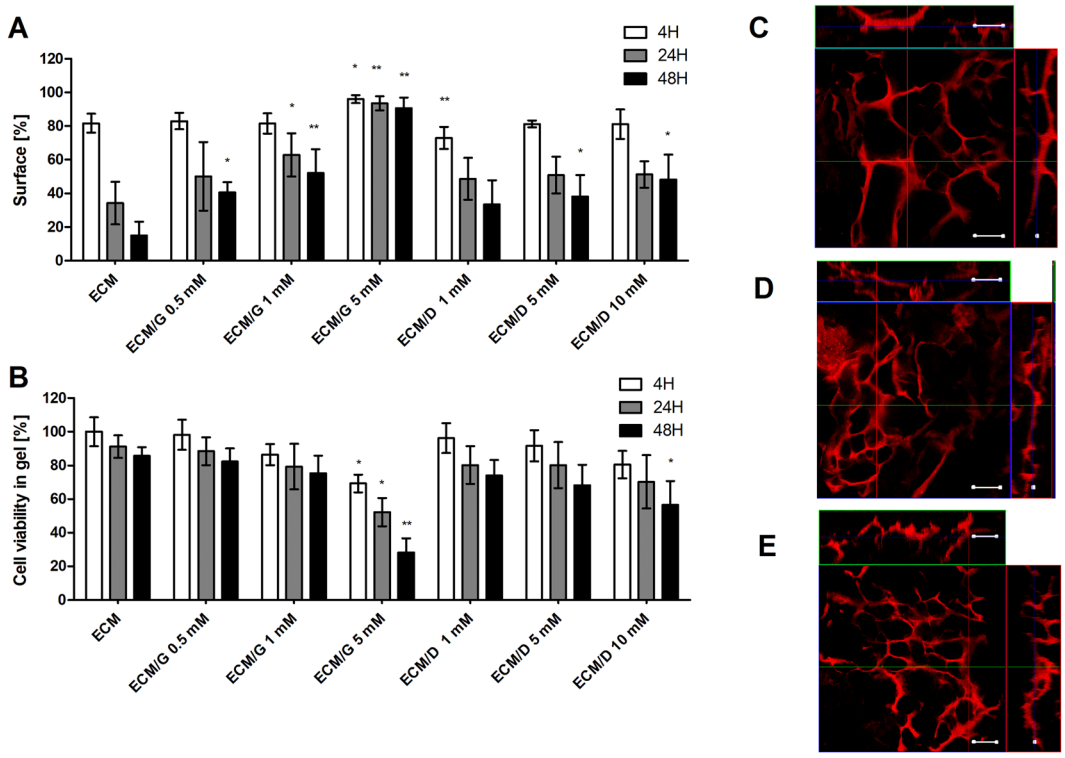

Figure 6. (**A**) Contraction of ECM, ECM/G and ECM/D hydrogel discs crosslinked with different concentrations of genipin and EDC, 4 h, 24 h and 48 h after 3D seeding with MSCs (5×10^5 in 200 µl of the hydrogel). Contraction is expressed as a percentage of the initial hydrogel disc area (*$p < 0.05$, **$p < 0.01$ vs. uncrosslinked ECM, n = 3). (**B**) Viability of MSCs seeded in ECM, ECM/G and ECM/D hydrogels crosslinked with different concentrations of genipin and EDC at 4 h, 24 h and 48 h after 3-D cell seeding. Viability is expressed as a percentage of the initial cell viability in uncrosslinked ECM (*$p < 0.05$, **$p < 0.01$ vs. uncrosslinked ECM, n = 3). (**C**–**E**) 3-D confocal micrographs of MSCs stained for phalloidin seeded on (**C**) ECM, (**D**) 1 mM ECM/G and (**E**) 1 mM ECM/D after 7 days of the culture. Scale bar: 100 µm.

cell viability within the ECM hydrogels was observed (Fig. 6B). The contraction was blocked with the genipin crosslinking of concentrations of 5 mM. On the other hand, EDC did not prevent hydrogel contraction, even at a concentration 10 mM of EDC. At concentration of genipin of 5 mM, and EDC of 10 mM, the viability of MSCs in 3-D cell culture significantly decreased (Fig. 6B). These findings are in line with the results from the mechanical strain which was improved after genipin but not after EDC crosslinking (Fig. 1B).

The ability of MSCs to grow from the surface into the ECM hydrogels was observed after 1 week of the culture (Fig. 6C–E). The cells formed an interconnected 3-D network within the uncrosslinked ECM as well as in ECM/G and ECM/D crosslinked by 1 mM genipin or EDC.

The effect of crosslinking on axonal growth. The effect of crosslinking of ECM hydrogel with 1 mM genipin and EDC was evaluated by analysis of the axonal growth of sensory neurons isolated from adult DRG. The percentage of neurons that displayed axonal growth was much lower than on the laminin coated glass cover slips (not shown) but did not show any significant differences among the uncrosslinked ECM, ECM/D and ECM/G (Fig. 7).

The effect of crosslinking on neural stem cell growth and differentiation. The proliferation of neural stem cells (SPC-01 line) was evaluated after 1 and 3 weeks of the culture on uncrosslinked ECM, ECM/D (1 mM) and ECM/G (1 mM). After 1 week, SPC-01 grew on all ECM hydrogels in distinct clusters (Supplementary Fig. 2). The values of cell density on various ECM hydrogels did not significantly differ at both time intervals (Supplementary Fig. 3). The differentiation of SPC-01 was then analysed after 3 weeks in culture. SPC-01 cells spread from the clusters and covered large areas on hydrogels and were positive for neuronal marker beta-III-Tubulin, mainly on the borders of spreading clusters. The minority of cells were also positive for astrocytic marker GFAP (Fig. 8). However, the cells did not tend to differentiate into oligodendrocytes. There were only individual cells positive for NG2 at this interval, either on ECM hydrogels or laminin coated coverslips (not shown).

***In vivo* evaluation of ECM/G hydrogel.** To prove the *in vivo* biocompatibility and degradation, ECM and ECM/G hydrogels were injected into the focal ischemic lesion created in the rat motor cortex to crosslink *in situ*. As is illustrated in Fig. 9A,E on collagen staining after 24 h, both ECM and ECM/G formed a compact hydrogel

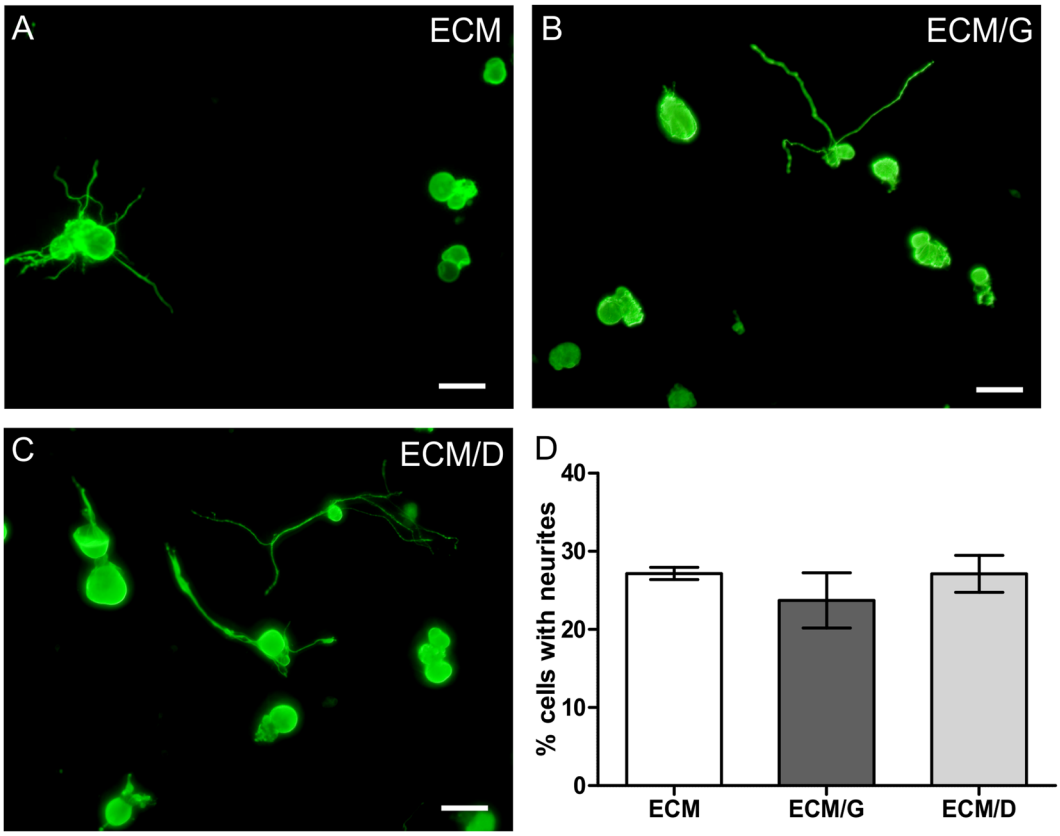

Figure 7. Axonal growth of dissociated adult dorsal root ganglion (DRG) neurons on the ECM, ECM/G and ECM/D hydrogels with crosslinker concentration 1 mM. (**A**–**C**) DRG culture on ECM hydrogels stained for beta-III-Tubulin. (**D**) Percentage of cells with neurites longer than cell body. Scale bars represent 50 µm (n = 3).

within the lesion and this was populated by the host cells, such as fibroblasts or macrophages. A remarkable infiltration of vimentin positive cells was observed in both the ECM and ECM/G hydrogels (Fig. 9B,F). The ECM and ECM/G hydrogel retention was then determined 2 weeks after the injection into the lesion. While uncrosslinked ECM degraded (Fig. 9C), ECM/G was still detected within the lesion without any sign of enhanced inflammatory reaction of fibrotic scarring (Fig. 9G,H). It is obvious that genipin crosslinking effectively enhanced ECM hydrogel retention within the lesion, while a gradual degradation was apparent in the surrounding tissue where the ECM/G fragments were highly infiltrated with the host cells. Unfortunately, due to the fragility of the lesion area, we were not able to perform a quantitative analysis that would reveal a hydrogel effect on cavitation and cell infiltration.

To determine the inflammatory reaction around the lesion treated by the ECM and ECM/G hydrogel, a relative number of microglia/macrophages positive for CD68 (ED1) and CD206 in the area surrounding the lesion were analysed after 2 weeks (Table 2). No significant differences were found between the group of ECM and ECM/G in the relative number of both ED1 and CD206 positive cells, which suggests that the genipin crosslinking of ECM hydrogel did not enhance an inflammatory reaction within the ischemic cortical lesion.

Discussion

Decellularized ECM tissues can be transformed to scaffolds of natural origin in a variety of applications in tissue engineering[32]. To remodel neural or other soft tissues, ECM in the form of hydrogels are acceptable in clinical practice as these materials offer minimally invasive delivery techniques using the advantage of injectability and retention of biologic activity.

In our previous study, we prepared and characterized ECM hydrogel derived from the human umbilical cord and found it comparable to ECM hydrogels derived from CNS and non-CNS porcine tissues[9]. However, despite the advantageous bioactive properties, physically crosslinked ECM hydrogels exhibit weak structural stability and rapid *in vivo* degradation when applied into acute or subacute CNS lesion, which in turn limit their use for *in vivo* application[10]. On the other hand, a slowing degradation may prolong the presence of the bioactive ECM matrix within the CNS lesion and thus allow the resident cells and axons to repopulate the ECM scaffold, enabling tissue remodelling and functional bridging of the lesion.

To solve this problem, in this study we aimed to enhance the *in vivo* degradation resistance of the ECM hydrogels by covalent crosslinking, and evaluate the feasibility of the crosslinked materials *in vitro*, with the focus being on their biocompatibility and neuro-promoting potential.

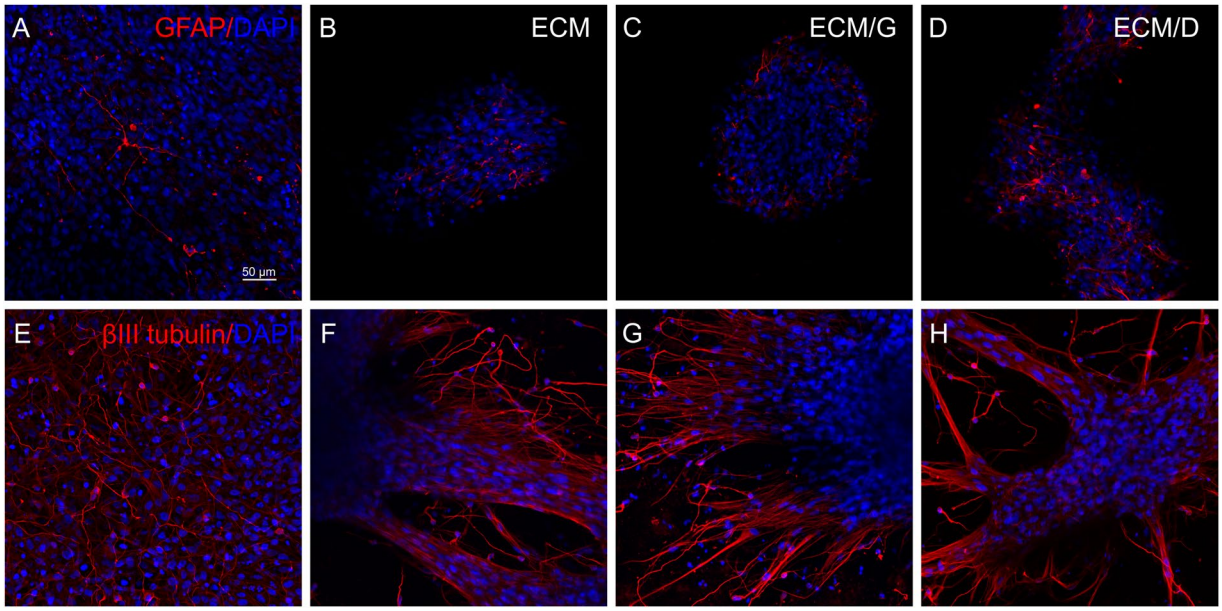

Figure 8. Neural stem cells (SPC-01) cultured (**A**,**E**), on the laminin coated glass coverslips, (**B**,**F**) uncrosslinked ECM, (**C**,**G**) ECM/G and (**D**,**H**) ECM/D. Cells were stained with (**A**-**D**) GFAP (red) and DAPI (blue) or (E-H) beta-III-Tubulin (red) and DAPI (blue). Scale bar: 50 µm.

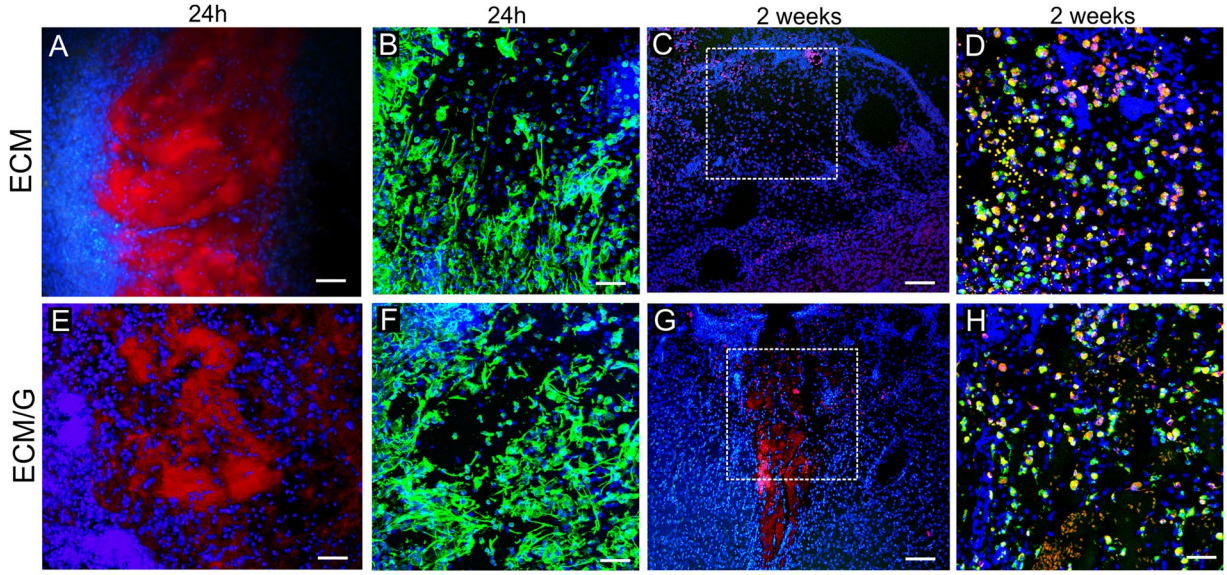

Figure 9. Coronal brain sections illustrating *in vivo* gelation and cellular infiltration of (**A**–**D**) ECM and (**E**–**H**) ECM/G hydrogel, (**A**,**B**,**E**,**F**) 1 day and (**C**,**D**,**G**,**H**) 2 weeks after the injection into the photothrombotic ischemic lesion in the rat motor cortex. (**A**,**C**,**E**,**G**) Staining for collagen I (red) and cell nuclei (DAPI, blue). (**B**,**F**) Staining for vimentin (green) and DAPI (blue). (**D**,**H**) The infiltration of macrophages (ED1, green) into the lesion with (**D**) uncrosslinked ECM hydrogel and (H) ECM/G 2 weeks after hydrogel injection into the lesion area. Cell nuclei were stained for DAPI (blue). The dotted squares in C, G show the area taken in D, H. Scale bars: (**A**,**E**,**C**,**G**) 100 µm, (**B**,**D**,**F**,**H**) 50 µm.

We compared two crosslinkers, genipin and EDC, which due to their relatively low cytotoxicity are commonly used for the stabilization of natural scaffolds, e.g. collagen, gelatine, chitosan or ECM matrices[19,33]. Both crosslinking agents bind proteins or peptides, such as collagen which is the most prominent compound of ECM. Furthermore, the ECM scaffold is composed of a substantial amount of glycosaminoglycans as well as other proteins that may form an additional substrate for the crosslinking process[9].

Importantly, the different principles of both crosslinking reactions and structures reflect the differences in the crosslinking degree and overall stability. While genipin primarily binds free amino groups with a wide

	ECM	ECM/G
ED1 (% cell number)	33.84 ± 1.09 (n = 5)	35.56 ± 3.17 (n = 5)
CD206 (% cell number)	28.05 ± 2.97 (n = 5)	30.09 ± 1.91 (n = 5)

Table 2. The percentage of ED1 and CD206 positive cells in the lesion area after ECM and ECM/G injection into the ischemic cortical lesion. (n = number of animals).

variety of covalent cross-links, EDC requires carboxyl groups and binds primary amino groups through an active O-acylisourea intermediate.

A higher crosslinking degree which elicits genipin rather than EDC has a substantial impact on the enhancement of storage modulus and the resistance of ECM hydrogels to enzymatic degradation. Moreover, a lower degree of crosslinking of the EDC-fixed tissue in comparison with genipin was also described in previous reports[16,17,34]. Notably, N-hydroxysuccinimide (NHS) has been reported to improve the efficiency of crosslinking collagen in conjunction with EDC. However, due to the organic origin and potential toxicity of NHS when used in the *in-situ* ECM gelling process, we did not use EDC coupling with NHS or sulfo-NHS agents.

The effect of genipin crosslinking on the enhancement of ECM hydrogel mechanical strength was further confirmed by the weakening hydrogel contraction after seeding with MSCs in 3D culture. The contraction of ECM matrices after the inoculation of MSCs or other fibroblast-like cell types represents a common phenomenon for collagen-based materials that might burden the ability of the matrix to fill the lesion cavity[7]. Crosslinking with 1 mM genipin significantly decreased ECM contraction without affecting MSC viability and thus improved the hydrogel ability to effectively fill the lesion when combined with MSCs.

When developing injectable hydrogels, the crosslinker dosage is limited by its toxicity as the ECM hydrogels have to crosslink *in situ* without the possibility of washing out the excess of crosslinkers from the matrix. While the genipin is covalently bound within the crosslinked matrix, EDC serves as an intermediate substance which does not take part in the linkage and remains within the scaffold in the form of isourea byproduct. This might limit the EDC as a crosslinker *in vivo*, as in effect it requires a higher concentration for the efficient crosslinking than genipin. In this study, we used crosslinkers concentration 1 mM that was found to be noncytotoxic. This concentration provided a significant ECM hydrogel resistance to *in vitro* degradation without a deleterious effect on cell proliferation, axonal sprouting, and neural stem cell growth and differentiation. The support of crosslinked ECM hydrogels for neural stem cells and MSCs is of great importance as proof of the neuro-promoting properties of ECM hydrogels as well as for cell delivery, as these cell types have been shown to enhance the therapeutic benefit of the ECM scaffolds[10,35].

To prove crosslinked ECM hydrogel stability *in vivo*, ECM and ECM/G were injected into the ischemic lesion to evaluate its retention within the lesion as well as the reaction of the host macrophages/microglia. Certainly, both ECM and ECM/G hydrogels formed a gel *in situ* and were infiltrated with the host cell, while genipin crosslinking enhanced ECM/G retention within the lesion for up to 2 weeks, when compared with uncrosslinked ECM hydrogels.

It has been reported that when applied *in vivo*, crosslinked collagen-based matrices induced a proinflammatory response, such as macrophage activation and the increase of proinflammatory cytokine release, while the host adverse response depends on the crosslinking degree[36]. In this study, the macrophage reaction did not reveal any significant changes that would indicate enhanced immunogenicity of ECM/G when compared to uncrosslinked ECM. Moreover, the prevalence of M2-like CD206 + macrophages was found in both ECM and ECM/G groups, similarly as in our previous reports[9,10]. This suggests that when exposed to the inflammatory environment of the subacute ischemic cortical lesion, the biocompatible concentration of genipin crosslinking (1 mM) was effective for *in situ* gelation and the prolongation of ECM hydrogel resistance without enhancement of inflammation reaction.

Apart from stabilization of the collagen matrix, genipin has been shown to have a significant effect on preventing cellular outgrowth[37]. In this study, we observed that MSCs were able to growth from the surface into the crosslinked ECMs *in vitro*. *In vivo*, the sparse host cell infiltration into preserved ECM/G was observed after 2 weeks. Nevertheless, gradual degradation of the ECM/G matrix and its replacement by endogenous tissue structures is apparent in the surrounding tissue. Therefore, longer time intervals are required to further assess the complete ECM/G degradation within the CNS lesion.

In summary, our study used genipin and EDC as crosslinkers to enhance ECM hydrogel stability. Both crosslinkers are well tolerated by various stem cells at concentrations of 1 mM, while genipin produced more stable hydrogels with a higher degree of crosslinking, enhanced storage modulus and resistance to *in vitro* degradation. Moreover, when crosslinked *in situ*, genipin prolonged the retention of the ECM/G hydrogel within the cortical ischemic lesion without any adverse or proinflammatory effects in the host tissue. To evaluate the feasibility of the ECM/G hydrogel in neural tissue repair, further *in vivo* study is required on the more appropriate models of CNS injury, such as SCI.

Conclusion

Injectable ECM hydrogel derived from human umbilical cord was stabilized with genipin or EDC crosslinking. Genipin, rather than EDC, improved the mechanical strength and bio-stability of the ECM hydrogel, when compared to uncrosslinked ECM. A concentration of 1 mM of both genipin and EDC was found biocompatible without affecting the ability of ECM hydrogels to support axonal growth and neural differentiation. *In vivo*, 1 mM genipin was suitable for the *in situ* ECM crosslinking and improved retention of ECM/G in the cortical ischemic lesion for up to 2 weeks when compared to uncrosslinked ECM.

Methods

Tissue decellularization and preparation of ECM hydrogels. Human umbilical cords were prepared according to the previously described protocol[9]. The cords were obtained from healthy full-term neonates after spontaneous delivery with the informed consent of the donors using the guidelines approved by the Institutional Committee at University Hospitals (Pilsen, Czech Republic). About 10–15 cm of frozen umbilical cord was aseptically transported to the lab, subsequently thawed and transversely cut into pieces (<0.5 cm length). The tissue pieces were agitated in PBS bath (48 h at 120 rpm, 4 °C). The deionized water (dH_2O) and PBS bath were exchanged three to five times before the tissue pieces were soaked in 0.02% trypsin/0.05% EDTA (120 min at 120 rpm, 37 °C, Sigma-Aldrich, Chemie GmbH Steinheim, Germany) and afterwards in a 0.1% peracetic acid in 4.0% ethanol bath (120 min at 300 rpm;) and in a series of PBS and deionized water (dH_2O) soaks. Finally, the tissue pieces were lyophilized for 24 h (FreeZone® 2.5, Labconco Corporation, Kansas City, MO, USA), powdered (Mini-Mill Cutting Mill, Thomas Scientific, Swedesboro, NJ, USA) and stored at −20 °C.

To prepare the hydrogel, powdered ECM samples were solubilized with 1.0 mg/ml pepsin in 0.01 N HCl (Sigma-Aldrich, Chemie GmbH Steinheim, GE) at a concentration of 10 mg ECM/ml and stirred at room temperature for 48 h to form a pre-gel solution (pH ~ 1.5–2.5). The pepsin-HCl ECM solution was neutralized to pH 7.4 with 0.1 N NaOH, isotonically balanced with 10x PBS, and diluted with 1x PBS to the final concentration of 8 mg/ml, which allows *in vivo* gelation[9,38]. The neutralized pre-gel was kept at 37 °C for ~120 min together with either genipin (Sigma) of required concentration solubilized in 50% DMSO to form genipin-crosslinked hydrogel (ECM/G) or with EDC (Sigma) of required concentration solubilized in H_2O to form EDC-crosslinked hydrogel (ECM/D).

Proteomic analysis. Proteins in ECM hydrogels and in the native umbilical cord tissue were identified by high-resolution LC–tandem mass spectrometry (MS/MS). The isolated proteins were digested with trypsin, concentrated and desalted using a trapping column (100 μm × 30 mm) filled with 3.5-μm X-Bridge BEH 130 C18 sorbent (Waters) and eluted onto an analytical column (Acclaim Pepmap100 C18, 3 μm particles, 75 μm × 500 mm; Thermo Fisher Scientific, Waltham, MA, USA). The analytical column outlet was directly connected to the Digital PicoView 550 ion source with PicoTip emitter SilicaTip (New Objective; FS360-20-15-N-20-C12). The analysis of the mass spectrometric RAW data files was carried out using the Proteome Discoverer software (Thermo Fisher Scientific; version 1.4) (Supplementary Materials).

Crosslinking degree determination by TNBSA protocol. The crosslinking degree was determined by 2,4,6-trinitrobenzen sulfonic acid (TNBSA) protocol and was defined as the ratio of the consumed amino groups in the crosslinked samples to the free amino groups in the corresponding uncrosslinked samples[31].

The amount of free amino groups in the test sample was determined by the optical absorbance of the solution at 335 nm recorded with a spectrophotometer (Infinite® 200 Pro, Tecan, Austria) using glycine at different concentrations (1.0, 2.0, 3.0, 4.0, and 5.0 mg/mL) as a standard. The samples were mixed in 0.01% TNBSA (Sigma) and 0.1 sodium bicarbonate (Sigma). After 2-hours incubation at 37 °C and adding 10% sodium dodecyl (Sigma) and 1 N HCl the amount of free amino groups in the tested samples was proportional to the optical absorbance of the solution. Both crosslinkers were tested also without gels to recognize no significant contribution of free crosslinkers to absorbance results.

The measured concentration (number of free amine moles in the sample per unit volume of dissolution) was divided by the sample number of moles and multiplied by the volume of dissolution, to obtain the free amine moles fraction in the sample. The degree of crosslinking was calculated following the equation (1):

$$\%\ \text{crosslinking} = \frac{X_{NH_2} - X_{NH_2\ cross}}{X_{NH_2}} \times 100 \tag{1}$$

where X_{NH_2} is the mole fraction of free amines in uncrosslinked samples and $X_{NH_2\ cross}$ is the mole fraction of free amines remaining in 120 min crosslinked samples. Three replicates of each concentration were evaluated.

Rheological measurement. Dynamic oscillatory shear tests were used to investigate the viscoelastic properties. ECM hydrogels crosslinked by 1 mM and 10 mM genipin or by 1 mM and 10 mM EDC were subjected to a sinusoidal deformation in a 40 mm parallel plate rheometer (Ares-G2, TA Instruments, New Castle, DE, USA) at 1 Pa stress and 10 °C to determine their mechanical response (displacement or strain) as a function of time. To prevent drying of the sample a thin layer of silicone oil was applied on the side of the sample which was not in contact with the plates, just before the measurement. The samples were placed between two plates of 25 mm or 12.5 mm in diameter. The bottom plate was a bowl with raised edge and defined space within the given diameter. The surface of both types of boards was finely roughened to prevent slipping. A frequency sweep test was run with the parameters of 5% strain, frequency 1–20 Hz, axial force: 0.01 N and temperature at 37 °C, 4 min duration. The test was repeated three times, at 12.5 mm and 25 mm diameter plates, with three independent samples in triplicate.

Turbidity gelation measurement. The turbidimetric gelation kinetics were determined as previously described[39] on a spectrophotometer (Infinite® 200 Pro, Tecan), which was pre-heated to 37 °C. ECM, ECM/G and ECM/D crosslinked by 1 mM and 10 mM genipin or EDC hydrogels were kept on ice at 4 °C until 100 μl were pipetted into each well of a 96 well plate, and inserted into a spectrophotometer. The absorbance was measured at 405 nm every 2 min for 120 min. Normalized absorbance, time to reach 50% and 95% maximal absorbance were determined as $t_{1/2}$ and t_{95}. The lag time (t_{lag}) was defined as the point where a line representing the slope at log

$t_{1/2}$ intersects the turbidimetry baseline with 0% absorbance. The gelation rate (S) was defined as the slope of the linear region of the gelation curve. The measurements were repeated three times with three independent samples in triplicate (Table 1).

$$Normalized\ Absorbance = \frac{A - A_0}{A_{max} - A_0} \quad (2)$$

1-D degradation assay. ECM hydrogels (0.5 mL, each sample n = 3) were crosslinked with genipin (0.5; 1 and 5 mM) or EDC (1, 5 and 10 mM) in a 2 mL cryotube (Scientific Specialties, Inc., US) and allowed to form a gel for 1, 3, 24, 48 and 72 h at 37 °C. 1 mL of collagenase I (0.1 wt %, 163 U/mg, Sigma) in PBS with 0.9 mM $CaCl_2$, was added on top of the gel and placed on a shaker at 150 rpm at 37 °C. After 3 h, the degradation medium was removed, the gels were rinsed with deionized water, frozen, lyophilized overnight, and weighed. The removal time was set by the degradation time for uncrosslinked ECM gels. The dry weights of the ECM hydrogels exposed to the collagenase were related to the weights of the control gel exposed to PBS for the same time; data are reported as % of the remaining weight.

3-D degradation assay. ECM hydrogels (0.5 mL, each sample n = 3) were crosslinked with genipin (0.5, 1 and 5 mM) or EDC (1, 5 and 10 mM) in a 2 mL cryotube and allowed to form a gel for 1 h or 48 h at 37 °C. The gels were then transferred into 24-well plates in PBS and exposed to collagenase I (0.1%, 1 mL, 163 U/mg) in PBS with 0.9 mM $CaCl_2$ on a shaker (150 rpm); the control gels were exposed to PBS. After 30, 60, 90, or 120 min, the collagenase was removed, and the gels were washed with PBS on a shaker for 20 min. The remaining gel samples were collected, lyophilized overnight, and weighed. The dry weights of the ECM hydrogels exposed to collagenase, were related to the weight of the control ECM hydrogels in PBS; data are reported as % of remaining weight. Half-life times were calculated as the time required to degradation of 50% of gel original mass (Table 2).

Mesenchymal stem cell culture. Human umbilical cord derived mesenchymal stem cells (MSCs) were used as described previously[40] (Supplementary materials). To reveal the cytotoxicity of the crosslinkers, the cells were seeded into a 96-well plate (5000 cells/cm^2 in 100 µl media) with an increasing concentration of genipin or EDC 0.5–10 mM in the media. After 4 h, 1 day, 4 days and 7 days of the culture, 10 µl of Alamar Blue reagent was added to each well containing 100 µl culture media and incubated for 3 hours at 37 °C. The fluorescence was measured using a Tecan-Spectra plate reader at 580 nm (emission) and 540 nm (excitation), the signal from the hydrogels without the cells was used for the fluorescence subtraction.

To determine the biocompatibility of the crosslinked hydrogels, the hydrogels were pipetted into a 96-well plate (90 µl/well) and seeded with cells (5000 cells/cm^2 in 100 µl media). The cell proliferation was measured using Alamar Blue assay after 4 h, 3 days, 7 days and 14 days of the culture. Each type of hydrogel was seeded in triplicate. Six independent experiments of three hydrogel batches were performed for each concentration. After 14 days in culture, the cells were visualized by Live/Dead Staining (Sigma, Supplementary Fig. 1).

ECM hydrogel contraction in 3D culture. In 3D cultures, MSC suspension in PBS was mixed with a neutralized liquid pre-gel solution for a final cell concentration of 2.5×10^6 cells/ml and crosslinked by 0.5–5 mM genipin and 1–10 mM EDC. 200 µl of the suspension was transferred inside the cylindrical mould (0.8 cm, Scaffdex, Tampere, FI) placed in the 24-well plates, and incubated at 37 °C for 45 min, to form a mechanically stable hydrogel disc seeded with the cells. Following this, the seeding moulds were removed, 1 ml of culture media was added to support living cells in the gel, and the hydrogel discs were incubated at 37 °C, and imaged after 0, 4, 24, and 48 h of the culture to quantify gel contraction. ImageJ (NIH) tracing module was used to measure the hydrogel areas at each time point and the values are shown as a percentage of the initial hydrogel area. The hydrogels were seeded in triplicate, and three hydrogel batches were used for the analysis. As a control, ECM hydrogel discs without cells were maintained in the culture under the same conditions.

To determine 3-D cell viability, ECM and ECM crosslinked by 0.5–5 mM genipin and 1–10 mM EDC were mixed with MSCs (5×10^4 in 20 µl of the hydrogel) and pipetted into a 96-well plate. After 45 min of gelation, the medium (100 µm) was added, and the cell proliferation was measured using Alamar Blue assay after 4 h, 1 and 2 days of the culture. The data were normalized to the initial viability values obtained after 4 h for the 3-D MSC culture in the uncrosslinked ECM.

To evaluate cell infiltration, 50 µl of ECM, ECM/G and ECM/D crosslinked by 1 mM genipin or EDC, were pipetted into the 96-well plate and let mature for 24 h. MSCs (5×10^3) were seeded on the surface of the hydrogels and cultured for 7 days. Cells were fixed with 4% paraformaldehyde in PBS and stained with immunofluorescent labelling for Alexa-Fluor 568 Phalloidin (1:400; Molecular Probes, Eugene, OR, USA). 3-D images were taken using the confocal microscope Zeiss LSM 5 DUO (Carl Zeiss, Jena, GE).

Axonal growth on the ECM hydrogels. Dorsal root ganglia (DRGs) were dissected from adult (2 months) male Wistar rats (Velaz, Unetice, CZ). The neurons were dissociated with 0.2% collagenase from Clostridium histolyticum and 0.1% trypsin (both from Sigma) and then centrifuged through 15% bovine serum albumin (BSA, Sigma). DRGs were cultured on coverslips coated with ECM, ECM/G, ECM/D hydrogels (300 µl, EDC/genipin concentration 1 mM) in DMEM (ThermoFisher, Waltham, MA, USA) supplemented with penicillin–streptomycin–fungizone (1%, Lonza, Basel, CH), ITS + (1%), NGF (10 ng/ml) and mitomycin C (0.5 µg/ml, all from Sigma) for 2 days. Cells were fixed with 4% paraformaldehyde in PBS and stained with anti-beta-III-Tubulin (1:1200; Abcam, Cambridge, UK) and goat anti-mouse IgG Alexa Fluor® 488 (1:400, Life Technologies, Eugene, OR, USA), and imaged on a fluorescent microscope AxioCam HRc Axioskop 2 Plus (Zeiss, Jena, GE) a 20x objective

and ImageJ software. For the analysis, a percentage of neurons with neurites longer than the cell body were calculated from 3 wells and 3 independent areas in each well. The experiment was repeated three times.

Neural stem cells growth and differentiation. The human fetal neural stem cell (NSC) line SPC-01, which is a conditionally immortalized cell line, was generated from 8-week-old human fetal spinal cord as described previously[41,42]. SPC-01 cells were cultured in tissue-culture flasks freshly coated with laminin 10 µg/ml (Sigma) in DMEM/F12 (GIBCO, Life Technologies, Grand Island, NY, USA) for 2 hours at 37 °C. Growth media comprising DMEM/F12 supplemented with human serum albumin (0.03%, Baxter Healthcare Ltd., Norfolk, UK), human apo-transferrin (100 µg/ml), putrescine DiHCl (16.2 µg/ml), human recombinant insulin (5 µg/ml), progesterone (60 ng/ml), L-glutamine (2 mM), sodium selenite (40 ng/ml), 4-OHT (100 nM) all from Sigma, human EGF (20 ng/ml), human bFGF (10 ng/ml) (PeproTech, London, UK) and primocin 100 µg/ml (InvivoGen, San Diego, CA, USA), was changed 3 times per week.

A suspension of 30 000 SPC-01 cells was seeded on laminin coated glass coverslips or 200 000 cells on ECM gels and cultured in a 24-well plate with a cultivation medium for 7 and 21 days. The cells were then fixed in 4% paraformaldehyde in PBS for 15 min and washed with PBS. The growth and differentiation of SPC-01 cells were analysed using immunofluorescent labelling for Alexa-Fluor 568 Phalloidin (1:400; Molecular Probes, Eugene, OR, USA), glial fibrillary acidic protein (GFAP, 1:800; mouse monoclonal IgG1 conjugated with Cy3; Sigma), beta-III-Tubulin (1:1200; rabbit monoclonal IgG; Abcam), NG2 chondroitin sulphate proteoglycan (1:400; rabbit polyclonal IgG; Abcam). Goat anti-rabbit IgG (H + L) conjugated with AlexaFluor 594 (1:400; Life Technologies) was used for visualization of beta-III-Tubulin and NG2 antibodies. The nuclei were visualized using 4′,6′, -diamidino-2-phenylindol (DAPI) fluorescent dye (1:1000; Life Technologies). Images were taken using the confocal microscope Zeiss LSM 5 DUO. The cell growth was determined from 10 random fields of view in each gel and analysed using ImageJ.

Injection of genipin crosslinked hydrogels into a rat model of cortical photothrombotic lesion. To test biocompatibility of ECM/G hydrogel *in vivo*, a focal brain photochemical lesion was created in the motor cortex in rats. Male Wistar rats (330 ± 30 g) (Velaz) were maintained at 22 °C on a 12 h light/dark schedule and given water and food *ad libidum*. To create the lesion, the animal was placed into the stereotactic apparatus under isoflurane (3%) anaesthesia, the scalp incision was created in the midline and the pericranial tissue was dissected to expose the bregma. Focal cerebral ischaemia was performed according to[43] as follows: Bengal Rose (Sigma) was injected via the right femoral vein (0.08 g/ml saline; 1 µl/g), and the skull was illuminated above the primary motor cortex (2 mm rostral and 2 mm dextrolateral to the bregma) with a fiber optic bundle of a cold light source (KL 1500 LCD; Zeiss) for 10 minutes. The skin overlying the cranium was then sutured.

Seven days after the focal cerebral ischaemia, a small opening in the lesion site was drilled into the scull of the animal and 10 µl of ECM (n = 5) or ECM/G (n = 5) in the form of pre-gel was injected into the lesion (in a depth of 2 mm) using a Hamilton syringe (Hamilton Company, Bonaduz, Switzerland) and stereotactic apparatus.

The animals were sacrificed 1 day and 14 days after the implantation with an overdose of anaesthesia and perfused with 4% paraformaldehyde in 0.1 M PBS intracardially. The brains were removed, fixed in 4% paraformaldehyde for 10 days and cut in frozen mode (local temperature −24 °C). Coronal slides, 40 µm thick, were stained for cell nuclei with DAPI (1:1000; Life Technologies), rabbit monoclonal IgG to vimentin (1:200, Abcam), mouse monoclonal IgG1 to CD68 (ED1; 1:150, Abcam), goat polyclonal IgG to CD206 (c-20; 1:250, Santa Cruz, Heidelberg, Germany) or mouse monoclonal IgG1 to collagen I (1:1000, COL-I, Abcam) diluted in 0.1 M PBS containing goat (or donkey – depending on the host organism of secondary antibodies) serum (1:10 both; Sigma) and Triton X-100 (0.1%) overnight in 4 °C. A staining solution lacking Triton-X was used only in the case of extracellular anti-collagen staining. As secondary antibodies, goat anti-mouse IgG conjugated with AlexaFluor 594 (1:400) for collagen I, donkey anti-mouse IgG conj. with AlexaFluor 488 (1:400) for CD 68 and donkey anti-goat IgG conj. with AlexaFluor 594 (1:400;) for CD206 (all from Life Technologies) were used.

Fluorescent images were taken using confocal microscope Zeiss LSM 5 DUO. The relative number of microglia/ macrophages (CD68+) and (CD206+) in the area surrounding the lesion was determined from sections taken by fluorescent microscope (Leica, Olympus Optical, Hamburg, Germany) using a 20x objective and ImageJ software. The quantity of the ED1 positive and CD206 positive macrophages was related to the number of all cell nuclei stained for DAPI in the area surrounding the lesion.

All experiments on the animals were performed in accordance with the European Communities Council Directive of 24th November 1986 (86/609/EEC), regarding the use of animals in research and were approved by the Ethical Committee of the Institute of Experimental Medicine Academy of Sciences Czech Republic, Prague.

Statistical analysis. Data were presented as mean ± standard error mean (SEM). The statistical significance was analysed using one-way ANOVA with Tukey's multiple comparison post hoc analysis (GraphPad Prism, San Diego, CA, USA) with a level of $p < 0.05$ considered statistically significant.

References

1. Schmidt, C. E. & Leach, J. B. Neural tissue engineering: strategies for repair and regeneration. *Annu Rev Biomed Eng* **5**, 293–347, https://doi.org/10.1146/annurev.bioeng.5.011303.120731 (2003).
2. Geller, H. M. & Fawcett, J. W. Building a bridge: engineering spinal cord repair. *Exp Neurol* **174**, 125–136, https://doi.org/10.1006/exnr.2002.7865 (2002).
3. Bellamkonda, R., Ranieri, J. P., Bouche, N. & Aebischer, P. Hydrogel-based three-dimensional matrix for neural cells. *J Biomed Mater Res* **29**, 663–671, https://doi.org/10.1002/jbm.820290514 (1995).
4. Kubinova, S. & Sykova, E. Biomaterials combined with cell therapy for treatment of spinal cord injury. *Regen Med* **7**, 207–224 (2012).
5. Saldin, L. T., Cramer, M. C., Velankar, S. S., White, L. J. & Badylak, S. F. Extracellular matrix hydrogels from decellularized tissues: Structure and function. *Acta Biomater* **49**, 1–15, https://doi.org/10.1016/j.actbio.2016.11.068 (2017).

6. Kubinova, S. Extracellular matrix based biomaterials for central nervous system tissue repair: the benefits and drawbacks. *Neural Regen Res* **12**, 1430–1432, https://doi.org/10.4103/1673-5374.215249 (2017).
7. Crapo, P. M. *et al*. Biologic scaffolds composed of central nervous system extracellular matrix. *Biomaterials* **33**, 3539–3547, https://doi.org/10.1016/j.biomaterials.2012.01.044 (2012).
8. Medberry, C. J. *et al*. Hydrogels derived from central nervous system extracellular matrix. *Biomaterials* **34**, 1033–1040, https://doi.org/10.1016/j.biomaterials.2012.10.062 (2013).
9. Koci, Z. *et al*. Extracellular Matrix Hydrogel Derived from Human Umbilical Cord as a Scaffold for Neural Tissue Repair and Its Comparison with Extracellular Matrix from Porcine Tissues. *Tissue Eng Part C Methods* **23**, 333–345, https://doi.org/10.1089/ten.TEC.2017.0089 (2017).
10. Tukmachev, D. *et al*. Injectable Extracellular Matrix Hydrogels as Scaffolds for Spinal Cord Injury Repair. *Tissue Eng Part A* **22**, 306–317, https://doi.org/10.1089/ten.TEA.2015.0422 (2016).
11. Ghuman, H. *et al*. Long-term retention of ECM hydrogel after implantation into a sub-acute stroke cavity reduces lesion volume. *Acta Biomater* **63**, 50–63, https://doi.org/10.1016/j.actbio.2017.09.011 (2017).
12. Yu, X. X., Wan, C. X. & Chen, H. Q. Preparation and endothelialization of decellularised vascular scaffold for tissue-engineered blood vessel. *J Mater Sci Mater Med* **19**, 319–326, https://doi.org/10.1007/s10856-007-3157-8 (2008).
13. Schoen, F. J., Harasaki, H., Kim, K. M., Anderson, H. C. & Levy, R. J. Biomaterial-associated calcification: pathology, mechanisms, and strategies for prevention. *J Biomed Mater Res* **22**, 11–36 (1988).
14. Schmidt, C. E. & Baier, J. M. Acellular vascular tissues: natural biomaterials for tissue repair and tissue engineering. *Biomaterials* **21**, 2215–2231 (2000).
15. Speer, D. P., Chvapil, M., Eskelson, C. D. & Ulreich, J. Biological effects of residual glutaraldehyde in glutaraldehyde-tanned collagen biomaterials. *J Biomed Mater Res* **14**, 753–764, https://doi.org/10.1002/jbm.820140607 (1980).
16. Sung, H. W., Chang, W. H., Ma, C. Y. & Lee, M. H. Crosslinking of biological tissues using genipin and/or carbodiimide. *J Biomed Mater Res A* **64**, 427–438, https://doi.org/10.1002/jbm.a.10346 (2003).
17. Sung, H. W., Huang, R. N., Huang, L. L., Tsai, C. C. & Chiu, C. T. Feasibility study of a natural crosslinking reagent for biological tissue fixation. *J Biomed Mater Res* **42**, 560–567 (1998).
18. Sung, H. W., Liang, I. L., Chen, C. N., Huang, R. N. & Liang, H. F. Stability of a biological tissue fixed with a naturally occurring crosslinking agent (genipin). *J Biomed Mater Res* **55**, 538–546 (2001).
19. Daniel, M., K., N. K. & Myron, S. Injectable Collagen–Genipin Gel for the Treatment of Spinal Cord Injury: *In Vitro* Studies. *Advanced Functional Materials* **21**, 4788–4797, https://doi.org/10.1002/adfm.201101720 (2011).
20. Wassenaar, J. W., Braden, R. L., Osborn, K. G. & Christman, K. L. Modulating *In Vivo* Degradation Rate of Injectable Extracellular Matrix Hydrogels. *J Mater Chem B* **4**, 2794–2802, https://doi.org/10.1039/C5TB02564H (2016).
21. Jiang, T. *et al*. Preparation and characterization of genipin-crosslinked rat acellular spinal cord scaffolds. *Mater Sci Eng C Mater Biol Appl* **33**, 3514–3521, https://doi.org/10.1016/j.msec.2013.04.046 (2013).
22. Wang, Y. *et al*. Genipin crosslinking reduced the immunogenicity of xenogeneic decellularized porcine whole-liver matrices through regulation of immune cell proliferation and polarization. *Sci Rep* **6**, 24779, https://doi.org/10.1038/srep24779 (2016).
23. Li, Y., Li, L. & Holscher, C. Therapeutic Potential of Genipin in Central Neurodegenerative Diseases. *CNS Drugs* **30**, 889–897, https://doi.org/10.1007/s40263-016-0369-9 (2016).
24. Zeeman, R. *et al*. Successive epoxy and carbodiimide cross-linking of dermal sheep collagen. *Biomaterials* **20**, 921–931, https://doi.org/10.1016/s0142-9612(98)00242-7 (1999).
25. Pieper, J. S., Oosterhof, A., Dijkstra, P. J., Veerkamp, J. H. & van Kuppevelt, T. H. Preparation and characterization of porous crosslinked collagenous matrices containing bioavailable chondroitin sulphate. *Biomaterials* **20**, 847–858 (1999).
26. Hanthamrongwit, M., Reid, W. & Grant, M. Chondroitin-6-sulphate incorporadted into collagen gels for the growth of human keratinocytes: the effect of cross-linking agents and diamines. *Biomaterials*, 775–780 (1996).
27. Buijtenhuijs, P. *et al*. Tissue-engineering of blood vessels: characterization of smooth-muscle cells for culturing on collagenand-elastin-based scaffolds. *Biotechnol Appl Biochem*, 41–49 (2004).
28. Park, S. N., Park, J. C., Kim, H. O., Song, M. J. & Suh, H. Characterization of porous collagen/hyaluronic acid scaffold modified by 1-ethyl-3-(3-dimethylaminopropyl)carbodiimide cross-linking. *Biomaterials* **23**, 1205–1212 (2002).
29. Ungerleider, J. L. *et al*. Extracellular Matrix Hydrogel Promotes Tissue Remodeling, Arteriogenesis, and Perfusion in a Rat Hindlimb Ischemia Model. *JACC Basic Transl Sci* **1**, 32–44, https://doi.org/10.1016/j.jacbts.2016.01.009 (2016).
30. Yan, L. P. *et al*. Genipin-cross-linked collagen/chitosan biomimetic scaffolds for articular cartilage tissue engineering applications. *J Biomed Mater Res A* **95**, 465–475, https://doi.org/10.1002/jbm.a.32869 (2010).
31. Satake, K., Okuyama, T., Ohashi, M. & Shinoda, T. The Spectrophotometric Determination of Amine, Amino Acid and Peptide with 2,4,6-Trinitrobenzene 1-Sulfonic Acid. *J Biochem-Tokyo* **47**, 654–660, https://doi.org/10.1093/oxfordjournals.jbchem.a127107 (1960).
32. Spang, M. T. & Christman, K. L. Extracellular matrix hydrogel therapies: *In vivo* applications and development. *Acta Biomater* **68**, 1–14, https://doi.org/10.1016/j.actbio.2017.12.019 (2018).
33. Ma, B., Wang, X., Wu, C. & Chang, J. Crosslinking strategies for preparation of extracellular matrix-derived cardiovascular scaffolds. *Regen Biomater* **1**, 81–89, https://doi.org/10.1093/rb/rbu009 (2014).
34. Yang, G. *et al*. Assessment of the characteristics and biocompatibility of gelatin sponge scaffolds prepared by various crosslinking methods. *Sci Rep* **8**, 1616, https://doi.org/10.1038/s41598-018-20006-y (2018).
35. Zaviskova, K. *et al*. Injectable hydroxyphenyl derivative of hyaluronic acid hydrogel modified with RGD as scaffold for spinal cord injury repair. *J Biomed Mater Res A* **106**, 1129–1140, https://doi.org/10.1002/jbm.a.36311 (2018).
36. Delgado, L. M., Bayon, Y., Pandit, A. & Zeugolis, D. I. To cross-link or not to cross-link? Cross-linking associated foreign body response of collagen-based devices. *Tissue Eng Part B Rev* **21**, 298–313, https://doi.org/10.1089/ten.TEB.2014.0290 (2015).
37. Macaya, D. J., Hayakawa, K., Arai, K. & Spector, M. Astrocyte infiltration into injectable collagen-based hydrogels containing FGF-2 to treat spinal cord injury. *Biomaterials* **34**, 3591–3602, https://doi.org/10.1016/j.biomaterials.2012.12.050 (2013).
38. Ghuman, H. *et al*. ECM hydrogel for the treatment of stroke: Characterization of the host cell infiltrate. *Biomaterials* **91**, 166–181, https://doi.org/10.1016/j.biomaterials.2016.03.014 (2016).
39. Gelman, R. A., Williams, B. R. & Piez, K. A. Collagen fibril formation. *Evidence for a multistep process. The Journal of biological chemistry* **254**, 180–186 (1979).
40. Krupa, P. *et al*. The Effect of Human Mesenchymal Stem Cells Derived from Wharton's Jelly in Spinal Cord Injury Treatment Is Dose-Dependent and Can Be Facilitated by Repeated Application. *Int J Mol Sci* **19**, https://doi.org/10.3390/ijms19051503 (2018).
41. Pollock, K. *et al*. A conditionally immortal clonal stem cell line from human cortical neuroepithelium for the treatment of ischemic stroke. *Exp Neurol* **199**, 143–155 (2006).
42. Cocks, G. *et al*. Conditionally immortalized stem cell lines from human spinal cord retain regional identity and generate functional V2a interneurons and motorneurons. *Stem Cell Res Ther* **4**, 69, https://doi.org/10.1186/scrt220 (2013).
43. Anderova, M. *et al*. Transplantation of embryonic neuroectodermal progenitor cells into the site of a photochemical lesion: immunohistochemical and electrophysiological analysis. *J Neurobiol* **66**, 1084–1100, https://doi.org/10.1002/neu.20278 (2006).

Acknowledgements
This work was supported by Ministry of Education, Youth and Sports of CR within CZ.02.1.01/0.0./0.0/15_003/0000419 and GAUK 300217. We thank Dr. Lucie Svobodova for technical support.

Author Contributions
S.K. and K.V. designed experiments and interpreted data; K.V., J.V. and Z.K. carried out most of experiments; K.K. and K.J. carried out neural cell experiments, J.H. provided rheological measurement, P.J. provided critical input to the overall research direction; K.V. and S.K. wrote the manuscript with input from all co-authors.

Additional Information
Supplementary information accompanies this paper at https://doi.org/10.1038/s41598-019-47059-x.

Competing Interests: The authors declare no competing interests.

Publisher's note: Springer Nature remains neutral with regard to jurisdictional claims in published maps and institutional affiliations.